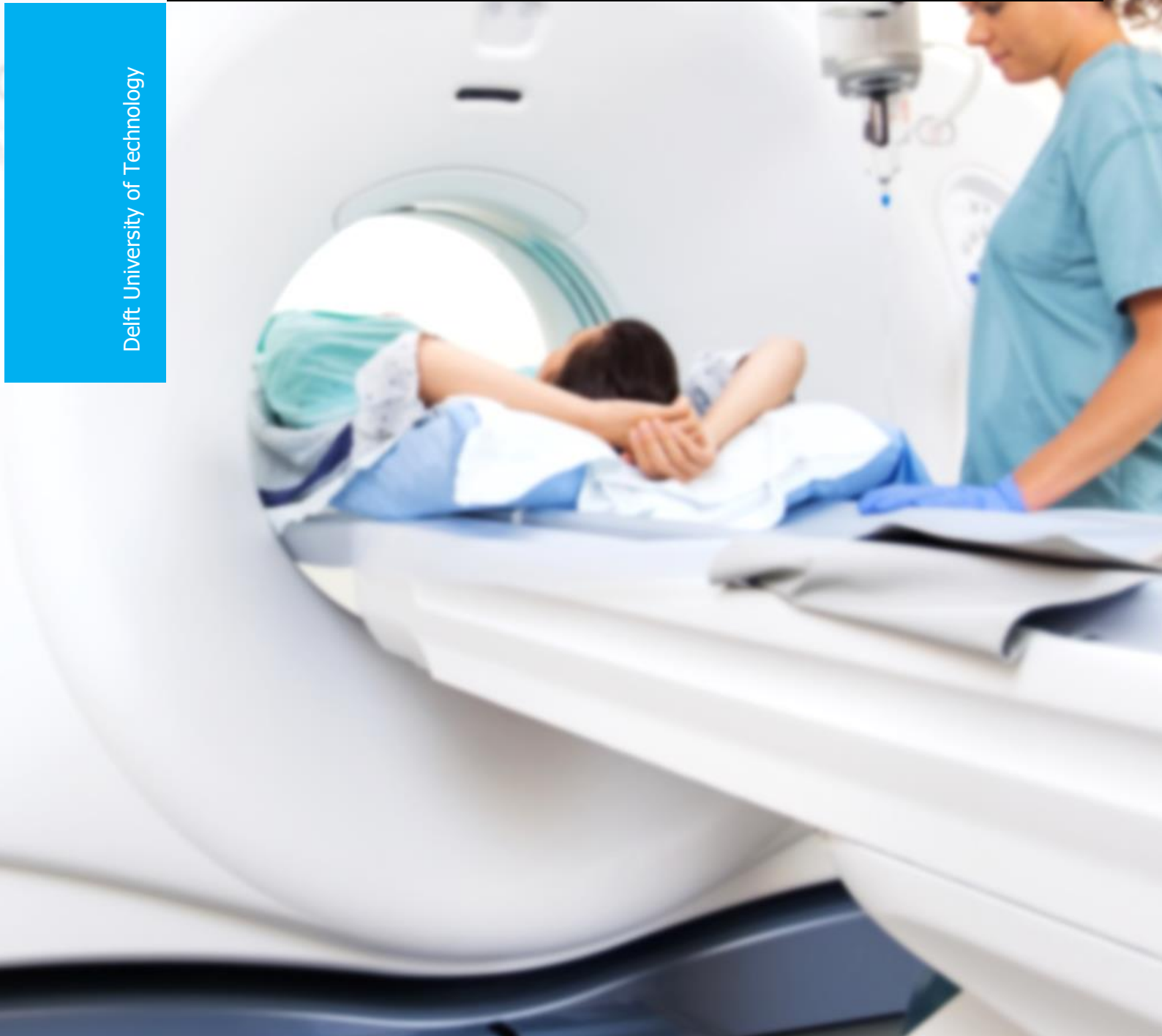


Improvement of tumour heterogeneity quantification in PET images

A study to design and develop a new PET heterogeneous phantom

L.M.H. Ghesquiere-Dierickx

Delft University of Technology



This page is intentionally left blank

ABSTRACT

Abstract

In medical images intra-tumour heterogeneity well translates specific cancer cells properties in a fast and non-invasive way. Medical community and researchers have developed proper tools (texture features, shape features...) permitting the quantification and the analysis of this tumour heterogeneity in particular in PET images. Yet so far, both doctors and researchers have mainly focused on the use of those tools before assessing their relevance and robustness. In this study, a new heterogeneous PET phantom allowing an extensive understanding of the key concept of heterogeneity quantification in PET images is designed and partially developed. This phantom aims at representing a complex enough environment mimicking clinical conditions to properly challenge PET heterogeneity data extraction and quantification methods further than commercial phantom already do. This study focusses, first, on defining sound specifications, design methodology and manufacturing method for this new object. Second, the study focusses on designing and developing the defined solution. Third, a proof-of-concept analysis is conducted within the study to test and validate the developed PET phantom prototype. It can be concluded that the produced PET phantom was successfully designed and developed and can be used by other operators; yet, there is still room for improvement. Finally, besides developing a novel PET phantom, this study yields recommendations to improve the work done toward a more handy, flexible and realistic tool.

This page is intentionally left blank

Improvement of tumour heterogeneity quantification in PET images

A study to design and develop a new PET heterogeneous phantom

By

L.M.H. Ghesquiere-Dierickx

in partial fulfilment of the requirements for the degree of
Master of Science
in Biomedical Engineering

at the Delft University of Technology,
to be defended publicly on the 10th of October, 2017 at 01:00 PM.

Student number:	4513932	
Supervisor:	Dr. ir. D.R. Schaart	TU Delft
	Dr. W. Grootjans	LUMC
Thesis committee:	Dr. ir. D. Lathouwer	TU Delft
	Dr. A.A. Zadpoor	TU Delft

This thesis is confidential and cannot be made public until October 10, 2017.

An electronic version of this thesis is available at <http://repository.tudelft.nl/>.

This page is intentionally left blank

PREFACE

This report presents the results of my graduation research, the final product of my Master in Biomedical Engineering, specialized in Medical Physics at Delft University of Technology. The topic of this study is the improvement of tumour heterogeneity quantification in PET images. This research was conducted at the Leids Universitair Medisch Centrum (LUMC), in a close collaboration with TU Delft and especially the TU Delft Electronic and Mechanical Support Division (Dienst Elektronische en Mechanische Ontwikkeling - DEMO). A previous report was handed in (in August 2017) containing the literature review completed for this study.

First, I would like to thank the Dennis Schaart and Willem Grootjans for giving me the opportunity to conduct this project. And I would like to thank the DEMO group and also the LUMC for the warm welcome I received at both places. Furthermore, I am deeply thankful to my thesis committee. Willem, thank you for all your answers on all my questions, regarding the topic. Denis, thank you for believing in me and giving me this amazing opportunity of work. Danny and Amir thank you both for your time and for being part of my graduation committee.

Additionally, there are multiple persons who contributed to this research and that I would like to thank. First, within the LUMC, I thank Joeri Kuil and Floris van Velden for their help with all of my experiments. Second, with the DEMO group, I thank Ernst van der Wal, Kevin Kamman who both always took the time to meet me, answer multiple questions by email and help me to build prototypes with them and by myself. Furthermore, I would like to also thank globally all of my colleagues in DEMO for their time, guidance, tips and insight whenever I needed help. I learned so much thanks to you all.

Lastly, I would like to thank my close friends from Delft and from abroad for their support, especially Thais and Timon who both were there for the good but also the bad moments to always support, cheer and motivate me. To finish, I would like to thank all of my family for their support, in particular my sisters and my mum, who always tried to help and encourage me even from abroad.

To you all: Thanks!

Laura Ghesquiere
The Netherlands
October, 2017

This page is intentionally left blank

TABLE OF CONTENT

Abstract.....	i
Preface.....	v
Table of Content.....	vii
List of Figures	ix
List of Tables	xi
List of Abbreviations	xii
Chapter 1: Introduction.....	1
1.1 Context.....	1
1.1.1 Clinical context.....	1
1.1.2 Positron Emission Tomography (PET)	2
1.2 Problem definition.....	3
1.3 Research objectives and research questions.....	4
1.3.1 Research objectives	4
1.3.2 Research questions.....	4
1.4 Relevance of the study.....	5
1.5 Practical contribution	6
1.6 Thesis Structure	7
Chapter 2: Research methodology	9
2.1 First phase: Analysis	9
2.2 Second phase: Design and Development	9
2.3 Third Phase: Test and validation	12
2.4 Fourth phase: Discussion and recommendations	12
Chapter 3: Literature study summary	13
3.1 PET heterogeneity quantification variability	13
3.2 How a heterogeneous PET Phantom can improve PET heterogeneity quantification?.....	14
3.3 Current state of the art of PET Phantoms.....	15
3.3.1 Current limitations of PET phantoms from the market.....	15
3.3.2 Current limitations of state-of-the-art PET research phantoms	16
3.4 Evaluation of a phantom quality.....	16
3.5 Literature review conclusion	18
Chapter 4: Design and Developments.....	19
4.1 Global phantom design overview: Box+ Inserts.....	19
4.1.1 Global phantom design requirements.....	19
4.1.2 Global phantom design description.....	21
4.2 Phantom box design	22
4.2.1 Phantom box preliminary design (V.0).....	24
4.2.2 Phantom box design (V.1.1 & V.1.2).....	26
4.2.3 Phantom box design (V.2.1, V.2.2, V.2.3 & V.2.4).....	27
4.2.4 Phantom box design (V.3.1 & V3.2).....	29
4.2.5 Phantom box design (V.4.1, V.4.2 & V.4.3)	30

4.2.6	Phantom box design (V.5)	30
4.2.7	Phantom box design (V.6.1 & V.6.2)	31
4.2.8	Phantom box design (V.7)	31
4.2.9	Phantom box design (V.8)	32
4.2.10	Phantom box design (V.9)	32
4.3	Phantom inserts design	33
4.3.1	Phantom inserts overview	33
4.3.2	Phantom inserts manufacturing	33
4.3.3	Phantom spherical inserts design	34
4.3.4	Phantom cubical inserts design	39
4.4	Design and development chapter summary	44
Chapter 5: Test and validation results		45
5.1.1	Pre-manufacturing glue selection test	45
5.1.2	Post-manufacturing spherical inserts circularity test	47
5.1.3	Post-manufacturing phantom water absorption test	48
5.1.4	Post-manufacturing phantom CT density test	50
5.1.5	Post-manufacturing cubical insert pillars influence test	55
5.1.6	Post-assembly leakages tests	56
5.1.7	Post-assembly estimated irradiation time	58
5.1.8	FDG PET/CT imaging test and proof of concept	60
Chapter 6: Recommendations		63
Chapter 7: Conclusion		65
References		67
Appendices		i
Appendix 0: Literature research method		ii
Appendix 1: Parameters influencing PET uptake values as found in the literature		iv
Appendix 2: Parameters influencing PET texture features as found in the literature		vi
Appendix 3: NEMA Body Phantom specific dimensions and requirements		viii
Appendix 4: Box design versions details		ix
Appendix 5: Spherical inserts design versions details		xi
Appendix 6: Cubical inserts design versions details		xii
Appendix 7: Protocols		xiii
Appendix 7.1: Radioactivity absorbance test of the photopolymer R05 protocol		xiii
Appendix 7.2: CT image background values extraction protocol		xiv
Appendix 7.3: Sphere shape analysis protocol		xv
Appendix 8: Master Thesis Log journal		xvi

LIST OF FIGURES

Figure 1 Four main contributions of the study	6
Figure 2 Theoretical design methodology workflow as pre-planned for the Master Thesis	10
Figure 3 Actual design methodology workflow followed during the Master Thesis	11
Figure 4 Global overview of the preliminary PET phantom design idea	21
Figure 5 Global overview of the latest PET phantom box design and its inserts	21
Figure 6 Exploded view of the latest PET phantom design	22
Figure 7 General overview of each design version of the phantom box	23
Figure 8 Top and bottom views of the SLA printing of a miniaturized version of the phantom box (V.0)	24
Figure 9 Lateral view of the SLA printing of a miniaturized version 0 of the phantom box (V.0)	25
Figure 10 PMMA tube and flanges assembly	27
Figure 11 Rubber gasket	27
Figure 12 Exploded view of the top part of the phantom box (V.2.3)	28
Figure 13 Side 3D view of phantom box design (V.3.1)	29
Figure 14 Side 3D view of phantom box design (V.3.2)	29
Figure 15 Filling cube from (V.4.1) (left) and filleted filling cube from (V.4.2) (right)	30
Figure 16 Screws (M3x10 left, M4x10 right)	31
Figure 17 PET phantom box assembly of the first prototype in the NEMA body PET box as designed in (V.7)	32
Figure 18 General overview of each design version of the spherical inserts and their manufactured prototypes	34
Figure 19 Photopolymer R05 as designed (left) and printed (right)	35
Figure 20 Phantom spherical insert design (V.1)	35
Figure 21 Phantom spherical insert design (V.2)	35
Figure 22 Phantom spherical insert design (V.3.2): spheres of 10, 13, 17, and 22mm ID	35
Figure 23 Phantom spherical insert design (V.3.2) SLA 3D printed with support	36
Figure 24 Phantom spherical insert design (V.5)	36
Figure 25 Phantom spherical FDM printed insert (V.5) with the four SLA printed spheres attached to one of its side	36
Figure 26 Phantom spherical insert design (V.6.1) and (V.6.2)	37
Figure 27 Phantom spherical insert prototype from sphere (V.3.2), (V.4) and plate (V.6.1) and (V.6.2)	37
Figure 28 Phantom spherical insert design (V.7)	38
Figure 29 Exploded view of the text volume developed by IBSI and used for the cubical inserts design	39
Figure 30 3D representation of the cubes according to their concentration	39
Figure 31 General overview of each design version of the cubical inserts and their manufactured prototypes	40
Figure 32 Cubical inserts (V.2.1)	41
Figure 33 Cubical inserts (V.2.2)	41
Figure 34 FDM print the cubical inserts (V.2.4)	41
Figure 35 Phantom cubical inserts (V.3.1) (left) and (V.3.4) (right)	42
Figure 36 SLA print of the phantom cubical insert (V.3.4)	42
Figure 37 Phantom cubical insert design (V.3.5) with diagonal pillars and extra external support	42
Figure 38 Imaging segment of 42mm containing: spherical insert (left) and cubical insert (right)	43
Figure 39 Additional external support added to design (3.6) by the SLA printed software: 3D design view (left), actual printed insert with supports (middle) and without (right)	43
Figure 40 Araldite 2020 (retrieved from Araldite website)	45
Figure 41 Araldite 2022-1 (retrieved from Araldite website)	46
Figure 42 Gluing strength comparison between Araldite 2020 (A)(C) and 2022-1 (B)(D)	46
Figure 43 Transversal CT image view of the spherical V.3 inserts in air	47
Figure 44 Ratio of the retrieved major & minor axis of the 3D printed spheres	47
Figure 45 CT images extracted from the different parts of the phantom	51
Figure 46 Retrieved CT density (HU) values of water from different imaging conditions	51
Figure 47 Retrieved CT density (HU) values of air from different imaging conditions	52
Figure 48 Retrieved CT density (HU) values of PMMA	52
Figure 49 Retrieved CT density (HU) values of NBR	52
Figure 50 Retrieved CT density (HU) values of PLA	52
Figure 51 Retrieved CT density (HU) values of the photopolymer R05 in air and water	53
Figure 52 Retrieved CT density (HU) values of the photopolymer R05 in water only	53
Figure 53 CT density scale (HU) from extracted values of air, water, PMMA, NBR, PLA and R05	54
Figure 54 CT acquisition of semi filled cubical insert	55
Figure 55 Assembly of the spherical inserts with their holding plate, leaks appear at the bottom of the plat where each sphere is closed by a M3 screw	56
Figure 56 Assembly of imaging segment (top) with an insert plate (blue), and a bottom segment held by M4 screws and bolt with a leak (arrow)	56
Figure 57 Picture of a M3 screw elongation of 1.27 mm (left) compared to a normal M3 screw with a global height of 12.5 mm (right)	58
Figure 58 Transversal section view (top) and side view (bottom) of the tested PET phantom segment which contains spherical inserts	60

Figure 59 PET phantom assembly of all the segments including the one containing the spherical inserts before filling (center).....60

Figure 60 Transversal view of the PET image reconstructed with set up #6, grey colour scale (left); thermal colour scale (centre) and (right)..... 61

Figure 61 Plot line of grey values from (Figure 60) containing spheres of 17mm, 17mm, and 22mm ID (left). Each spheres true concentration and background are added in red (left). 61

Figure 62 Plot line of grey values from (Figure 60) containing spheres of 10mm, 22mm and 10mm ID..... 62

Figure 63 Plot line of grey values from (Figure 60) containing (left spheres of 10mm, 22mm and 10mm ID and 17mm, 22mm, 17mm ID (right))..... 62

Figure 64 Geometric shapes that can be developed later on 63

Figure 65 PRISMA flow chart of the literature study ii

Figure 66 3D drawing of the NEMA Body PET Phantomviii

Figure 67 Transversal engineering drawing view of the NEMA Body PET phantomviii

Figure 68 Frontal engineering drawing views of the NEMA Body PET phantomviii

Figure 69: ImageJ® toolbarxiv

Figure 70 Shape selection in CT images using ImageJ..... xv

Figure 71: Results retrieved from shape extraction protocol..... xv

LIST OF TABLES

Table 1: Influencing parameters of PET uptake and texture features quantification	14
Table 2 Current PET Phantom limitations	15
Table 3 Ideal PET phantoms requirements	16
Table 4 Summary of advantages and disadvantages of cutting-edge PET phantoms	17
Table 5 Research scope, requirement and guidelines for this Master Thesis' phantom design	20
Table 6 General properties of PMMA (Ide-mat 2003).....	27
Table 7 General properties of NBR (Matweb 2017)	27
Table 8 Parts list of box design (V.2.3)	28
Table 9 Parts list of box design (V.2.4)	28
Table 10 Parts list of box design (V.6.1)	31
Table 11 Comparative table of FDM and SLA additive manufacturing techniques	33
Table 12 General properties of R05 (EnvisionTEC 2015).....	35
Table 13 General properties of PLA (Ultimaker 2017)	36
Table 14 Phantom design trade-offs summary.....	44
Table 15 General properties of Araldite® 2020 (Huntsman 2020a, 2020b).....	45
Table 16 General properties of Araldite® 2022-1 (Huntsman 2022b, 2022a).....	46
Table 17 Water absorption literature values found for the different materials used in the phantom	48
Table 18 Results of the radioactivity absorbance test	49
Table 19 Literature HU values for typical human tissues types	50
Table 20 Tested configuration overview for spherical insert closing leak tests.....	56
Table 21 Tested configurations overview for assembly leak tests	57
Table 22 Chosen reconstruction parameters for the PET/CT image acquisition validation test	61
Table 20 Vocabulary used during first literature review	ii
Table 21 Vocabulary used during second literature review	iii
Table 22 Biological or physiological parameters influencing PET uptake values	iv
Table 23 Pre-acquisition parameters influencing PET uptake values.....	iv
Table 24 Acquisition parameters influencing PET uptake values	v
Table 25 Image reconstruction parameters influencing PET uptake values	v
Table 26 Biological and physiological parameters influencing PET texture features.....	vi
Table 27 Acquisition parameters influencing PET TF.....	vi
Table 28 Reconstruction and Post-processing Parameters influencing PET texture features	vi
Table 29 Feature extraction parameters influencing PET texture features	vii
Table 30 Phantom Box design iterations details	ix
Table 31 Spherical inserts design iterations.....	xi
Table 32 Cubical insert design iterations	xii

LIST OF ABBREVIATIONS

Units:

Becquerel	Bq	standard International Unit (USI) of radioactivity representing 1 nuclear decay/second.
Gray	Gy	standard International Unit (USI) representing the deposit of a joule of radiation energy in a kg of matter.
Sieverts	Sv	standard International Unit (USI) representing the biological health effects on the human body of the absorption of a joule of radiation energy in a kg of human tissue.
Hounsfield unit	HU	unit of measurement used on a computed tomography machine (CT) representing the linear attenuation coefficients of a certain material compared to water

List of symbols:

α	alpha particle, identical to a helium nucleus (also written α^{2+} , He^{2+})
β	beta particle: can be either β^+ (positron) or β^- (electron)
γ	gamma radiation, photon

List of acronyms:

3D	Three Dimensions or Three Dimensional Space
AM	Additive Manufacturing
CT	Computed Tomography
^{18}F -FDG	Fluorine-18 labelled [F-18] fluorodeoxyglucose
^{18}F -FLT	Fluorine-18 labelled [F-18] 39-deoxy-39-fluorothymidine
^{18}F -FET	Fluorine-18 labelled O-(2-[F-18]-fluoroethyl)-L-tyrosine
^{18}F -FMISO	Fluorine-18 labelled [F-18]-fluoromisonidazole
^{11}C -MET	Carbon-11 labelled l-(methyl-[11C])-methionine
FDM	Fused Deposition Modelling
FOV	Field Of View
GLCM	Grey Level Co-occurrence Matrix
GLRLM	Grey Level Run Length Matrix
GLSZM	Grey Level Size Zone Matrix
HU	Hounsfield unit
IAEA	International Atomic Energy Agency
IBSI	Image Biomarker Standardisation Initiative
ID	Inside Diameter
LOR	Line Of Response
MRI	Magnetic Resonance Imaging
MATV	Metabolic Active Tumour Volume
NBR	Nitrile Butadiene Rubber
NGTDM	Neighbourhood Grey-Tone Difference Matrix
NGLDM	Neighbourhood Grey-Level Difference Matrix
OD	Outside Diameter
PET	Positron Emission Tomography
PLA	Polyactic acid
PMMA	Poly(methyl methacrylate)
R05	Photopolymere EnvisionTec named R05
RT	Radiation Therapy
ROI	Region Of Interest
SLA	Stereolithography
SNR	Signal to Noise Ratio

SPECT	Single-Photon Emission Computed Tomography
STP	Standard Temperature and Pressure
SUV	Standardized Uptake Value
TA	Texture Analysis
Tc ^{99m}	Technetium-99m
TF	Texture Features
TLG	Total Lesion Glycolysis
TOF	Time Of Flight
US	UltraSounds
VOI	Volume Of Interest

This page is intentionally left blank

1

CHAPTER 1: INTRODUCTION

This first report chapter aims at presenting the context of the research and its organisation. First, the Master thesis context scope is detailed, followed by definitions of the key concepts of this work like cancer heterogeneity, positron emission tomography (PET) general principles and heterogeneity extraction methods. Then, the research problem is established and detailed. Following this, the research objectives and questions are laid out. Next, the relevance and the contribution of this Master study are explained. The chapter ends with an outline of the Master thesis research.

1.1 CONTEXT

1.1.1 CLINICAL CONTEXT

Cancer is a generic term for a large group of complex diseases characterized by the fast proliferation of abnormal cells unable to become functional tissues, it is caused by diverse intrinsic genetic mutations that can affect any organ of the human body (Hanahan and Weinberg 2000). The term *tumour heterogeneity* includes variability regarding many features of variability in tumour cells themselves (e.g. cells morphology, size, shape, surface receptors) and their functionality (metabolisms, cell-to-cell interactions, proliferation rate, metastatic potential, radiation response). Tumour heterogeneity can be separated into three categories: (1) *inter-tumour* heterogeneity where each tumour is globally different from another one in another patient. (2) *Intra-tumour heterogeneity* which states that there are specific tissue compositions within the tumour as a consequence of different sub-cell population and properties in the same tumour. And (3) *temporal heterogeneity* which refers to the tumour changes that occur over time (stress, growth, treatment etc.) (Welch 2016). In this report, only *intra-tumour heterogeneity* is considered, thus the term "*tumour heterogeneity*" refers to "*intra-tumour heterogeneity*" alone.

It is known that tumour vascularisation, proliferation, metabolism (Hanahan and Weinberg 2011) plays an important role in such observed tumour heterogeneity, leading to intrinsic and acquired treatment resistance (Marusyk, Almendro, and Polyak 2012). Similar to the Darwinian evolution mechanisms, the cells adapted best to a specific environment will have a higher survival probability and have the potential to multiply the most. This mechanism explains why the most resistant cells will be promoted to survive during anti-cancer therapy, reducing the chances of curing the patients from cancer (M Gerlinger and Swanton 2010). Personalising treatment includes a selection of appropriate systemic therapy (e.g. chemotherapy or biological agents) or an adaptation of radiation dose to the specific composition of the tumour which could improve patient survival (O'Connor et al. 2015). This is why identification of tumour types and intra-tumour heterogeneity is one of the main challenges of this decade and why we focussed here on improving the understanding and precision of heterogeneity quantification.

Usually invasive biopsies are performed to analyse patient tumour cells composition. However biopsies only sample a specific part of the tumour at a specific time. Such biopsy samples thus contain no or little information regarding the global tumour composition (M Gerlinger and Swanton 2010; Marco Gerlinger et al. 2012). On the other hand, imaging techniques like X-ray, ultrasounds (US), magnetic resonance imaging (MRI), computed tomography (CT), positron emission tomography (PET) or single-photon emission computed tomography (SPECT) can non-invasively analyse the entire tumour composition and precisely track its global changes over time.

Among all the different imaging techniques available in oncology, the author chose to focus here, within the context of this Master thesis, on Positron Emission Tomography (PET) modality.

1.1.2 POSITRON EMISSION TOMOGRAPHY (PET)

Positron Emission Tomography (PET) is a commonly employed non-invasive imaging technique which uses biological molecules radiolabelled with positron (β^+) emitter radionuclides to detect and delineate regions of biological interest in human body (Phelps 2004). Once injected to the patient, PET radiotracers like ^{18}F -FLT, ^{18}F -FET, ^{18}F -FMISO, ^{18}F -HX4 or ^{11}C -MET... are delivered to the entire body and distributed in tissues according to the biological interest of their molecule component.

The goal of *PET image quantification* is to calculate image metrics that properly represent the radiotracer distribution. Quantitative inaccuracies, due to noise and other degrading factors, should be kept to a minimum. PET image quantification quantifies the uptake of the radiotracer; but can also quantify its spatial distribution and heterogeneity, thus we will separate PET image quantification in two terms: (1) *PET image uptake distribution quantification* and (2) *PET image heterogeneity quantification*.

Analysing the radiotracer uptake distribution in PET images can give valuable information regarding a lot of different tissue properties such as proliferation (Juhász et al. 2014), hypoxia (Rajendran and Krohn 2015), cell activity (Fletcher et al. 2008), vascularisation (Hjelmgren et al. 2014), etc.

But analysing the radiotracer uptake heterogeneity in PET images can provide even more information regarding tumour characteristics than PET uptake distribution values alone. For example heterogeneity quantification gives a better understanding of tumour proliferation (Willaime et al. 2013), vascularization (Tixier, Groves, et al. 2014), and hypoxia (van Elmpt et al. 2016). Intra-tumour heterogeneity is also usually predictive of treatment resistance (Junttila and de Sauvage 2013). The association of quantitative heterogeneity features on medical images with patient prognosis was recognized and resulted in the creation of the term: *radiomics*.

First defined by (Lambin et al. 2012) after the promising results of (El Naqa et al. 2009) and (Tixier et al. 2011), *radiomics* is the analysis of high dimensional image data set (more than 400 features values extracted medical images, mainly heterogeneity values via texture and shape quantification) that provides additional valuable information. Radiomics permits to make correlation between tumour heterogeneity and tumour biology through extraction of valuable information regarding tumour resistance, survival rate, new patients' prognostic values (Aerts et al. 2014; Tixier, Hatt, et al. 2014; O'Connor et al. 2015; Gillies, Kinahan, and Hricak 2016).

At the end, from this first clinical context section and regarding the interesting results found in the recent literature (O'Connor et al. 2015), (Gillies, Kinahan, and Hricak 2016), (S. S. F. Yip and Aerts 2016) it is now easy to understand the importance that has been given during the last past years to the topic of intra-tumour heterogeneity quantification in oncology, patient treatment adaptation and outcome prediction. However, even though PET heterogeneity quantification and its use in radiomics seem to give very promising results, few recently published papers try to retain the current research enthusiasm by emphasizing the limitations of heterogeneity quantification (Brooks 2013), (Chalkidou, O'Doherty, and Marsden 2015), (Hatt et al. 2017). In the light of those papers, the next section of this introduction chapter aims at understanding the true extent of PET tumour heterogeneity quantification limitations and which solution can overcome them.

1.2 PROBLEM DEFINITION

The outline of the research problem was drawn from the preliminary reading of three publications: (Brooks 2013), (Chalkidou, O'Doherty, and Marsden 2015) and (Hatt et al. 2017) which stressed the fact that heterogeneity quantification images and radiomics analysis in PET have been proven to show good results, but that those good results unfortunately shades the actual limitations and unresolved issues faced by the core concept of PET tumour heterogeneity quantification. Hence, this paragraph which tries to give a non-exhaustive list of the limitations of heterogeneity quantification showing that radiomics and especially heterogeneity quantification in PET images still need to be better investigated.

First, as there is still no standardized method to analyse heterogeneity and due to the large number of texture features defined over the years by different authors (Haralick, Shanmugam, and Dinstein 1973; Galloway 1975; Chu, Sehgal, and Greenleaf 1990; Dasarathy and Holder 1991; Sun and Wee 1983; Thibault et al. 2009) the redundancy and differences in texture features definition or formulae make their use complex and their values difficult to analyse or compare to each other. The need for standardization of texture feature calculation is huge and has therefore been expressed in a lot of other papers (Cheng, Fang, and Yen 2013), (Brooks 2013), (Orlhac et al. 2014), (Nyflot et al. 2015) (Hatt et al. 2017).

Secondly, heterogeneity quantification is based on the spatial analysis of voxel uptake values like SUV. but it has been shown that from the same acquired ground truth object those calculated values are noise-, acquisition- and image reconstruction-dependent (Galavis et al. 2010) (Hatt et al. 2013). As small changes in texture values can lead to significant change in the prognostic values extracted from radiomics analysis, (Hatt et al. 2013), the use of non-robust texture features in big-data analysis like radiomics can lead to confounding results that can be misinterpreted (Hatt et al. 2017) and should therefore not be employed.

Third, one of the main limitations of PET tumour heterogeneity quantification is the current lack of knowledge regarding texture features clinical interpretation. Indeed, the link between PET image values and the underlying biology of tissues (metabolism, hypoxia, necrosis...) is based on assumptions or limited correlations and not enough studies have been done yet to improve the understanding of those relationships (Hatt et al. 2017). Due to that, some texture feature might not be representative of any true heterogeneous biology and therefore completely irrelevant. Studies should therefore first investigate the biological/physiological interpretation of heterogeneity quantification before using them for interpretation; but among all the papers that were considered for this review, only one publication studies the influence of uptake heterogeneity on texture features values (Orlhac et al. 2017).

Lastly, in small populations overfitting of data is usually a big problem. (Chalkidou, O'Doherty, and Marsden 2015) statically analysed publications results regarding quantification heterogeneity and radiomics and yield to the conclusion that even though the statistical models used in radiomics publications were specifically fitted to the population, they would not necessarily be predictive in a random other cohort due to the usual small cohort size used in radiomics. Usually test and validation cohorts are needed, but this is not considered in most of the studies (because there are not enough patients). Furthermore, (Hatt et al. 2017) also detailed statistical issues existing due to the strong trend of only publishing positive results where publications running counter to the current direction of radiomics promising results are rare and not especially well recognized, which leads to bias in the overall literature regarding this topic.

At the end, all of these remarks highlight current uncovered gaps in the literature regarding PET heterogeneity quantification limitations and drawbacks. These remarks are explained by a lack of knowledges regarding radiomics commonly used tools and they all emphasize the need of improving the PET heterogeneity quantification core concept. To this end the Master thesis, and especially its literature review, were defined to invest all the remarks described by those three papers, and to confront them with the whole current literature on heterogeneity quantification in PET images in order to proper assess all existing issues regarding PET heterogeneity quantification and how to overcome them.

To sum up, the following problems are identified:

- (1) Bias: so far most of the research has only focussed on clinical radiomics applications.
- (2) Core concept is unprecise: some papers tend to suggest that the basic concept of heterogeneity quantification in PET images faces great limitations that are not overcome yet
- (3) Limitations have started to be listed: those limitations arise from lack of standardisation, value extraction dependency, lack of knowledge regarding the link between heterogeneity values and what biology they truly represent and wrong statistics.
- (4) Unknown other limitations can exist: those limitations can arise from other issues that still need to be investigated.

1.3 RESEARCH OBJECTIVES AND RESEARCH QUESTIONS

1.3.1 RESEARCH OBJECTIVES

Globally, this Master study aims at investigating and answering the aforementioned problems by understanding the true extent of PET tumour heterogeneity quantification and by finding a way to improve it. To this end we defined two main research objectives: a theoretical and a practical one that will need to be fulfilled by the end of the Master thesis. The theoretical objective of this Master study is to properly assess the current issue with heterogeneity quantification in PET images and its causes. The other practical objective of this Master thesis is to first propose a solution to improve standardization of PET heterogeneity quantification, namely a PET heterogeneous phantom, and to, second, study its relevance and feasibility; then, third, to implement a design methodology and build the solution as well as, fourth, assess its efficiency compared to what was expected from it.

1.3.2 RESEARCH QUESTIONS

Those global objectives were, first, translated in a literature review question:

What are the limitations of tumour heterogeneity quantification and how do current available tools fail to overcome those limitations?

This question was answered in a literature study (handed in August 2017) which addressed the following theoretical/methodological sub-questions (answered in the literature review and in Ch.3):

- a. What are the causes, background and interrelated aspects of the issue with PET heterogeneity quantification and how is it currently described in the literature? What parameters influence PET heterogeneity quantification?
- b. In theory, how we improve tumour heterogeneity quantification in PET images? How will creating a heterogeneous PET phantom help?
- c. What is the state of the art in PET phantoms development?
- d. What are the limitations of current PET phantoms?
- e. In theory, what are the measures that can be used to evaluate a phantom quality?
- f. How current PET phantom perform according to those criterion?

From those answers a global Master thesis research question was defined:

How can a heterogeneous PET phantom be developed and help to improve current PET tumour heterogeneity quantification limitations?

From this global question, a cluster of several practical sub-questions were formulated (to be answered here):

- g. What design methodology should be follow during this Master study? (cf.Ch.2)
- h. What workflow and iterations were needed to build a new PET phantom? (cf. Ch.4)
- i. Is the built phantom fulfilling its requirements? (cf. Ch.5) (Test and validation)
- j. What are the challenges faced during the Master Thesis? (cf. Ch.5) (Discussion)
- k. Which phantom part could be improved and how? (cf. Ch.6) (Recommendation)

The global research question cannot be answered without first answering to the literature review question. Thus, the current report will briefly re-present the conclusion drawn from the literature review but, then, it will mainly focus on answering the Master thesis research question.

1.4 RELEVANCE OF THE STUDY

In this section, the relevance of the Master thesis is assessed by comparing the expressed research objectives of the Master thesis to the scientific needs and gaps found in the available literature. As the Master thesis is focused on developing a heterogeneous PET phantom to improve PET heterogeneity quantification, first the relevance of the topic is checked and the relevance of improving the understanding of PET tumour heterogeneity quantification will be reminded first in this section. Second, the relevance of our global solution for that topic –i.e. a PET phantom applied to heterogeneity quantification- is checked and an analysis of all scientific papers regarding PET phantom applications for PET image heterogeneity quantification improvement is described. Third, the relevance of our precise solution in a more precise way –i.e. a heterogeneous PET phantom applied to heterogeneity quantification- is checked and all scientific papers regarding heterogeneous PET phantom are examined to check if the needs of such a tool has been expressed and/or already covered.

First, as detailed in (§1.1.1 Clinical context) over the last 8 years a large number of publications has been focussed on the analysis of PET image heterogeneity and its prediction power, most exhibiting very good results (El Naqa et al. 2009; Gillies, Kinahan, and Hricak 2016) and suggesting that PET heterogeneity quantification is a topic of very high importance in the current oncology research field. For more details, please refer to (S. S. F. Yip and Aerts 2016) for the latest detailed review of PET heterogeneity quantification applications and results. However, as stated in (§1.2 Problem definition) and in the literature review report, a lot of parameters influence PET heterogeneity quantification meaning that, even though PET image heterogeneity and its prediction power show promising result, they still need to be improved. As suggested by several papers (including (Hatt et al. 2017)) a reference standard needs to be developed for heterogeneity quantification definition, quantification protocols, and feature analysis to overcome these issues with PET heterogeneity quantification. One way we chose here to do so is by creating a standardized complex ground truth object, in the form of a *heterogeneous PET phantom*.

Second, usually PET phantoms are developed in order to simply assess PET image *uptake* quantification (and not PET image heterogeneity). In the literature only few very recent papers have developed and used PET phantoms for PET image heterogeneity quantification: (Nyflot et al. 2015), (Forgacs et al. 2016), (Cortes-Rodicio et al. 2016), (Shiri et al. 2017), (Carles et al. 2017). By using ground truth objects and fixed experimental conditions these papers have tried to assess PET variability in heterogeneity quantification by analysing patient biology, size, lesion size, noise influence (Nyflot et al. 2015), volume of interest (VOI) dependency, heterogeneity influence (Forgacs et al. 2016), reconstruction settings (Cortes-Rodicio et al. 2016), (Shiri et al. 2017) and respiration motion and reconstruction influence (Carles et al. 2017). All of these scientific papers are less than 2 years old which proves the relative recent need of improving PET heterogeneity quantification using PET phantoms.

Third, among those five papers using PET phantoms for image heterogeneity quantification only two papers (Forgacs et al. 2016) and (Carles et al. 2017) actually developed and used *heterogeneous* PET phantoms. One paper (Forgacs et al. 2016) used syringes filled with different concentration and the other paper (Carles et al. 2017) used alginates inserts mould with different radioactivity concentration. But both of them faced some limitations: (Forgacs et al. 2016) syringes have plastic walls, non-realistic tumour shapes and do not present a great flexibility of use whereas (Carles et al. 2017) moulded alginates insert presented a great flexibility in tumour shape and size with can lower the reproducibility of the phantom results and increases set-up time. As none of these heterogeneous phantoms is perfect, the need of designing and developing another heterogeneous PET phantom for heterogeneity quantification is still huge. The last three other papers (Shiri et al. 2017), (Nyflot et al. 2015) and (Cortes-Rodicio et al. 2016) only used homogeneous phantom. However, both (Nyflot et al. 2015) and (Cortes-Rodicio et al. 2016) suggest that the next step of their work for a better evaluation of features influence and robustness would be to use heterogeneous phantoms as they would better investigate changes in heterogeneity variations which, again, confirms the necessity of developing such a tool .

In the end, all of this highly emphasizes the present need of improving PET heterogeneity quantification using PET phantom and more especially using heterogeneous PET phantom and support the global relevance of this Master thesis.

1.5 PRACTICAL CONTRIBUTION

In this section the Master thesis contribution is summarized; which permit to already have in the report's introduction a good overview of the work achieved during the thesis and what still needs to be done. The practical contribution of this study can be separated in four main contributions (cf. Figure 1).

First, an extensive analysis of the scientific literature was performed to fully understand the issue regarding PET heterogeneity quantification and the current gaps that were needed to be filled. Due to the total novelty of this project, this analysis phase was considered as a key step of the study and a lot of efforts were put in this contribution to properly analyses but also define the set-ups and direction of the project for the first time. This "definition and analysis" contribution is detailed in (Chapter 1: Introduction), (Chapter 2: Research methodology) and (Chapter 3: Literature study summary).

Second, once the project direction was defined, a clear description of a research solution was completed which constitutes the second main contribution of the study. Precise requirements of the solutions were listed according to current the state of the art of PET phantom limitations and regarding the global aim of the study. This "solution definition" contribution is detailed in (Chapter 3: Literature study summary). From the detailed solution specifications, a design could be developed.

Third, then, the design and development of a partial solution proceeded and constitute the third main contribution of the study. This contribution is the central point of the study as it aims at specifically answering the project problem. The solution development yields to several sub-contributions in the form of: design process definition and workflow, design files and engineering drawings of a solution, techniques and manufacturing knowledges regarding PET phantom creation, limitation and usual trade-off faced while designing an object. All of these sub-contributions expend the research solution development contribution with gained knowledges and additional produced information. This "solution design and development contribution and its sub-contributions are described in (Chapter 4: Design and Development) and (Chapter 5: Results and discussion).

Last, the fourth contribution of the study stems from the limitation and un-resolved issues faced while developing the study solution. As the project is very new, there is room for a lot of improvement and applications. This last contribution is the creation of recommendations and suggestion of new directions for further work regarding this project which is described in (Chapter 6: Recommendations).

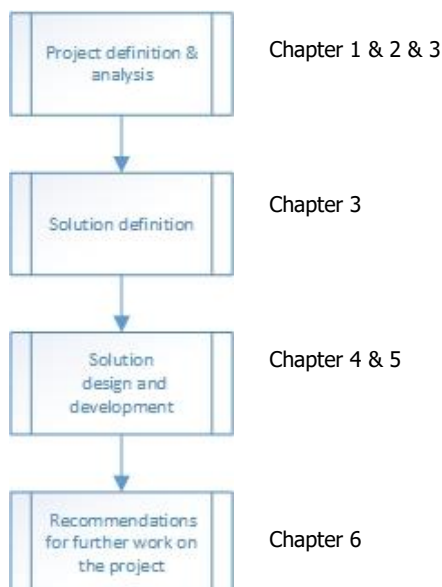


Figure 1 Four main contributions of the study

To conclude, all of the four contributions of the study: project analysis, solution definition, solution development and recommendation for further work appeared to be as important as the others. Regarding the complete newness of the project, each contribution by itself could have been developed into four entire study projects. However the author here decide scan them all, and to globally deal with all of them together in one project as it permits to quickly move forward with a -almost- functional produced solution.

1.6 THESIS STRUCTURE

In this last section the Master thesis structure is detailed. The Master Thesis yielded two reports: a literature study report and a Master thesis one. The previous literature report already has been handed in in (August 2017). This report, here, forms the global Master thesis report. It is built in 7 chapters containing four major phases: (1) analysis, (2) design and development, (3) results; and (4) discussion and recommendation as described below:

Chapter 1: Introduction

- Research context
- Problem statement
- Research objectives & question

Methodology

Chapter 2: Research methodology - conceptual phase-

- Phase 1: Analysis
- Phase 2: Design methodology and process
- Phase 3: Manufacturing / Development
- Phase 4: Test and Validation

Phase 1: Analysis

Chapter 3: Literature study summary

- Knowledge gap identification
- Design directions description
- Selection of a solution direction

Phase 2: Design and development

Chapter 4: Design and development

- Design overview
- Design iterations
 - Box design
 - Inserts design
- Trade offs
- Manufacturing

Phase 3: Test and Validation

Chapter 5: Test and validation results

- Test
- Validation

Phase 4: Discussion and Recommendations

Chapter 6: Discussion and Recommendations

- Design remarks
 - Box design
 - Inserts design
- Recommendations

Chapter 7: Conclusion

This page is intentionally left blank

2

CHAPTER 2: RESEARCH METHODOLOGY

In this entire chapter the research method followed before and when developing the research solution of the Master thesis is described. This methodology reflects preliminary thinking as well as theoretical and actual steps that the Master thesis followed. The chosen research methodology is separated in four phases: (1) analysis phase, (2) design and manufacturing phase, (3) test and validation phase and (4) discussion and recommendation phase. The global aim of each of those four phases is described in this chapter 2. At the end, all together these phases lay the foundations of this research report, thus each of these phases will be translated and detailed in an appropriate chapter of this report, namely: (Chapter 3: Literature study summary) for the analysis phase, (Chapter 4: Design and Development) for the design and development phase, (Chapter 5 Test and validation results) for the test and validation phase and finally (Chapter 6: Discussion and recommendations) for the discussion and recommendation phase.

2.1 FIRST PHASE: ANALYSIS

This first preliminary phase aims at analysing the context of the research project and defining a precise research solution according to scientific literature and the highlighted gaps found in it. In other words: this phase is the literature review. A complete report of this phase already has been handed in, but a summary will be presented in next chapter (Chapter 3: Literature study summary). During that phase the research context, the research problem and the relevance of the study were first detailed and analysed. A research solution was then proposed; namely the "Design and fabrication of a heterogeneous PET phantom to improve heterogeneity quantification" according to directions suggested in the scientific literature. Lastly, precise limitations of the proposed solution, its requirements and its stakeholders were defined and analysed. Globally after this first analysis phase, all the key elements needed to design and develop our research solution are known, which leads us to the second phase: the design and development phase.

2.2 SECOND PHASE: DESIGN AND DEVELOPMENT

This second phase permits to define the design approach that will be followed during the entire research study: from the preliminary design of the solution to its final prototype. This phase is done directly following the literature review and permitted to draw the global direction of the thesis work (design method) as well as defining and following its specific steps (design process). This phase is therefore separated in two sub-phases: the design methodology sub-phase, described here, and actual design work sub-phase, described in Chapter 4 of this report. For the design methodology described here, a preliminary theoretical method and workflow were defined (cf. §2.2.1). But, both were found to be more complex than planned, and were, second, updated during the thesis (cf. §2.2.2).

2.2.1 Planned design method and process

Among all the different available design methods, a linear design methodology was chosen, which eventually permitted to follow a single design version at a time. The planned methodology was quick and straightforward, as only one design exist and the latest design's version can be updated via a single feedback loop which translates issues or limitation faced by the previous design' version. The processes were organized in a linear way from a preliminary design toward a final prototype (cf. Figure 2) following four consecutive steps: pre-manufacturing analysis, design, manufacturing, and post-manufacturing test and validation.

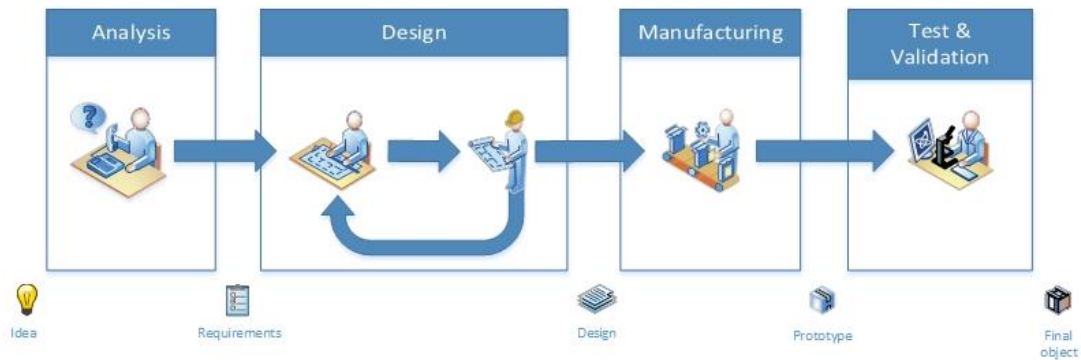


Figure 2 Theoretical design methodology workflow as pre-planned for the Master Thesis
 Four phases following each other in a linear way: analysis, design, manufacturing and test and validation

Inside the design step, a single iterative loop permitted to update the design once at a time. This process has been chosen because it is very cost efficient: the design phase is extremely important, iteration and changes in the design are only made during this phase, this avoids the manufacture of unnecessary parts, it only produces one prototype and test it afterwards.

2.2.2 Real design method and process

In reality, this planned design process was updated during the research study to become more complex in an unpredicted way, leading to the creation of several parallel branches and various feedback loops in the design workflow as presented in another graphic next page (cf. Figure 3). This was mainly due to a lot of limitations and unforeseen events that are summarized in the following paragraphs:

First reason, the manufacturing step has been shown to be at least as complex as the design step compared to what was planned. Iterations and updates of the design were made while manufacturing pieces of the phantom; and limitations due to the available materials, broken pieces, un-fitted parts, directly affected the design phase. This intrinsic relationship between design and manufacturing phases contributed to the creation of a unique phase called "Design and Development" combining those two steps together and leading to a design workflow of three phases instead of four.

Second reason, the previous planned design process was simply linear, permitting to follow only an action at a time. But in reality, the design of the phantom has rapidly been split in three parallel designs:

- the design of the phantom box
- the design of the phantom spherical inserts and
- the design of the cubic inserts.

These three parallel designs were especially convenient during unforeseen events like material delivery delays, machine maintenance, or staff holiday, permitting to switch from one bottlenecked design to another one. Ultimately this permitted to be way more time efficient. Plus, all of those parallel designs needed to be tested and assembled. Therefore three tests phases followed by one assembly step were added in the second workflow within the Design and Development phase.

Third reason, iterations and updates of the different designs were arising from almost all the different steps of the design workflow. Manufacturing pieces, testing pieces, assembling them, led to issues that needed to be taken into account in a new design update. Moreover each separate phantom pieces specifications like their size, shape, material... influenced the design other pieces, thus a lot more feedback /updating loops were added, arising from almost all the processes and object of the workflow.

At the end, analysis, design, manufacturing, and test & validation steps were still existent in the second design workflow but were all complemented with extra tests and assembling phases and with designs updates feedback loop from all along the workflow. This design workflow will precisely be detailed later on in (Chapter 4: Design and Developments).

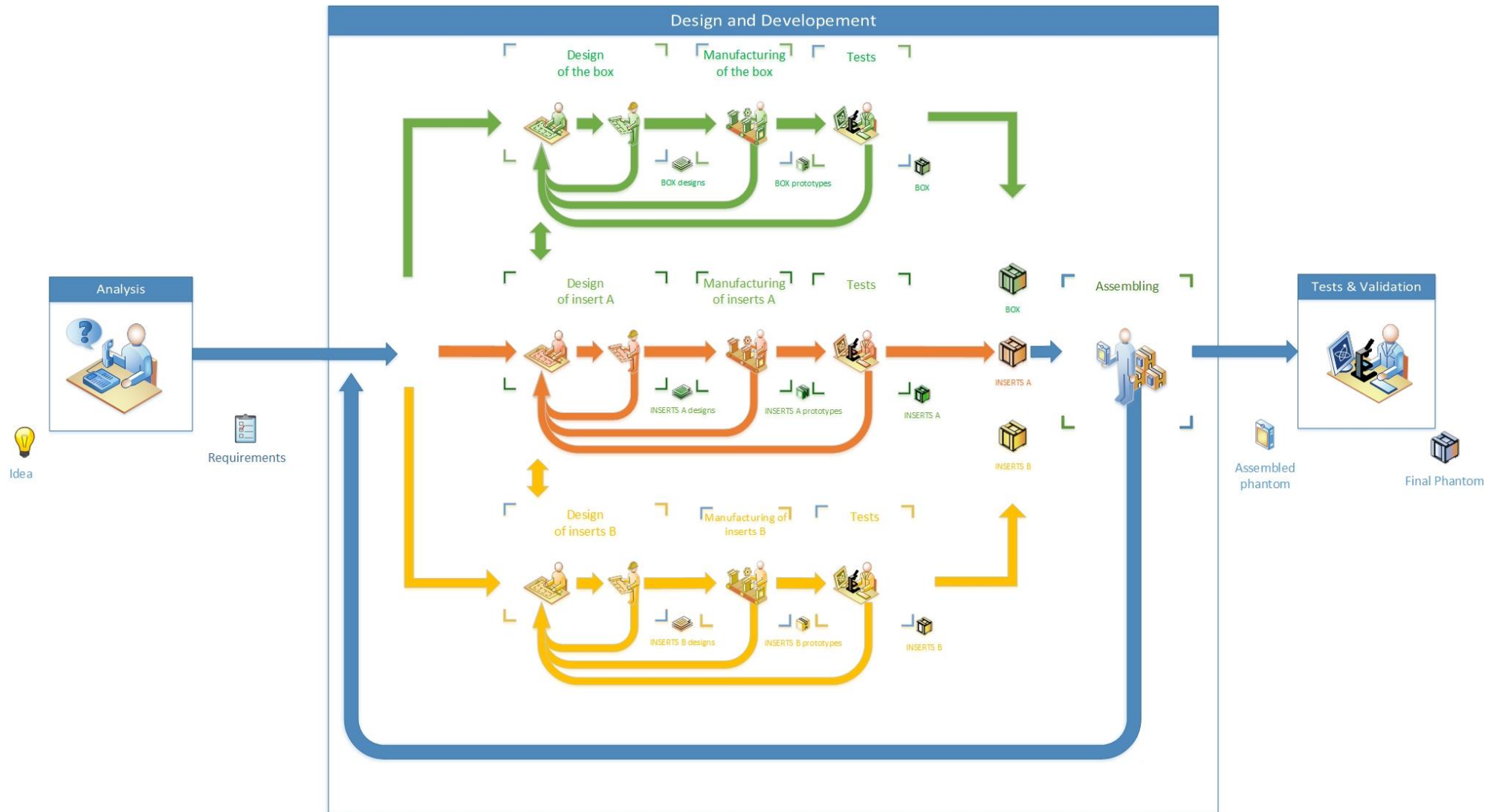


Figure 3 Actual design methodology workflow followed during the Master Thesis

In the previous theoretical workflow, the design was unique and including all the different parts of the phantom. In reality the design was split in three parts: the phantom box and its inserts A (spheres) and B (cubes). The theoretical four steps process (Analysis/Design/Manufacturing/Tests& Verification) has been reformed in a six steps process (Analysis/Design/Manufacturing/Test/Assembling/Test& Validation). In the previous theoretical workflow, only the design step was iterative using an unique feedback loop. Here each design, manufacturing, test and assembly steps also create feedback loops that update the design of each phantom part.

2.3 THIRD PHASE: TEST AND VALIDATION

This step (presented in Chapter 5: Test and validation results) aims at detailing all the results coming from the design, development and validation of the research solution. This phase also acts as a proof of concept of the research solution within a specific experimental setup.

This phase was planned on being one of the main phases of the research leading to a consequent number of results and conclusions. However, the prior design and development phase of the research happened to be more difficult and time consuming than expected. Thus, this phase mainly focussed on testing and validating separately each part of the phantom, and not really focussed on actually using the phantom as a whole in several setups.

2.4 FOURTH PHASE: DISCUSSION AND RECOMMENDATIONS

Last, but not least, phase of the study is the discussion and recommendation phase (described in Chapter 6). Due to the total novelty of the project and the number of faced limitations, there is still a lot of room for improvement. This last phase focusses on giving a list of directions and recommendations for further solution development and also for further uses and applications of the prototype.

At the end, this chapter 2, permitted to properly define the Master thesis research methodology, separated in four phases: (1) analysis phase, (2) design and manufacturing phase, (3) test and validation phase and (4) discussion and recommendation phase; all translated and detailed in an appropriate chapter of this report.

3

CHAPTER 3: LITERATURE STUDY SUMMARY

This chapter quickly presents the literature summary which is relevant to the contextualisation and the understanding of this Master thesis research. The literature report (previously handed in) aimed at answering the after mentioned sub-questions: What are the causes, background and interrelated aspects of the issue with PET heterogeneity quantification and how is it currently described in the literature? What parameters influence PET heterogeneity quantification? In theory, how can we improve tumour heterogeneity quantification in PET images? How will creating a heterogeneous PET phantom help? What is the state of the art in PET phantoms in the market and in development? And what are the limitations faced by PET phantoms?

Therefore, in this summary chapter, PET heterogeneity quantification variability is first detailed, followed by a brief section on how creating a PET heterogeneous solution is beneficial, and another section on the limitations of current and newly developed PET phantoms. The chapter finishes with a list of requirements extracted from all of these remarks. These requirements were already defined in the literature review as a preliminary step to foresee and avoid any already existing design limitations while developing a new PET phantom solution.

For further details please refer to the other literature report.

3.1 PET HETEROGENEITY QUANTIFICATION VARIABILITY

This section summaries the causes, background and interrelated aspects of the issue with PET heterogeneity quantification as described in the literature review. It mainly focused on presenting PET heterogeneity quantification variability causes, with first what influences PET radiotracer uptake distribution and, second, what influences PET heterogeneity quantification. During the literature review, 212 papers have been screened and 54 have been read entirely to understand the limitations of tumour heterogeneity quantification (cf. the PRISMA chart in Appendix 0).

All the influencing parameters found in the literature to affect PET uptake distribution are listed in (Appendix 1) and have been separated in three categories:

- (1) True Biological changes
- (2) Un-wanted biology variability
- (3) Technical variability: from pre-acquisition variability / from acquisition variability / from post-acquisition variability

All the influencing parameters found in the literature to affect PET heterogeneity quantification are all listed in (Appendix 2) and (Table 1). PET heterogeneity quantification was approximated in the literature review to PET texture features quantification (from first to higher order) only. These texture features defined by (Haralick, Shanmugam, and Dinstein 1973; Galloway 1975; Chu, Sehgal, and Greenleaf 1990; Dasarathy and Holder 1991; Sun and Wee 1983; Thibault et al. 2009) have been proved to depends on SUV distribution (Brook and Grigsby 2015) (Hatt et al. 2015). Therefore all the parameters influencing PET uptake previously listed were also considered as influencing PET heterogeneity quantification. Other influencing parameters found to also affect heterogeneity quantification were classified in a fourth category (4):

- (1) True biological changes
- (2) Un-wanted biology variability
- (3) Technical variability: from pre-acquisition variability/ from image acquisition variability / from post-acquisition variability
- (4) Heterogeneity quantification variability itself

At the end, by looking at those four categories, it was easier to understand from where global PET heterogeneity variability can occur. Limiting the impact of each influencing parameters in each category, will permits PET images reproducibility and comparison to be improved. Ideally if the variability arising from (2) un-wanted patient biology, (3.a 3.b 3.c) image pre-acquisition, acquisition, post-acquisition and (4) quantification is reduced, the only change displayed in PET images would be from true patient biological changes (1) which is exactly what PET images are trying to quantify.



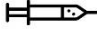

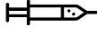


 True biological changes	 Un-wanted biology variability	 Technical variability			 Quantification variability
		 pre-acquisition	 acquisition	 post-acquisition	
Tissue type Biologic heterogeneity ...	Plasma glucose level Insulin level FDG plasma clearance Menstruation Inflammatory processes Breathing activity Colonic /bowel activity Urinary activity Testicular activity Skeletal muscle activity Radiotracer uptake period Patient size/weight/BMI Tumour volume Tumour rotation and deformation motion Uptake heterogeneity (radiotracer distribution) ...	Scanner calibration Dose calibration Net dose given Injection protocol Clocks synchronisation ...	Noise Acquisition mode Acquisition protocol Scanner type ...	Image reconstruction Image correction Normalization ...	ROI segmentation Extraction methods ROI size Discretization Matrix choice Formulae choice ...

Table 1: Influencing parameters of PET uptake and texture features quantification

3.2 HOW A HETEROGENEOUS PET PHANTOM CAN IMPROVE PET HETEROGENEITY QUANTIFICATION?

This section re-explains how PET heterogeneity quantification can be improved by developing a heterogeneous PET phantom. *Phantoms* are physical objects representative of a known ground truth and imitating a clinical situation. They describe non ideal phenomenon like attenuation, scattering, random coincidences and permit to understand tissues' and scanners' characteristics. Their main requirements are the following ones: (1) provide a reliable ground truth (lesion activity concentration, size and location), (2) be realistic, and simulate imaging situations and (3) provide reproducible results. PET phantoms are mainly used to evaluate system performance or validate theories by reproducing a simplistic but realistic clinical environment. Creating a standardized complex ground truth object in the form of a *heterogeneous phantom* will permit to develop a reference standard for heterogeneity quantification definition, quantification protocols, and feature analysis. First, this will permit to only evaluate the variability coming from image acquisition, reconstruction, post-reconstruction and quantification processes, excluding all influences arising from the true biology and physiology changes. Imaging this ground truth object will permit to understand to which extent acquisition, reconstruction and quantification parameters influence PET pixel values and will ensure searchers that the heterogeneous images they are analysing contain the correct complex same values than the complex underlying imaged object. Second, if this complex ground truth object could undergo a heterogeneity quantification analysis. This will permit to compare the texture feature values with a known heterogeneous ground truth; which will help to understand of the link between textural features retrieved from PET images and the underlying biology of complex heterogeneous tumour cells that are imaged and will also permit to assess, compare and approve current texture analysis formulas.

3.3 CURRENT STATE OF THE ART OF PET PHANTOMS

This section, presents a summary of the limitations found in the literature of current and newly developed PET phantoms. Analysing those limitations has been done in order to understand the possible limitations that might be faced during the Master thesis while developing a new PET phantom.




3.3.1 CURRENT LIMITATIONS OF PET PHANTOMS FROM THE MARKET

The most commonly used PET phantoms are: NEMA phantoms (NEMA NU-2 2001 or NEMA NU 2-1994), the Jaszczak SPECT Phantom and Flangeless Deluxe PET and SPECT Phantoms. All of them consist of "hot" fillable spheres and/or "cold" solid inserts made of transparent polymethyl methacrylate (PMMA) placed in a cylindrical fillable compartment. Some non-fillable inserts (made of Teflon, air, foam etc) can also be added to those phantoms to better evaluate the accuracy of PET attenuation and scattering corrections.

As described in (Table 2 Current PET Phantom limitationsTable 2), current PET phantoms have globally the same design limitations when trying to mimic realistic human tissue properties as a ground truth. First, the simplistic shapes, regular geometry and homogeneity of current PET phantoms inserts are not really representative of realistic irregular tumours. Sizes and shapes flexibility of current phantom is still quite limited, with only circular shapes of specific diameters available. Plus, phantoms have glass or plastic walls of 1 to 3 mm thickness that do not contain any radioactivity (*cold walls*) which differs from realistic tumour environments where tumours with a high activity are in direct contact with a lower background activity. Additionally, cold walls of small spheres enhance undesired effects in images like partial volume effects (PVE) and spill-over effects (Phelps 2004). Both of these effects lower the contrast between areas of high activity by underestimating their concentration and spreading their location, leading to inaccuracies on volume and activity estimation especially for small objects (e.g. small spheres or tumours placed inside a high activity background will appear bigger and with less activity) (Berthon et al. 2013).

The same goes for current PET phantoms' uniform homogeneous background chambers. As PET phantoms' background can only be filled with a unique radioactive solution, it too simplistic to represent realistic heterogeneous noisy human tissue background. Adding non fillable insert can permit the creation of more complex background areas with different attenuation coefficients which permit to properly assess the accuracy of PET attenuation and scatter correction, but available phantoms in the market only use unfillable inserts, creating zero activity regions which still not represent well realistic clinical situations.

Table 2 Current PET Phantom limitations

Properties	Inserts					Background	
	Design			Composition		Design	Composition
	Wall-less	Realistic shapes	Flexibility	Heterogen.	Realistic density	Realistic	Heterogen.
 PET-CT Phantom	1-2 mm wall (-)	Spheres (-)	Only 6 insert sizes (-)	Pouring of homogeneous solution (-)	PMMA density is different than tissue density (-)	Simplistic (-)	Pouring of homogeneous solution (-)
 NEMA Phantom	1-2 mm wall (-)	Spheres (-)	Only 6 insert sizes (-)	Pouring of homogeneous solution (-)	PMMA density is different (-)	Simplistic (-)	Pouring of homogeneous solution (-)
 Flangeless Deluxe PET and SPECT Phantom	1-3.2 mm wall (-)	Spheres (-)	Only 6 insert sizes (-)	Pouring of homogeneous solution (-)	PMMA density is different (-)	Simplistic (-)	Pouring of homogeneous solution (-)

Thus, according to the literature and basic observation of the phantoms, the current PET market phantoms used in oncology present several important limitations that we decided to separate in two categories: (1) inserts design and composition limitations and (2) background design and composition limitations.

3.3.2 CURRENT LIMITATIONS OF STATE-OF-THE-ART PET RESEARCH PHANTOMS

A lot of research phantoms have been developed to improve previously mentioned current PET phantom inserts and background design and composition limitations. All of them tried to improve and complicate tumour and background mimicking. Some phantoms contained irregular inserts made of wax, gel or zeolites to avoid the existence of unrealistic "cold-walls" (Turkington, Degrado, and Sampson 2002), (Hamill et al. 2005), (Bazañez-Borgert et al. 2008), (Marie Sydoff Sören Mattsson, Sigrid Leide-Svegborn 2014) , (Carles et al. 2017), (Zito et al. 2012; Soffientini et al. 2017). Though, the use of these new tools brought around new limitations like higher experiment set-up times, toxicity or wastes and lower reproducibility. Other phantoms, tried to use fillable porous materials (DiFilippo et al. 2004), (Hunt, Easton, and Caldwell 2009), (Wollenweber 2014) as a more flexible tool, faster and easier to set-up but, here again, new limitations like material density difference and manufacturing time arose. Finally, realistic phantoms also have been developed to globally represent realistic human shapes as a whole using gel poured in a mould (Skretting et al. 2013), a stack of A4 paper printed with radioactive ink (Holmes, Hoffman, and Kemp 2013), (Markiewicz et al. 2011), (Berthon et al. 2015) or directly using 3D printing (Miller and Hutchins 2007). But, as previously said, these complicate phantom designs still lead to the creation of other restricting limitations like larger manufacturing or set-up times, the creation of disposable phantoms with a lower reproducibility.

Thus, trying to overcome current PET market phantoms limitations leads to the creation of other limitations that we decide to classify in a category named "experimentation" which include low set-up time, low repeatability, difficult standardization, toxicity and waste. Table 4 summarize the trade-offs made by state-of-the-art research phantoms between all of those design limitations¹.

3.4 EVALUATION OF A PHANTOM QUALITY

This section focuses on describing the measures that can be used to evaluate a phantom quality and summarize previous sections in a way that permits to gain knowledges on commonly and already made trade-offs in order to better understand the customary dynamic of phantom design and development.

Phantoms need to provide a reliable ground truth (lesion activity concentration, size and location), to be realistic and to simulate imaging situations as well as to provide reproducible results. From the literature study, and by analysing current phantom limitations and state of the art, a list of ideal PET phantoms characteristics has been defined (in Table 3). During this Master thesis, when developing our solution, limitations from Table 4 and requirements from Table 3 will always be kept in mind and whenever a trade-off will be needed, the taken decision will be select by trying to fulfil at best those requirements

Table 3 Ideal PET phantoms requirements

Category	Requirement
Tumour design	Wall-less Realistic shape Flexible in size and in shape
Tumour composition	Heterogeneous activity Heterogeneous density
Background design	Realistic shape
Background composition	Heterogeneous activity Heterogeneous density
Handling	Low set-up time Repeatability Standardisable Non toxicity No wastes

¹ Last remark: most of the analysed state-of-the-art PET phantoms in this literature review were not made for PET heterogeneity quantification. However, design ideas from these phantoms can still be used to build one for PET heterogeneity quantification that already overcome most of previously mentioned limitations.

Table 4 Summary of advantages and disadvantages of cutting-edge PET phantoms
 +: the design contains this advantage, -: it does not contain it, -/+: it does contain it but only to a certain extent

Properties		Tumour					Background		Experimentation					
		Design			Composition		Design	Composition	Low set up time	Repeatability	Standardisable	Nontoxicity	No wastes	
		Wall-less	Realistic shapes	Flexibility	Heterogen.	Realistic density	Realistic	Heterogen.						
NEMA Phantom		-	-	-	-	-	-	-	+	+	+	+	+	
Inserts	Irregular plastic spheres	+	+	-	-	-	-	-	+	+	+	+	+	
	Moulded wall less	18F wax	+	-	-	-	-	-	-	-	-	-	-	-
		18F Gelatine	+	-	-	-	-	-	-	-	+	+	+	-
		68Ge silicone	+	-	-	-	-	-	-	+	+	+	+	+
		18F alginate	+	+	+	+	-	-	-	-	-	-	+	-
	Solid zeolites	+	+	-	-	-/+	-	-/+	-	+	-	+	+	
Fillable	Handmade fillable porous	+	-/+	+	+	+	-/+	+	+	+	+	+	+	
	3D printed fillable porous	+	-/+	+	+	+	-/+	+	+	+	+	+	+	
	Polyhedrons	+	-	+	-	-	+	+	-	-	-/+	+	+	
Realistic	Fillable Hoffman	-	+	-	-	-	-	-	+	+	+	+	+	
	Fillable gel phantom	-	+	-	-	+	-	-	+	+	+	+	-	
	2D radioactive inkjet	+	+	+	+	-	+	+	-	+	+	+	-	
	3D printed organs+inserts	-	-/+	+	-	-	+	-	+	+	+	+	-	
	3D radioactive organs	+	+	+	-	+	-	-	-	+	+	+	-	

3.5 LITERATURE REVIEW CONCLUSION

First, it has been found that PET heterogeneity quantification is mainly limited by its non-robustness and variability. This variability is dependent on both biological changes (true biological events or unwanted biological events), and on technical changes (pre-acquisition preparation, acquisition, and post-acquisition and/or quantification methods). This is explained by the fact that heterogeneity values are extracted following non robust methods that are biologically and technically dependent.

Second, to improve PET heterogeneity quantification, robust standardized acquisition and extraction methods need to be defined so variability arising from true biology changes can be separated from variability arising from technical changes. Once patient preparation, acquisition, reconstruction and quantification processes are set to only produce robust, un-variable heterogeneity values, unwanted biology changes and technical variability will be reduced. Thus, both the medical community and researchers will be sure that PET images they are looking at are only influenced by underlying biology changes and therefore heterogeneity quantification those changes will be relevant. Thanks to the literature review an idea of the solution needed to reach this situation has been found: complex enough heterogeneous phantoms from which heterogeneity values can be extracted will permit to fix the underlying biology to a known truth. By fixing this biology, the influence of biological changes in PET heterogeneity quantification is also fixed, and only changes arising from technical variability are present in the extracted images. This stationary ground-truth object can, in the first place, permit to improve PET images quality by finding all technical settings that influence heterogeneity quantification and suppressing them; and later on, it can also permit to develop user-friendly standardized protocols by evaluating and comparing textures features values to only keep robust and meaningful ones.

Third, to be sure of the feasibility of the project, the literature study also focussed on analysing state-of-the-art PET phantoms to list all their limitations, classified as inserts design and composition limitations, background design and composition limitations or experimentation limitations. Remark was made that trade-offs almost always needs to be made between simple unrealistic design and more complex but realistic ones.

Last, the literature review provided a list of global PET phantom requirements that need to be fulfilled and that can be used as a base to develop a new object.

For further details please refer to the other literature report.

4

CHAPTER 4: DESIGN AND DEVELOPMENTS

In this fourth chapter, the entire Master thesis “Design and Development” phase is detailed. First a global design overview is given to help the reader understand the limited design scope and requirements followed during the Master thesis. This overview also details the different parts names and characteristics of the designed phantom, permitting the reader to already have a good idea of the designed solution before entering in the details of its development. Following this overview a thorough description of the phantom design phase is given, from the preliminary version (V.0) to the last update of it. As the design has been separated in three sub-designs, this description is also separated in this report in three different sections: first, the design of a phantom box and its separated chambers (§4.2. Phantom box design) followed by, second, the design of fillable spherical inserts (§4.3.3. Phantom spherical inserts) and, third, the design of fillable cubical inserts (§4.3.4. Phantom cubical inserts). This fourth chapter ends with a list of the current design global limitations and introduces the next fifth chapter (Chapter 5: Test and validation results) which will focus on analysing all the tests results done during the “Design and Development” phase of the Master thesis.

4.1 GLOBAL PHANTOM DESIGN OVERVIEW: BOX+ INSERTS

4.1.1 GLOBAL PHANTOM DESIGN REQUIREMENTS

As stated in (§1.3.1. Research objectives, p.4 of this report), the main goal of this Master thesis is to improve the heterogeneity quantification in PET images by developing a heterogeneous PET phantom and following must-have requirements. Considering the limited time frame of the Master thesis the precise list of requirements extracted from the previous literature study needed to be restricted to our Master thesis scope. Therefore the requirements listed in (Table 3) were updated in a (Table 5, cf. next page). Some requirements being better detailed, whereas others were removed in order to re-focus the research study into something doable in 8 months.

In the end, due to the limited allocated time for the Master thesis and due to the novelty of the project, a focus was set on the development of, first, a simple version of a working PET phantom box containing inserts with complex shapes that can be easily designed, updated, manufactured and connected to each other. Thus, requirements regarding the heterogeneous density of the inserts and the realistic shapes of the background were not considered here as they would both lead to an increasingly complex design if taken into account now. However those aspects can still be taken into account in a later –and more complex- design of the phantom (cf. Chapter 6: Recommendations).

Research scope:	The development of a working PET phantom box containing inserts with complex shapes that can be easily designed, updated, manufactured and connected to each other.	
Category	Ideal requirements	Guidelines and solution requirements
Tumour design	Realistic inserts shape Flexible in size & shape Wall-less inserts	Complex inserts' design formed via 3D printed inter-changeable plates Each plate should be easily interchangeable with a modular design Wall thickness of the phantom insert as thin as possible (~1mm)
Tumour composition	Heterogeneous activity	Different fillable phantom segments containing inserts with different radioactivity
Background design	Realistic shape	<i>Out of the Master thesis scope</i>
Background composition	Heterogeneous activity Heterogeneous density	Different fillable phantom segments with different radioactivity <i>Out of the Master thesis scope</i>
Handling	Low set-up time Repeatability Standardisable Non toxicity No wastes	Easy to use. Fast and easy filling Solid fillable inserts. Re-usable. Not deformable 3D printings of inserts using CAD shared files Follow radiation safety measures Watertight (no leaks) Limiting user time exposure Should resist several uses Good impact resistance (not easily breakable)
Added requirement	Miscellaneous	Completely transparent to visually check for air bubbles Smooth surface to avoid any air bubble formation Should fit within the NEMA body PET phantom ² : 1 Top extrusion: cylinder of 50 mm diameter by 5 mm height 2 Bottom extrusion: cylinder of 50 mm diameter by 3 mm height 3 A total phantom height of 202 mm (including the extrusions)

Table 5 Research scope, requirement and guidelines for this Master Thesis' phantom design

² All the NEMA body PET phantom dimensions were retrieved from the literature or measured in the available NEMA phantom in the LUMC and are detailed in (Appendix 3: NEMA Body Phantom specific dimensions and requirements). A 3D representation of the NEMA phantom was created as a reference in Inventor®

4.1.2 GLOBAL PHANTOM DESIGN DESCRIPTION

Once the precise research solution scope and requirements were set, a global idea of the PET phantom design emerged and evolved. In this sub-section, the global design idea -from which the Master thesis started- and the final design idea -from which the Master thesis stopped- are detailed in order to familiarize the reader with the name and purpose of each pieces composing the designed PET phantom.

The phantom was first defined as fillable cylindrical box fitting inside the NEMA body PET phantom and containing several separated fillable *segments* (also called *chambers*). The adjoining walls of these chambers (called *plates* or *inserts*) have been designed to be modular, 3D printed and able to be shaped in complex interconnected profiles. (Figure 4) gives a global idea of how the phantom was planning on looking like at the beginning of the Master thesis.

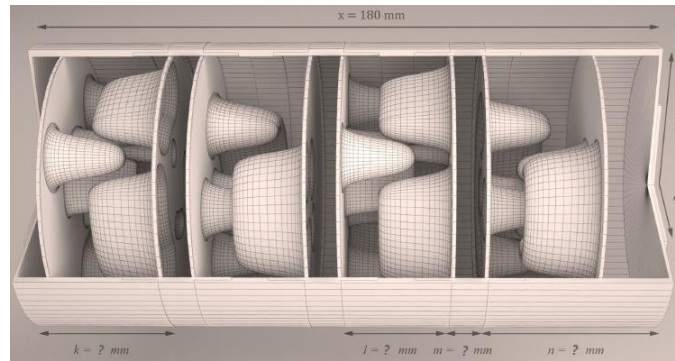


Figure 4 Global overview of the preliminary PET phantom design idea
Cylindrical phantom box made of different segments and separated by several 3D printed inserts-plates forming complex heterogeneous shapes and all fillable with different radioactivity concentration. General dimensions like the cylinder radius r , or each segment number or heights l , k , n and m are not fixed yet when the Master thesis started. Only the global height of the structure was fixed to fit in the NEMA body PET phantom.

During the Master thesis, the global design of the phantom has been separated in several sub-designs: the design of (1) the phantom cylindrical box and (2) the design of its inserts-plates. During the designing of its plates, several ideas of shapes have been developed and the plates design split in two main directions: (2.a) the design of spherical inserts and (2.b) the design of cubical inserts. (Figure 5) represents the global design from which the Master thesis ended and (Figure 6) present the vocabulary of each designed part.

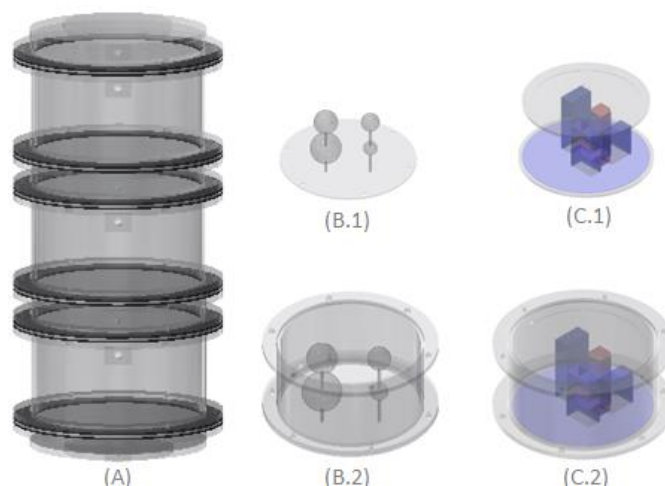


Figure 5 Global overview of the latest PET phantom box design and its inserts
PET phantom cylindrical box (left) composed of a pilling of seven different segments with fixed dimensions. (B-1) represents a spherical inserts plate as designed in the thesis containing four fillable spheres. (B-2) is the assembly of the spherical insert plate with one of the imaging PET phantom segments. (C-1) represents a cubical insert plate containing a stack of cubes (fillable with three different radioactivity solutions) and (C-2) is the assembly the cubical insert plate with one of the imaging PET phantom segments.

Top // – Image – // Fill // – Image // – Fill // – Image – // Bottom

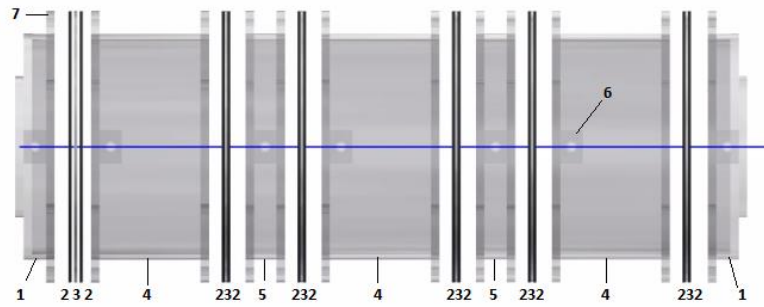


Figure 6 Exploded view of the latest PET phantom design

(1) *Top and bottom caps* which fit in the NEMA body PET phantom and are also considered as *filling segments* for nearby inserts, i.e. considered as segment from which inserts are filled. (2) *Rubber gaskets* are sealing rubber rings placed at the junction of each segment and plate, they are held together by the pressure applied from neighbouring *flanges* (7). Flanges are the locking rings glued around each segment which possess six screw holes to tight and assemble each segment to another. (3) *Insert plates* are the plates where heterogeneous inserts are attached to. (4) *Imaging segments* or *imaging chambers* are the biggest segments where inserts protrude and from where PET images will be acquired. These segments are fillable with background radioactivity concentration directly via a hole at their surface. (5) *In between segments* or *filling chambers* are the small segments from which inserts are filled with different radioactivity concentrations. Finally (6) *filling cubes*, are the small pierced cubes from where each segment is filled and closed using a M3 screw (screws of 3mm dia).

During the Master thesis, the phantom box design spread from 0 to 9 different versions. The phantom spherical inserts design spread from 1 to 7 versions. And the phantom cubical inserts spread from 1 to 3.7 versions. Each design version is named "V.X" and can be derived in a sub-version called "V.X.Y" where "Y" represents a small change in the designed version "X".

4.2 PHANTOM BOX DESIGN

Now that the reader is familiar with each pieces of the phantom, the process of the design of each of these pieces will be presented here, starting with the design of the phantom outside box. Therefore, in this section the entire phantom box design process is described. This section first starts with a general overview of the phantom box designs in (Figure 7). Followed by a description of each version of the phantom box details, advantages, drawbacks and trade-offs; one version per paragraph of this section. This section finally ends with a small conclusion regarding the phantom box design and where the study stopped.

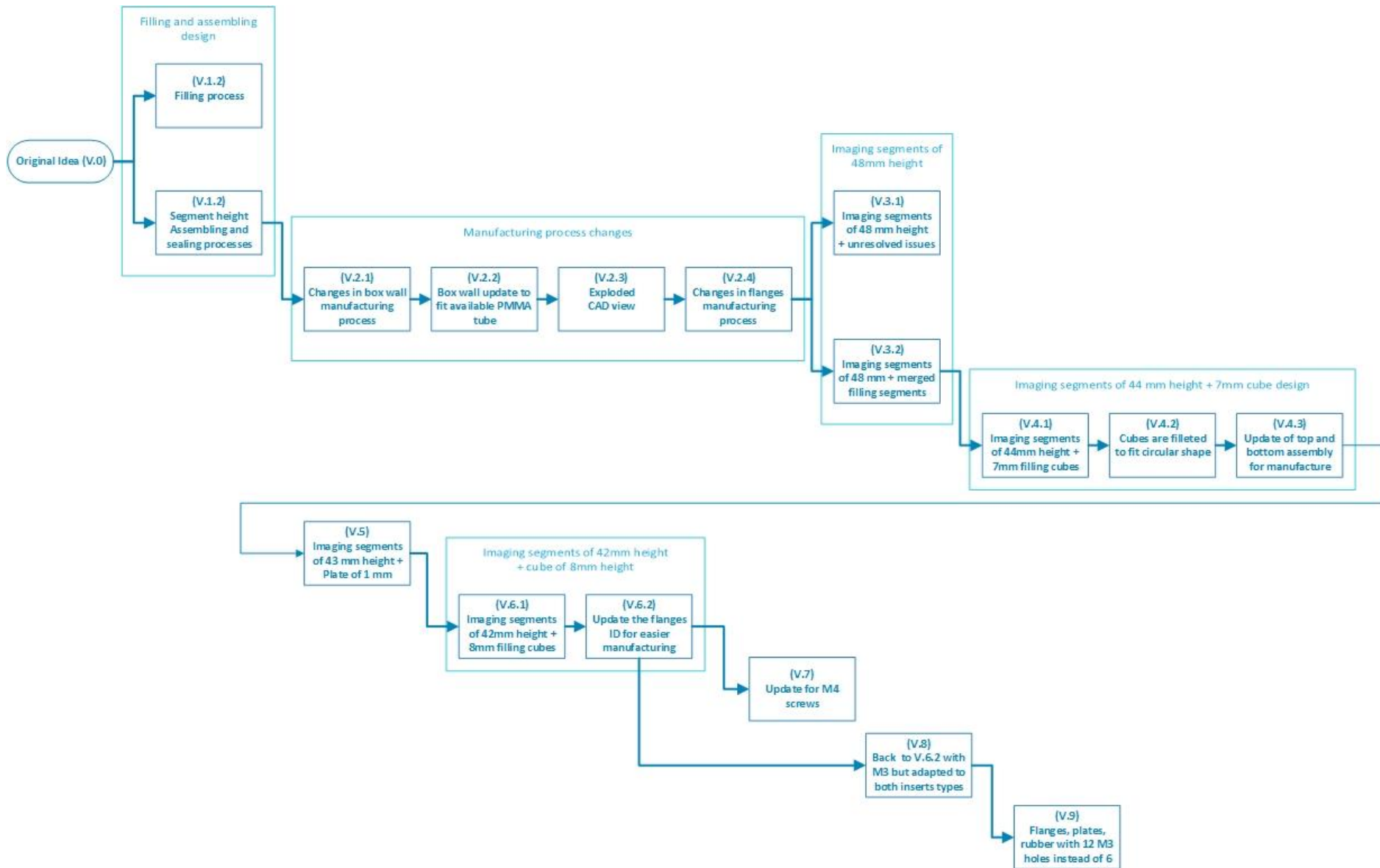


Figure 7 General overview of each design version of the phantom box

4.2.1 PHANTOM BOX PRELIMINARY DESIGN (V.0)

The Master thesis started based on the preliminary work of Willem Grootjans (LUMC), Dennis Schaart (TU Delft) and Ernst van der Wal (DEMO group at TU Delft). Some design ideas were drafted in a version named version zero (V.0). This preliminary version gave the general wished direction of the PET phantom solution.

Design: Phantom Box (V.0) characteristics:

Version zero (V.0) of the phantom box was composed of several cylindrical segments (respectively designated A, B, and C). Segments A representing the top and bottom parts of the phantom. Segments B, the longest ones, forming the imaging segments from where images would be extracted. And segments C being the in-between segments from where the phantom would be filled with radioactive solution. These segments stacked all together formed the cylindrical PET phantom. The stacking of all the segments was designed to fit in the already existing NEMA body PET phantom (cf. Appendix 3 for a summary of the NEMA dimensions retrieved and used during this Master thesis). Only segments A and C were supposed to contain filling holes (called *access ports*): four in total per segment, on either side, rotated by 90 degrees; through which a radioactive solution could be provided to the inner compartments of the phantom. The filling holes functioned in pairs, where one port was planned to be used for filling a specific compartment of the phantom while the other opposite one used for de-airing the same compartment. Since the presence of the ports can cause scattering of emitted photons (due to the presence of additional material), the ports should be placed as far as possible from the imaging segment of the phantom (i.e. as far as possible of the segments B). Therefore, in the design (V.0), the ports were only placed on the A and C segments and the filling of the adjacent B segments was accomplished by using an internal routing configuration (named *corridors*) coming from segment A or C and discharging in segment B.

Characteristics of the phantom box preliminary idea (V.0):

- Entirely 3D printed using the precise additive manufacturing technique of stereolithography
- Assembling process based on interference fit
- Four filling/de-airing holes per segments for segment A and C (two filling / two de-airing)
- No filling holes for the imaging segments B
- Filling corridors running along the imaging segment B
- Thin ring of rubber to seal the junction of the segments

A SLA printing of (V.0) in a smaller scale using SLA Envisiontec printer and made of the photopolymer R05 was performed (cf. Figure 8 and Figure 9). As no attaching process was defined yet between the plates and the segment in this preliminary version zero, the insert plates were printed attached to the imaging segments. From this printing the following remarks were made: Only one semi-opaque R05 material is available for SLA printing and it seems still too opaque for our PET phantom purpose. SLA printing technique is convenient, precise but still faces some limitation when printing flat surfaces. The filling-corridors as designed in this version are too thick when running along the imaging segment B. The corridor material quantity present in the imaging segment is too large compared to the inserts.

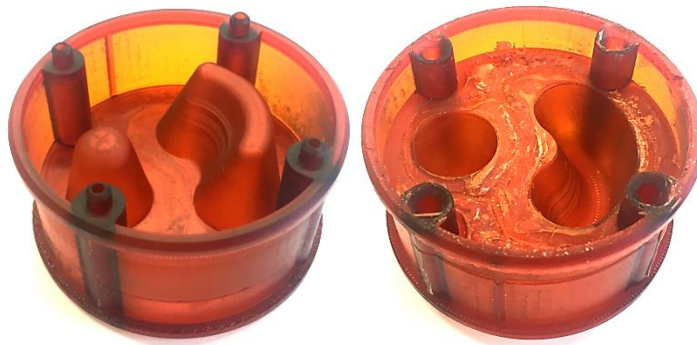


Figure 8 Top and bottom views of the SLA printing of a miniaturized version of the phantom box (V.0) Wall thickness of 1mm. Top view (right) the inside shapes and filling corridors are well defined. Bottom view (left) the flat surface of the inside plate is not well printed



Figure 9 Lateral view of the SLA printing of a miniaturized version 0 of the phantom box (V.0)
Even if a thin wall thickness (1mm) the printed material is too opaque for the phantom imaging segments.

Limitation of version (V.0):

- × No precise number of segment defined yet
- × No precise assembling process defined yet
- × No precise insert plate shape and attachment defined yet
- × The already defined filling process using corridors running along the imaging segment should be improved (corridors too thick)
- × No precise closing system of the filling-holes defined yet
- × Manufacturing of the phantom using SLA and R05 material seems not transparent enough

Questions that need to be answered by next version of the phantom:

- How many segments per phantom should be designed?
- How these segments will be stacked together?
- How the phantom plate will be attached to the phantom box?
- How improving the already existing filling system?
- How closing the filling holes?
- How manufacture a transparent enough phantom chamber?

4.2.2 PHANTOM BOX DESIGN (V.1.1 & V.1.2)

Designs (V.1.1 and V.1.2) are described together in this paragraph as no major design evolutions occurred between those two designs. They both focussed on well defining the number of needed segments as well as their height, their filling and their assembling processes.

First, the number and height of each segment were defined given the fact that the total height of the PET phantom needs to fit in the NEMA body PET phantom box (202mm height) and that each imaging segment B needs to be as tall as possible to produce large field of views. As the total length of the phantom is fixed by the NEMA body phantom inside height, the following trade-off appears: increasing the number of imaging segment B automatically results in a substantial decrease in their height and therefore in a decrease of the imaging field of view. Therefore a compromise needed to be made between the number of segments and their height. Two segments of 10mm for segments A, two segments of 10mm C and three segments of 45mm for imaging segment B were thus designed. (Remark: $2 \times 10 + 2 \times 10 + 3 \times 45 = 175\text{mm}$ and $175\text{mm} < 202\text{mm}$, because inserts plates and sealing rubber rings sandwiched between each segment will add some millimetres more to the global assembled structure).

Second, the filling process of each of these segments was refined. Due to the extra material thickness of the corridor running along the imaging segments B and its photons scattering property; it has been decided to not use this filling process anymore. Instead each segment was designed to be filled directly by a single hole at its surface. These 2mm holes will be reinforced with a small cubic extrusion at the surface of the segment, the cube extrusion was thick enough to allow nylon screws of 2mm diameter (M2 screws) to be tight in it and to close the holes. As imaging segments are now directly filled via a small 2mm hole through their wall, thick corridors are not compulsory anymore. Plus, by using a syringe thin enough to pour liquid in the segment while letting air escape via the same hole, only one hole is needed to fill each segment instead of the two filling/draining holes previously designed.

Last, in the previous version (V.0) not proper assembling process was detailed; thus, in these (V.1.1 and V.1.2) versions an assembling process of the different PET phantom segments altogether was defined. Locking rings –*flanges*– were designed to be attached at the extremities of each segment. Each flange is pierced on both side with six 2mm holes and can be screwed to another flange using long plastic screws of 2mm diameter (M2 screws). At the interface of two segments, in between their two flanges, a rubber ring, followed by a shaped insert plate and another rubber ring can be sandwiched. This “flange-rubber-plate-rubber-flange” stack permits to seal the junction between each segment as well as the addition of shaped plates in-between each segment.

Questions answered by this design (V.1)

- How many segments per phantom should be designed?
 - Seven segments:
 - Three of 45mm height for segment B
 - and two and two 10mm for segments A and C
- How these segments will be stacked together?
 - Extra rings (flanges) running along each segment and screwed together using M2 screws
- How the phantom plate will be attached to the phantom box?
 - Sandwiched in between each segment and rubber gaskets
- How improving the already existing filling system?
 - One filling hole per segment, no corridors
- How closing the filling holes?
 - Holes are closed using cube extrusions and M2 screws
- How manufacture a transparent enough phantom chamber?
 - Not answered

Limitation of version (V.1):

- × Manufacturing of the phantom using SLA and R05 material seems not transparent enough

Questions that need to be answered by next version of the phantom (V.2)

- How manufacture a transparent enough phantom chamber?

4.2.3 PHANTOM BOX DESIGN (V.2.1, V.2.2, V.2.3 & V.2.4)

Phantom box designs (V.2.1, V.2.2, V.2.3 and V.2.4) have been created all together in order to answer the remaining question "How manufacture a transparent enough phantom chamber?".

First, design version (V.2.1) was produced to define a proper manufacturing process of the designed PET phantom. In Design (V.2.1) the walls of the different phantom segments are made of 78mm inside diameter (ID) and 80mm outside diameter (OD) (i.e. 78/80mm ID/OD) tubes made of Poly(methyl methacrylate) (PMMA), also known as Perspex® or Plexiglas®, from Vink® (as shown in Figure 10). In this same design (V.2.1), other PMMA tubes of 80/90mm ID/OD are used for the flanges (aslo shown in Figure 10). Top and bottom ceiling and covering caps were cut from PMMA sheets of 5 and 3 mm thick (from Snijlab®).

Poly(methyl methacrylate) (PMMA) material was chosen here for its resistant properties (cf. Table 6) and its general availability. Existing PET phantom in the market such as the PET-CT Phantom, or the NEMA body PET phantom are also made of PMMA which prove the compatibility of this material for the development of a PET phantom.



Figure 10 PMMA tube and flanges assembly (extracted view from Inventor®)

Table 6 General properties of PMMA (Ide-mat 2003)

Name	Poly(methyl methacrylate) (PMMA)
Sector of use	Almost all: transport, medical, implant, art...
Supplier	Vink® and Snijlab®
Physical state	Solid and resistant
Colour	Cristal clear
Odour	No odour or sulfur-like
Initial boiling point range	High: 200°
Flash point	High: >250°
Vapour pressure	29.25 mm Hg (at 20°)
Density	1,170-1,200 g/cm ³ (at 25°)

However after some researches, it appears that no tubes with such diameter (80mm ID) were available for order with only a thickness of 1 mm (only 2mm, 4mm, 6mm or 10mm thick). Thus, a second trade-off needed to be made between: available PMMA tubes size of 80mm diameter and tube thickness. To solve this issue several solutions were possible:

- the manufacturing process can be changed again (no cut from already existing tubes),
- the manufacturing process can be kept but the material can be changed again, (from 80mm diameter tubes but not from tubes in PMMA)
- the manufacturing process and material can be kept but the size of the material and the imaging segment can be reduced, (from tubes in PMMA but with a smaller ID than 80mm)
- the manufacturing process, material, and size can be kept (the PMMA tube of 80mm ID will be eroded to reach 1mm thickness) but its transparency will be reduced to a milky appearance.

A second design (V.2.2) permitted to find an acceptable compromise for this issue. The manufacturing process and PMMA material were kept but the size of the tube was updated to a thicker one (2mm thick instead of 1mm with the available tube of 76/80mm ID/OD). This tube, available for order via Vink® website, is a little too thick but is not smaller so the imaging segments stay large enough for proper image acquisitions, and does not necessitate extra manufacturing processes so does not affect the transparency of the PET phantom imaging segment.

In parallel of the definition of a manufacturing process for the phantom segments, a manufacturing process of the sealing gasket was designed: the gaskets will be directly laser cut from Nitrile butadiene rubber (NBR) sheet (as shown in Figure 11).. NBR is also called Nitrile rubber, or known as Bu-na-N, Perbunan, or acrylonitrile butadiene rubber (general properties of NBR as fund in Table 7).

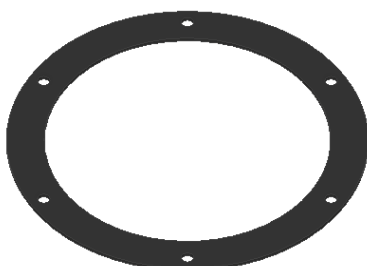


Figure 11 Rubber gasket (extracted view from Inventor®)

Name	Nitrile Rubber (NBR, Acrylonitrile-Butadiene Rubber)
Sector of use	Almost all: construction, industry...
Physical state	Elastic solid
Colour	Light yellow to black, (here black)
Odour	Mid aromatic, rubber like
Flash point	224.8-350°C
Density	0.95-1, 65 g/cm ³ , depends on the rubber type

Table 7 General properties of NBR (Matweb 2017)

Then, once the global phantom manufacturing processed ideas and materials were clarified, a third exploded design (V.2.3) of the phantom box was produced (cf. Figure 12). This design permitted to seize the interconnections and requirement of each separated phantom box part that needed to be produced, ordered and assembled together. Proper list of the needed materials, their quantity and supplier were extracted from this design (as detailed in (Table 8)).

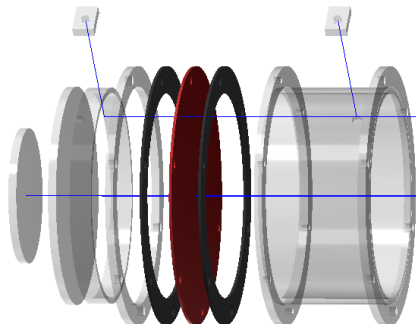


Figure 12 Exploded view of the top part of the phantom box (V.2.3)

(from left to right): top cap; top ceiling; filling (or in-between) segment; flanges; rubber gasket (black); insert plate (red); rubber gasket (black). Un-exploded imaging segment composed of two flanges and a tube is visible on the right

Table 8 Parts list of box design (V.2.3)

Quantity	Part Name	Manufacturing process
1	Top_cap	PMMA sheet 5mmthick
1	Bottom_cap	PMMA sheet 3mmthick
2	Top_Bottom_ceiling	PMMA sheet 3mmthick
3	Imaging_segment_wall	PMMA tube 76/80mmID/OD x 45mm height
4	Inbetween_segment_wall	PMMA tube 76/80mmID/OD x10 mm height
6	Insert-plate	(to be defined in §4.3 & 4.4)
12	Flange	PMMA tubes 80/90mmID/OD x 3mm height
12	Rubber gasket	NBR sheet 1mmthick
7	Filling_cube	PMMA sheet 7mm thick
36+7	M2 assembling and closing screws	Buy M2 nylon screws

A last update (V.2.4) of the design was created when enlarging the flanges from 80/90mm ID/OD to 80/96mm ID/OD. In the previous version (V.2.3) the flanges were supposed to be cut off from a 80/90mm tube. Yet the width of these flanges (5mm width) soon appeared to be too small to host screws holes. Consequently, flanges were designed larger (80/96mm ID/OD) and laser cut from a PMMA sheet of 3mm thick (cf. Table 9 update) as no PMMA tubes were available for the new flanges dimensions. These newly designed larger flanges of 8 mm width permitted to uses bigger and more resistant nylon M3 screws instead of the M2 screws used in previous designs.

Table 9 Parts list of box design (V.2.4)

Quantity	Part Name	Manufacturing process
1	Top_cap	PMMA sheet 5mmthick
1	Bottom_cap	PMMA sheet 3mmthick
2	Top_Bottom_ceiling	PMMA sheet 3mmthick
3	Imaging_segment_wall	PMMA tube 76/80mmID/OD x 45mm height
4	Inbetween_segment_wall	PMMA tube 76/80mmID/OD x10 mm height
6	Insert-plate	(to be defined in §4.3 & 4.4)
12	Flange	PMMA tubes 80/90mmID/OD x 3mm height PMMA sheet 3mm thick
12	Rubber gasket	NBR sheet 1mmthick
7	Filling_cube	PMMA sheet 7mm thick
36+7	M2 assembling and closing screws	Buy M2 nylon screws
36	M2 closing screws	Buy M3 nylon screws
7	M3 assembling screws	Buy M2 nylon screws

Limitation of version (V.2.4):

- × Thicker tubes composing segment walls (2mm instead of 1mm thick)
- × Larger flanges (8mm thick instead of 5mm thick) to host M3 screw hole
- × Larger but stringer M3 screws instead of M2 screws

The phantom box design version 2 (V.2) finishes with this small sub-design (V.2.4) and does not contain major unresolved issues or question that still need to be answered. Next design (V.3) is therefore focussed on enhance the phantom box design and push its limits.

4.2.4 PHANTOM BOX DESIGN (V.3.1 & V3.2)

Phantom box designs (V.3.1 and V.3.2) have been created all together in order improve the latest phantom box design (V.2.4). They do not answer to a specific issue but mainly focussed on improving the existing design by increasing the imaging segment height while still keeping a global height of the phantom of less than 202 mm so it still fits in the NEMA body box.

The different designs were produced with an imaging segment height of 48mm instead of 45mm as shown in (Figure 13) and (Figure 14).

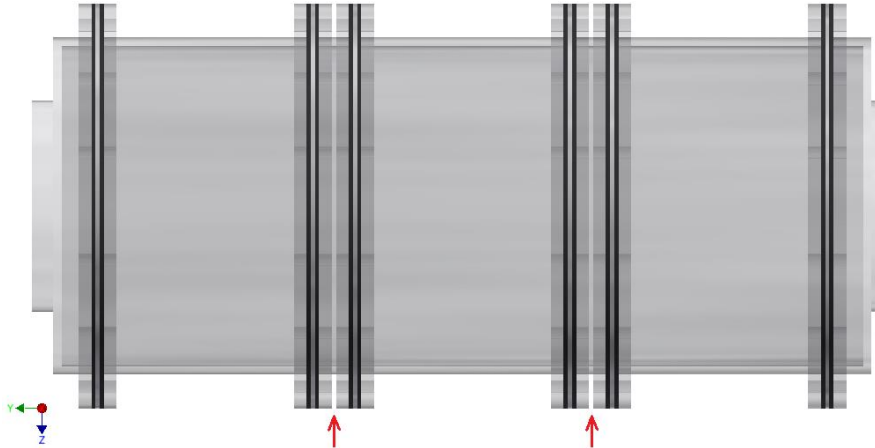


Figure 13 Side 3D view of phantom box design (V.3.1)

The increase of imaging segment from 45mm thick to 48 mm in the design (V.3.1) compressed the in-between segments so much that the space left to screw the flanges together was almost reduced to nothing (see red arrows in (Figure 13)). Design (V.3.2) merged these nearby flanges together in a thick locking ring that also served as a filling segment (cf. red arrows in (Figure 14)). However this design required elongated M3 screws of at least 20mm long to assemble the flanges together and was also composed of a lot of additional inert material near the imaging segments which as we said, could cause scattering effects in PET images. Therefore this (V.3.2) design was not ideal.

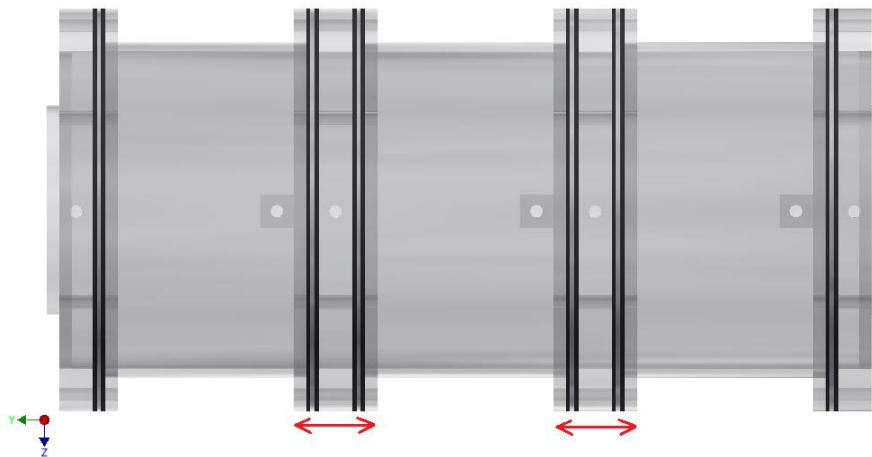


Figure 14 Side 3D view of phantom box design (V.3.2)

Limitation of version (V.3):

- × Filling segments are too small in (V.3.1)
- × Removing imaging segments in (V.3.2) forces the use of long and thin M3.20 screws
- × M3.20 screws are long to screw, easily breakable, less ideal than M.3.8 screws

Both designs (V.3.1 and 3.2) were inconclusive and comfort the idea that an imaging segment height of more than 45mm is difficult to design without creating other compromises on other PET phantom box parts. Thus, the design V.3 aborted and following update of the phantom box stemmed from box design V.2 instead of design V.3.

4.2.5 PHANTOM BOX DESIGN (V.4.1, V.4.2 & V.4.3)

Starting back from design version (V.2.4), the phantom box designs (V.4.1, V.4.2 and V.4.3) have been created all together in order ameliorate some details of the previous design toward a properly buildable phantom box.

First, imaging segments size was set back to 44 mm height, for 7.5mm for top/bottom filling chambers height and 13mm for in-between filling chamber height in (V.4.1). Once done, filling cubes that permit the filling and closing of each segment were adapted to each new segment height: i.e. cubes were designed to have the following dimensions: 7x7.5x3mm for the top and bottom filling segments and 7x7x3mm for the rest of the segments.

Second, in design (V.4.2) the back surface of the filling cubes was filleted to better fit the cylindrical surface of the segments they are glued to (as shown in Figure 15). Moreover, in this (V.4.2) design, each M3 hole size was also adapted to either be 2.7mm diameter if the hole needs to host a M3 thread or to be 3.4mm diameter if not. And same goes for M2 hole size which was either updated to 1.7mm or 2.4mm diameter.

Third and last, top and bottom closing cap were slightly expended in a versions (V.4.3) for an easier gluing of them on the tubes.

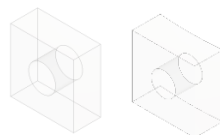


Figure 15 Filling cube from (V.4.1) (left) and filleted filling cube from (V.4.2) (right)
The back surface of the right filling cube (V.4.2) is not totally straight is slightly curved

Limitation of version (V.4):

- × None yet
- × But limitation from the parallel design the insert plates forces the segment height to be updated in a version (V.5)

4.2.6 PHANTOM BOX DESIGN (V.5)

All of these small previous updates (V.4.1, V.4.2 and V.4.3) drove the PET phantom box design closer its prototype construction. However, as the reader probably recall, the phantom box design was done in parallel of two other designs: the phantom cubical and spherical insert plates designs. Some limitations arose from the designs of the phantom inserts design which (at that time) were done in parallel. In turn, limitations arising from the SLA printing technique forced the insert plate thickness to be increased from 0.5mm to 1mm thick and thus forced the phantom box design to be updated in a version (V.5).

Indeed, the PET phantom box is designed as a stack of cylindrical segments, sealing rubber rings, and insert plates that needs to fit in the NEMA body phantom box. Thus, if the thickness of the insert plates changes, the height of each segment needs to be adapted to still fit in the NEMA body box. Version 5 of the phantom box is a direct consequence of this intrinsic relationship between the design of the phantom box and of its inserts. In (V.5) the imaging segments height was reduced from 44mm to 43mm.

Limitation of version (V.5):

- × None yet
- × But a limitations arise from the manufacturing process and ordering of the phantom material parts which forces the design to be updated in a version (V.6)

4.2.7 PHANTOM BOX DESIGN (V.6.1 & V.6.2)

In the last step before manufacturing the phantom box another issue arose while verifying the material availability for each phantom part. It appeared that PMMA sheet of 7mm could not be ordered, as only PMMA sheets of 5mm or 8mm thick are available to be laser cut. This led to the creation of a design (V.6.1) which updated the cube sized which were 7mm and 7.5mm height to now 8mm height (cf. Table 10).

Table 10 Parts list of box design (V.6.1)

Quantity	Part Name	Manufacturing process
1	Top_cap	PMMA sheet 3mmthick
1	Bottom_cap	PMMA sheet 3mmthick
2	Top_Bottom_ceiling	PMMA sheet 3mmthick
3	Imaging_segment_wall	PMMA tube 76/80mm
4	Inbetween_segment_wall	PMMA tube 76/80mm
6	Insert-plate	<i>(to be defined in §4.3 & 4.4)</i>
12	Flange	PMMA sheet 3mm thick
12	Rubber gasket	NBR sheet 1mmthick
7	Filling_cube	PMMA sheet 7mm thick PMMA sheet 8mm thick
36	M3 assembling screws	Buy M3 nylon screws
7	M2 closing screws	Buy M2 nylon screws

Moreover, no special tolerance interval has been included in the designs of the phantom box so far. However, the manufacturing of some pieces might produce bigger or smaller parts than designed. Among all of the different manufactured pieces, only the flanges, rubber gasket and cubes were not produced by TU Delft but by a supplier. Therefore, the dimensions of those pieces could not be precisely tracked while manufactured. To avoid any assembling problem, especially with critical pieces like the flanges which hold the entire phantom together, special dimension tolerance were added in a design (V.6.2). In this version, for example, the flanges inner diameter was updated to ensure that, once laser cut by the supplier, these flanges would stay larger than the 76/80mm ID/OD tubes they are supposed to surround. As a final point, this design (V.6.2) is taken as a reference to start the ordering and manufacturing of the PET phantom box.

Limitations of version (V.6):

- × None yet
- × But limitations arise when receiving the ordered phantom parts which forces us to update the design and produced prototype in a version (V.7)

4.2.8 PHANTOM BOX DESIGN (V.7)

Yet, even though the latest box design version (V.6.2) seemed perfect, some post manufacturing design updates needed to be implemented. The new design (V.7) described in this section stemmed from the unfortunate realization than the designed and ordered flanges screws holes of 2.7mm and 3.4mm do not support well M3 screws thread because they already are too big. As the flange were already ordered, manufactured, delivered, and assembled, the only solutions were to either update each M3 hole in the flanges to a bigger M4 holes, or to re-order all the flanges with new dimensions and to completely rebuilt another prototype. To solve this issue, another version (V.7) was designed with bigger M4 screw holes in the flanges. Doing so permitted to resolve the issue of flanges threads that matches exiting screws without having to start the manufacturing from the beginning. However, it also led to another issue: when switching from M3 screws to bigger M4 screws not only the threaded holes need to be enlarged but also the space around the new M4 screws head. As shown in (Figure 16) hexagonal M4 screws have a bigger head than M3 screws and this bigger head appeared to touch each segment wall while fastening the screws which implied the need of manually erode each segment wall enough to let the M4 screws head pass.



Figure 16 Screws (M3x10 left, M4x10 right)

Once updated in such a way, the phantom box manufacturing continued and finished, producing the first PET phantom box prototype known as version (V.7) (cf. Figure 17). However this prototype faced several issues: first, it was not leak tight, and second M4 screws were very difficult to tight so the assembling of the phantom was still problematic.



Figure 17 PET phantom box assembly of the first prototype in the NEMA body PET box as designed in (V.7)

Limitation of version (V.7):

- × Bigger M4 screws used
- × Erosion of the imaging segment wall impairing the imaging segment transparency
- × Not watertight
- × M4 screws are difficult to fasten
- × Assembly is challenging and time consuming
- × Not enough time to reproduce an entire phantom prototype

4.2.9 PHANTOM BOX DESIGN (V.8)

Hence, the quick design and production of another prototype (V.8) build to overcome the previously mentioned limitations. This time M3 holes on the flanges were correctly. Plus, as a new design was created for this prototype, another update was added to this design version (V.8) consequently to other issues faced in the parallel design of inserts plates. As it will be explained later on in (§4.3.4 Phantom cubical inserts design), imaging segments height needs to be adaptable to the kind of inserts used inside the PET phantom. Thus, imaging segments in this (V.8) were designed to either be produced with a 42mm height or with a 40mm height.

However, due to the limited allocated time of the Master thesis, the production of the entire prototype (V.8) would have taken too much time with no clear promise of a functional phantom at the end. A choice was therefore made to only build few pieces of this phantom box version (V.8) together with its following version (V.9) and to both test these parts in a leak test (§5.1.6 Post-assembly leakages tests). By doing so, the designs were partly tested and validated before their mass production which permitted to be more time and cost efficient.

4.2.10 PHANTOM BOX DESIGN (V.9)

Following the previous statement regarding the production of only some PET phantom box pieces for leakages tests before a big entire prototype manufacturing, another design (V.9) was developed. This design is based on an increase of the number of M3 screws holes in the flanges (from 6 to 12 holes) which was engineered to reduce the strength applied to each of the M3 screws and to homogeneously compress the rubber gasket all around the flange using more pressure points. This might permit the rubber flange to work more efficiently and therefore to reduce the leaks at the junction of each segment.

Finally the phantom box design stopped at those two version (V.8) and (V.9). At the end, once produced, the semi-prototypes (V.8) and (V.9) were tested at the very end of the master thesis and were both validated as leak tight. Thus, the manufacturing of the rest of these phantom boxes (V.8) and (V.9) is suggested as the following step of the Master Thesis if continued by another student.

4.3 PHANTOM INSERTS DESIGN

4.3.1 PHANTOM INSERTS OVERVIEW

Parallel to the design of the PET phantom box, PET phantom inserts have been developed. In order to develop complex heterogeneous shapes, first a proof of concept of the box design as well as the insert manufacturing techniques needs to be done. Once the concept of the phantom is validated with simple shapes, a development of more complex inserts can be done. To this end, simple shapes (spheres and cubes) have been first designed and developed to be incorporated in our PET phantom box. The two following sections focus on detailing the development of such inserts.

4.3.2 PHANTOM INSERTS MANUFACTURING

Additive manufacturing (AM) process (also known as "3D printing") is a manufacturing process that is based on the creation of object using the addition of layers on top of each other. This technique is commonly used in the development of new design as it presents several advantages over other manufacturing techniques such as: flexibility (complex shapes and geometry possible), customization, no tools and mould needed, lower fixed cost, fast easy, less waste... Additive manufacturing was originally developed by (Hull 1986) who invented the first 3D printing technique called stereolithography (SLA). Since then, a lot of additive manufacturing techniques have been developed but only three of them (Stereolithography (SLA), Fused Deposition Modeling (FDM) and Selective Laser Sintering (SLS)) were available for the DEMO group in TU Delft where the Master study was conducted.

Stereolithography (SLA) is based on the polymerisation of liquid photopolymer (usually referenced as resin) using a laser beam. The build platform is soaked in a liquid resin tank. Each layer is created by solidifying in a (x,y) plan the bottom liquid layer of the tank. When a layer is done in the (x,y) direction; the build platform where the cured resin is attached moves up, and another layer of resin can be solidified below the previous one.

Fused Deposition Modeling (FDM) is based on the deposition layer by layer of melted plastic on a build platform. A plastic filament is heated and processed through the printer nozzle and deposited on a (x,y) plan. Once the layer is completed the build platform is lowered in the z direction and another layer can be put on top of the previous one.

Lastly, Selective Laser Sintering (SLS) is based on the melting and re-solidification of powdered material like metal using a laser beam. Each layer is built in the (x,y) direction by the melting of a layer powder put on a build platform. Once solidified, the previous (x,y) layer on this platform is lowered in the z direction and is covered by a new layer of powder. SLS uses metal, in the context of this study, is not an adequate material.

Thanks to the great flexibility of shape and geometry of additive manufacturing, the PET phantom inserts were designed to be manufactured by additive manufacturing process. A comparison between the two available and suitable additive manufacturing techniques: SLA and FDM, was conducted to evaluate which printing technique is the most suitable process for those parts (cf. Table 11). SLS techniques was not taken into account as it uses metal powder and any metal is strictly forbidden in the design of a PET phantom as it leads to artefacts creation during image reconstruction. At the end both SLA and FDM techniques can be used and will be used for the phantom inserts prototyping according to what properties prevail and are most needed.

Table 11 Comparative table of FDM and SLA additive manufacturing techniques

Printer name	Materials	Resolution	Advantages	Disadvantages
SLA Envisiontec P4 Mini	ABStuff, ABflex, ABS Flex EC500/ EC3000 , EPIC, PIC 100, PIC100G, HTM140, LS600, WIC100G, WIC300, E-Shell 200, Photosilver, QView, R5, R5 Gray, R11, RCP30, RC31, RC70, RC90	xy: 33 or 19 µm z: 15 to 150 µm	- precision -semi-transparent material available	- cost of the photopolymers - 1st layer isn't flat - vibration sensitive - only semi-transparent material available - build platform width < 8cm -less available
FDM Ultimaker Original	thermoplastics :, PLA, Nylon, ABS, CPE (transparent), CPE+, PVA, PC , TPU 95A	20 to 200 µm	- simple to use -available - widely used - lot of tutorials	- slow: 8mm ³ /s - less precise - no transparent materials available

4.3.3 PHANTOM SPHERICAL INSERTS DESIGN

In this section, the design of simple spherical insert is described. Spheres of the same dimensions and smaller than the already existing NEMA PET phantom spheres have been designed and produced during this master thesis. As presented in the following paragraphs, the design of these spheres appeared to more complex than expected leading to the creation of a final solution slightly different from what was planned. (Figure 18) gives a good overview of the different sphere design versions and each of their main characteristics.

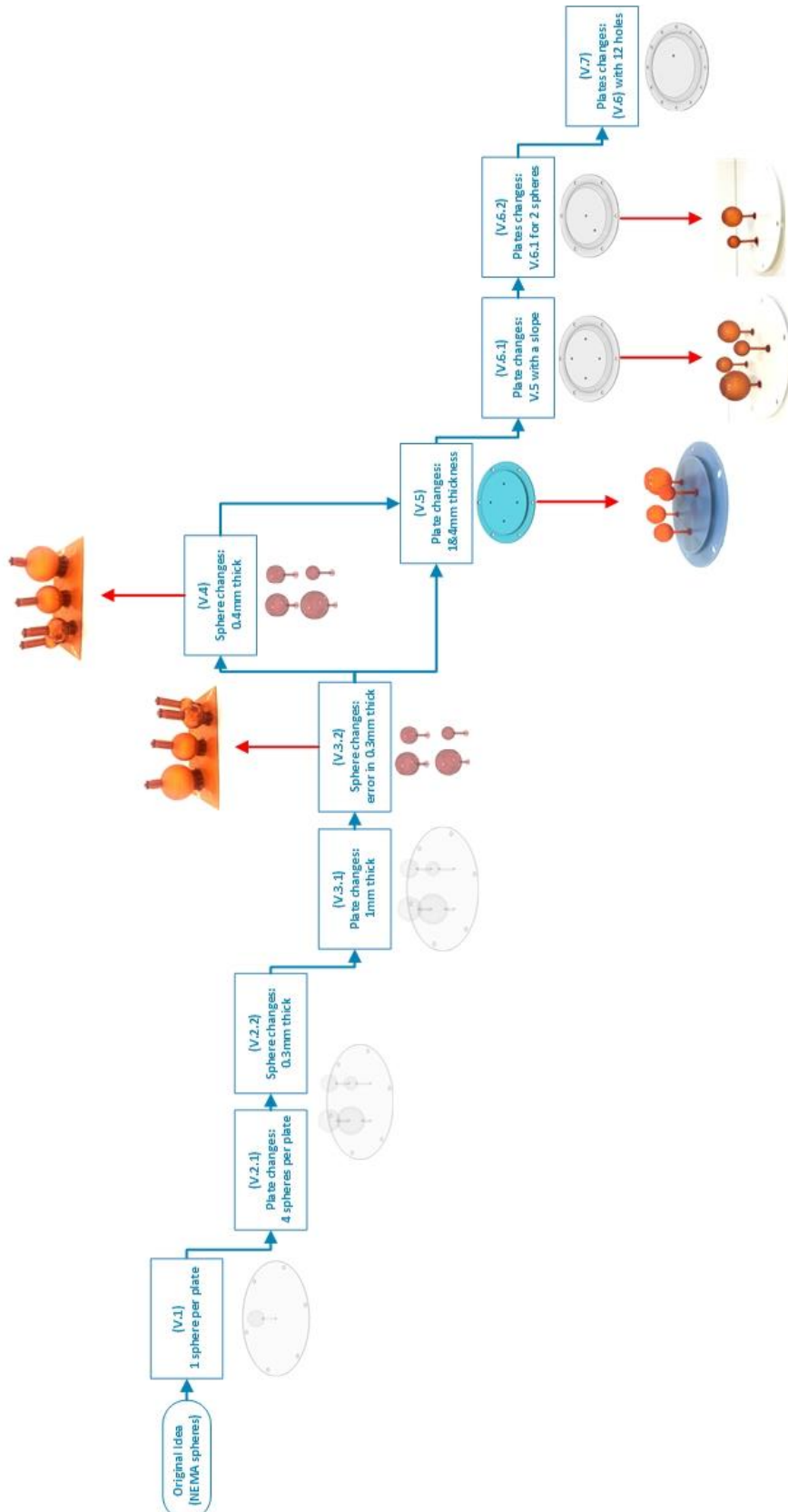


Figure 18 General overview of each design version of the spherical inserts and their manufactured prototypes

First, similar to the already existing NEMA spheres, four different spheres of 10, 13, 17, and 22mm inside diameter (ID) with a wall thickness of 1mm and fillable via a hollowed capillary tube of 1mm have been designed in a version (V.1). Each sphere was centred and attached to the phantom insert plate as presented in (Figure 20) and was planned on being manufactured using the precise additive manufacturing modality of stereolithography (SLA) as it permits the manufacture of precise object (of only a few tenth of a millimetre thick) and permits to print with R5 a semi-transparent red liquid photopolymer from EnvisionTec® (cf. Figure 19). (Table 12) summarizes the general properties of the material R05.



Figure 19 Photopolymer R05 as designed (left) and printed (right) (extracted view from Inventor®)

Table 12 General properties of R05 (EnvisionTEC 2015)

Name	Photopolymer R05
Sector of use	Light curing resin for EnvisionTec's family Computer Aided Modeling Devices
Supplier	Envisiontec® GmbH
Physical state	Liquid
Colour	Clear - Red
Odour	Acrylate
pH	6.8-7.2 (at 25°)
Initial boiling point	>100°
Flash point	>100°
Vapour pressure	0.0015 mm Hg (at 25°)
Density	1.08-1.12 g/cm ³ (at 25°)
Dynamic viscosity	400-900 mPa.s (at 25°)

Second, this design was updated in a version (V.2.1) where the four spheres were attached to one insert plate as shown in (Figure 21). In order to produce something innovative and improved than what already exists, all of the spheres were made thinner than the already existing NEMA spheres (from 1mm thick to 0.3mm thick) in a following version (V.2.2).



Figure 20 Phantom spherical insert design (V.1)

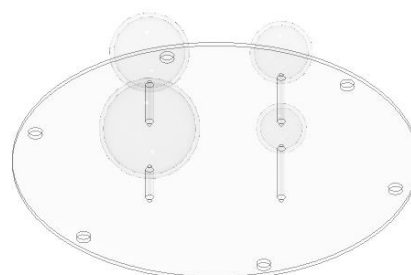


Figure 21 Phantom spherical insert design (V.2)

Third, the selected manufacturing process: SLA appeared to face some limitations when printing thin and flat plate of less than 1mm thick. Therefore (V.3.1) updated the plate thickness from 0.5mm to 1mm and version (V.3.2) corrected from some error in sphere wall thickness. This version (V.3.2) (cf. Figure 22) was then manufactured using SLA additive manufacturing with EnvisionTEC Perfactory® P4 Mini printer, at EWI workshop (cf. Figure 19 and Figure 23).



Figure 22 Phantom spherical insert design (V.3.2): spheres of 10, 13, 17, and 22mm ID



Figure 23 Phantom spherical insert design (V.3.2) SLA 3D printed with support

Fourth, the printed version (V.3.2) of the sphere presented few holes at the surface of the spheres. Thus, another version (V.4) designed thicker spheres of 0.4mm instead of 0.3mm thick to check if a thicker sphere wall will have fewer holes at its surface when being manufactured. Once produced, the 0.4 mm spheres also presented holes at their surfaces which, together with the 0.3 mm spheres holes, were filled using glue.

As spheres of 0.4mm did not performed better than 0.3mm thick ones, the spherical inserts design shifted back to thinner 0.3mm thick spheres. Ideally three sets of four spheres – 3 times 10, 13, 17, and 22mm ID- should have been produced in 0.3mm thick, unfortunately the SLA printer used to produce such sets was removed from TU Delft for maintenance on the 20th of July 2017 and since then no further spheres could have been produced. Therefore, due to the limited allocated time of the Master thesis, a decision was made to keep the only two prototype sets of 0.3 and 0.4mm thick spheres already printed and to develop a unique prototype using those non ideal, but at least available, spheres.

Fifth, as the 0.3mm and 0.4mm prototype spheres were already produced, a special focus was set on their support plates. The plate design was updated in a version (V.5) with a disk extrusion of 4mm that permit the addition of closing screws throughout the plate which can closes each sphere separately. (Figure 24) shows the 4mm disk extrusion on top of the plate. On this extrusion, 4 holes are designed, each hole will be closed on one side by a M3 screw and on the other side by a sphere as shown in (Figure 25). This version (V.5) was manufactured using FDM additive manufacturing with the Ultimaker printer at the RID workshop. Here, FDM printing machines printed inserts plate with polylactic acid (PLA) plastic filament (Table 13 summarizes the general properties of PLA). FDM manufacturing process was chosen here for the availability of the printer and its relative short manufacturing time. The plates did not especially needed to be transparent as no air is supposed to be retained in the plates. The only region of interest within the spherical insert is inside the spheres and those spheres are already printed in semi-transparent R05 photopolymer using SLA technique.

Table 13 General properties of PLA (Ultimaker 2017)

Name	Polylactic acid PLA
Sector of use	FDM printing devices
Supplier	Ultimaker® or MakerPoint ®
Physical state	Solid filament
Colour	Available in white, black, red, blue etc..
Odour	Slight
Melting poin	145-160°C
Flash point	388°C
Density	1.24 g/cm ³

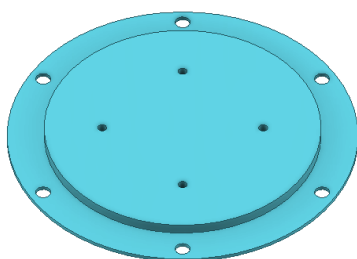


Figure 24 Phantom spherical insert design (V.5)



Figure 25 Phantom spherical FDM printed insert (V.5) with the four SLA printed spheres attached to one of its side

Sixth, as leak tests were performed by assembling with the different produced inserts plates with phantom box imaging segment (V.7) and rubber gaskets. From these tests unsatisfying results, some updates were made on insert plate (V.5) to improve the sealing function of the gaskets brought in contact therewith. Indeed, the 4mm extrusion present in (V.5) caused some changes in the opposite surface of the plate that might have impaired the sealing property of the rubber gaskets to its contact. Thus, versions (V.6) and (V.6.1) were designed and FDM printed with a less abrupt extrusion (small slope of 45° instead of a 90° angle) as shown in (Figure 26) which was engineered to create less surface variation on the opposite surface of the plates and supposedly improve the sealing power of the rubber gasket to its contact.

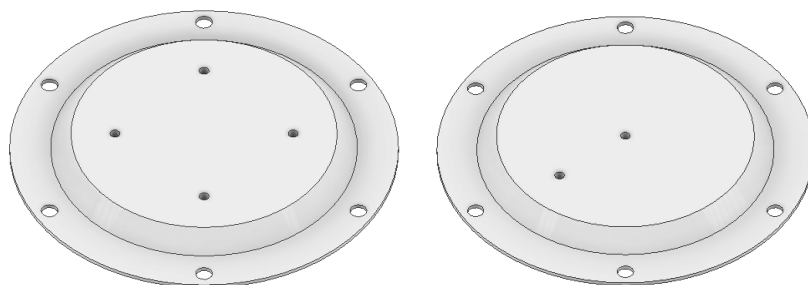


Figure 26 Phantom spherical insert design (V.6.1) and (V.6.2)

Unfortunately, as it will be presented later on in this report in (§5.1.6 Post-assembly leakages tests), these design updates did not led to less leak.

Therefore, due to the limited allocated time of the Master thesis, a decision was made to create a simple water tight box which glued all together imaging segment and insert plate and that did not necessitate the use of rubber gaskets. This prototype, as presented in (Figure 27), uses already printed plate versions (V.6.1 and V.6.2) and contains all the available spheres. Creating such a prototype permitted to have at least of a proof of concept on the designed insert spheres even though the assembly process between the imaging segments and inserts plates would not be finished. Fortunately, this prototype has assessed and validated it sill be described in (§5.1.8 FDG PET/CT imaging test and proof of concept, p.60).

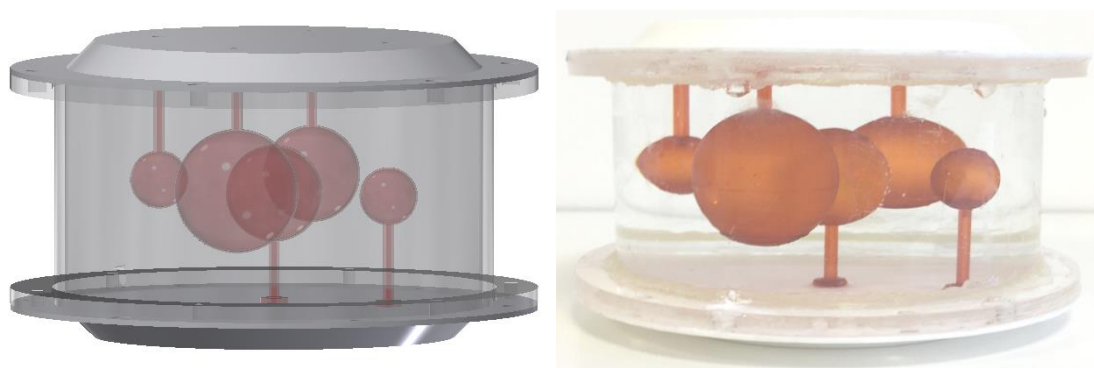


Figure 27 Phantom spherical insert prototype from sphere (V.3.2), (V.4) and plate (V.6.1) and (V.6.2) As designed (left) and as produced (right). The prototype contains five spheres: two of 0.4mm thick (10 and 17mm ID filled by the bottom plate of the figure) and three of 0.3mm thick (10, 17 and 22mm ID, filled by the top plate of the figure).

Seventh and last, parallel to the PET phantom box design (V.9) a plate (V.7) (cf. Figure 28) was design to fit 12 holes flanges contained in the last version of the phantom box for further leak tests. This plate permitted to test the sealing power of 12 holes gaskets, where the increasing number of M3 screws holes in the flanges (from 6 to 12 holes) is engineered to reduce the strength applied to each of the M3 screws and, thus, to homogeneously compress the rubber gasket all around the flange using more pressure points, which might ensure a better sealing. This design might permit the rubber flange to work more efficiently and therefore to reduce the leaks at the junction of each segment.

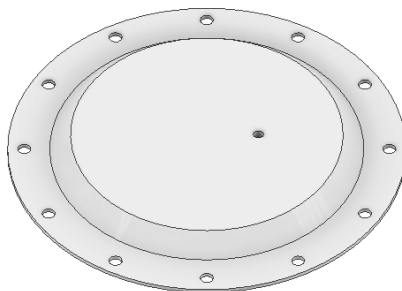


Figure 28 Phantom spherical insert design (V.7)

Once printed this design (V.7) was tested with PET phantom box design (V.9). As presented later on in this report in (§5.1.6 Post-assembly leakages tests), this assembly is watertight, and the construction of an entire phantom using this assembly process can be considered as the direct following step of this Master thesis.

However, having more holes to tight implies a longer setting up time for the phantom assembly; which, in the case of PET phantom image acquisition preparation, leads to a higher irradiation of the person handling the phantom. It is therefore suggest to continue the leak tests and to find a water tight solution that does not involve the use of 12 holes flanges and rubber gaskets.

4.3.4 PHANTOM CUBICAL INSERTS DESIGN

Following the idea of first developing simple shapes that will be complexified more and more, cubical intricate inserts shapes were also designed in parallel of the phantom box design and the spherical inserts design during the Master Thesis. This section first starts with a general overview of the phantom cubical insert design (cf. Figure 31, next page). Followed by a quick description of each version of the cubical insert details, advantages, drawbacks and trade-offs. This section ends with a small conclusion regarding the last cubical design and where the study stopped.

First, the design of these inserts was based on an upcoming publication of the image biomarker standardisation initiative (IBSI) and focussed on creating three different milieus interconnected to each other and filled with three different radioactivity concentrations as defined in (Figure 29).

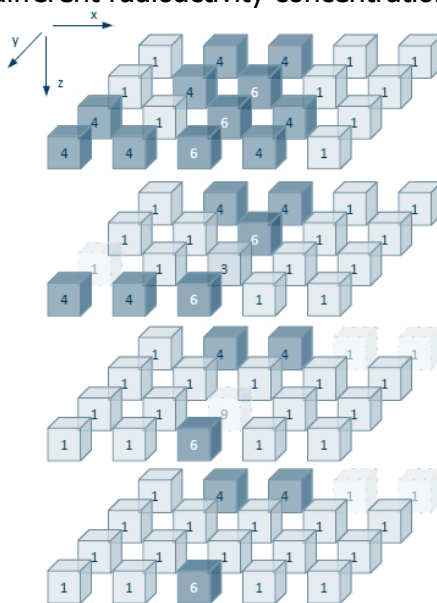


Figure 29 Exploded view of the text volume developed by IBSI and used for the cubical inserts design. The number in each voxel corresponds to its grey level. Semi-transparent pixels are included in the design as background pixels with a grey value of 1 for all of them.

From it, a representation of each volume was designed (cf. Figure 30). As no pixel size dimensions were detailed in the upcoming publication, different cube sizes were tested: 2x2x2mm, 4x4x4mm, 8x8x8mm and 16x16x16mm. Considering the limited amount of space available within the PET phantom box imaging segment and the relative low resolution of PET scanners (roughly between 4v and 7mm) the design continued to be updated using 8x8x8mm cubes, as they are big enough to be visible alone in PET images but small enough to have a stack of 5 cubes contained in a 45mm height segment. From this idea several design were developed as presented in (Figure 31) and some were manufactured using SLA additive manufacturing, chosen for its flexibility and precision when compared to other additive manufacturing techniques.

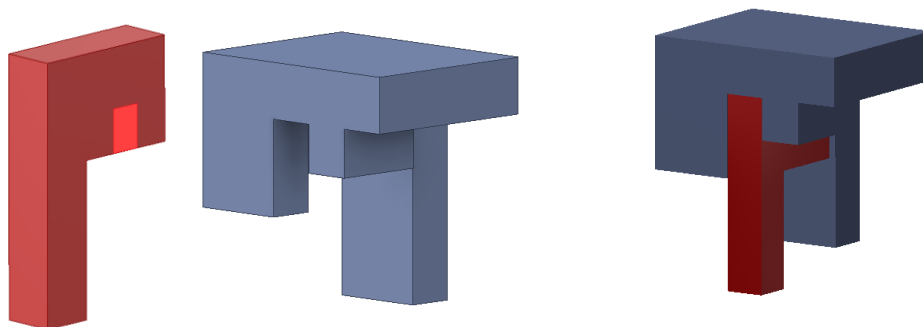


Figure 30 3D representation of the cubes according to their concentration. 3D representation of the stack of all the cubes with a high grey level of 5 and 6 (i.e. high radioactivity concentration) extracted from Figure 29 (left). 3D representation of the stack of all the cubes with a lower grey value of 4 (centre) and their assembly together (right).

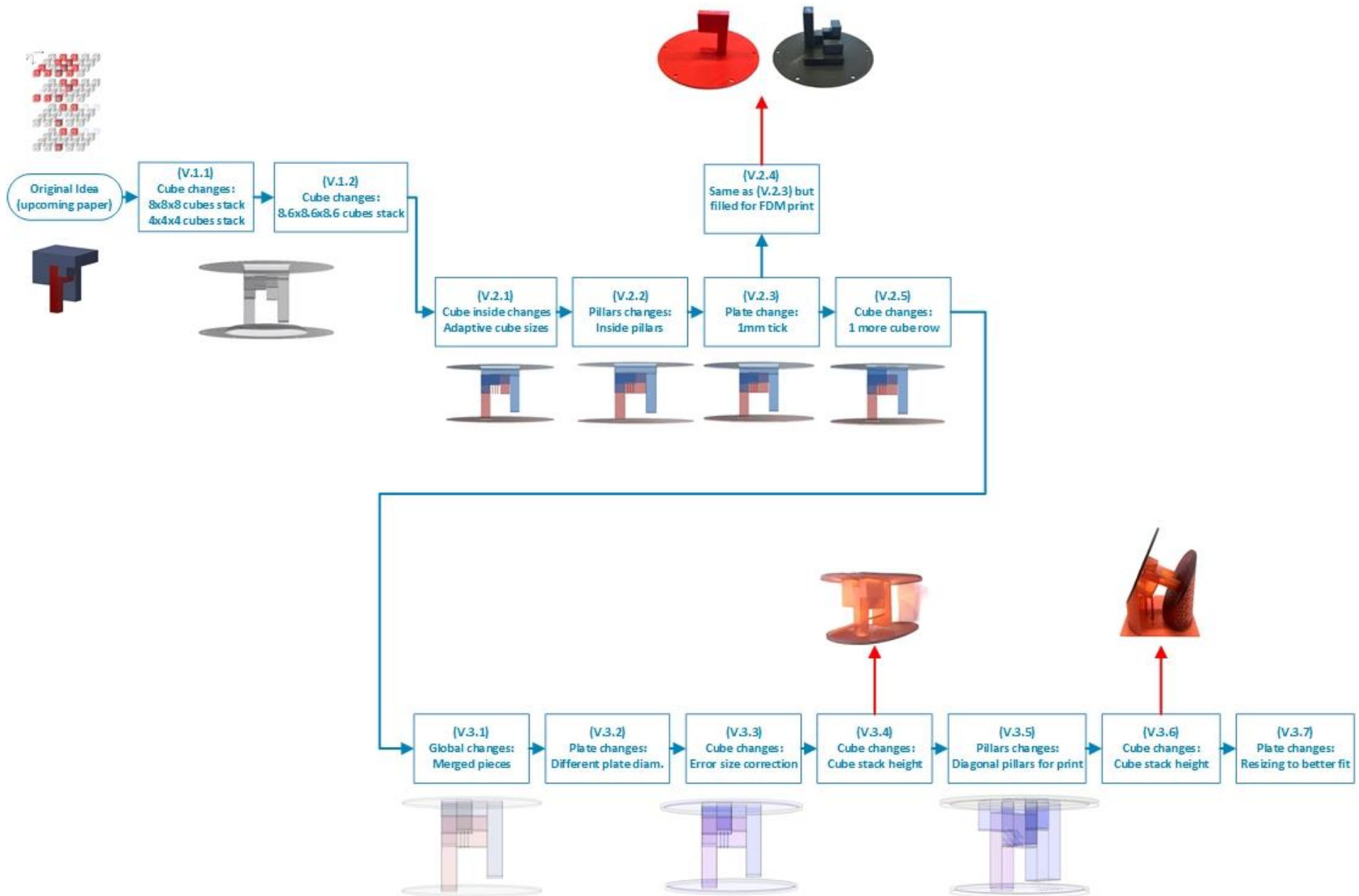


Figure 31 General overview of each design version of the cubical inserts and their manufactured prototypes

Second, from this design idea and definition, two stacks of hollowed cubes of outside dimensions 8x8x8mm (V.1.2) and of 8.6x8.6x8.6mm (V1.2) have been designed. These were developed as cubical extrusions coming out from two insert plates of a wall thickness of 0.3mm. Each plate and its shaped cube stack can be filled with a specific radioactivity concentration (4 or 6 times the background) and can be assembled together as detailed in in (Figure 30). However, both of these designs faced the following limitation: when assembled together the cube stack of lower grey value and higher grey value were not perfectly aligned. Misalignment in the Z direction is explained by the fact that each cube stack ends at some point and has a ceiling wall with a thickness of few millimetres that is in direct contact with the ceiling wall from the other concentration stack. This ceiling walls superposition misaligns the stacks of few millimetres from neighbouring stacks.

Third, to overcome this problem, a new version (V.2.1) uses adaptive cube size of either 8 or 8.6 mm height with an adaptive wall thickness of 0.3 or 0.6 mm, as represented in (Figure 32). Moreover, in this version, the middle pixel, which is only containing a radioactivity concentration of 3, was designed to be half filled with pillars. These pillars are engineered to slightly influence the global concentration of radioactivity contained in the insert at that position. Indeed, by adding an extra inert material the global radioactivity concentration contained in a specific volume should be lowered. However as the background concentration is already low, the pillars as designed in (V.2.1) (Figure 32) would lower even more the radioactivity in this volume to half of the background concentration. This does not correlate with the middle cube grey value defined as equal to three times the background concentration. Thus, a version (V.2.2) (Figure 33) updated the pillars to include them in the red shape stack which has a grey value of 6 and can be half lowered to 3.

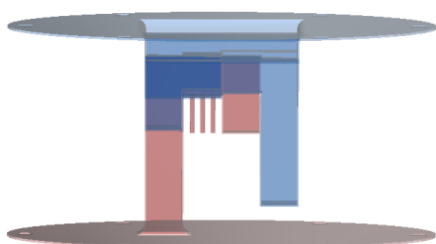


Figure 32 Cubical inserts (V.2.1)

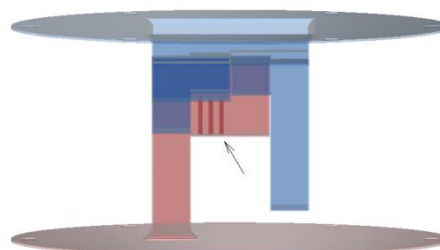


Figure 33 Cubical inserts (V.2.2)

As described in (§4.2 Phantom box design) and (§4.3.3 Phantom spherical inserts design), all insert plates went from 0.5mm thick to 1mm thick due to the SLA printer thickness limitation. This led to the creation of a new cubical insert version (V.2.3) with a thicker base of 1mm instead of 0.3mm. From this design version, a filled design was realized (V.2.4) and FDM printed (cf. Figure 34). This print permitted to visualized the dimensions of the inserts and to check how good the two printed plates inter-connected. Even though the printing technique used here (FDM) is different to the printing technique planned on being used to print the inserts (SLA), the printed

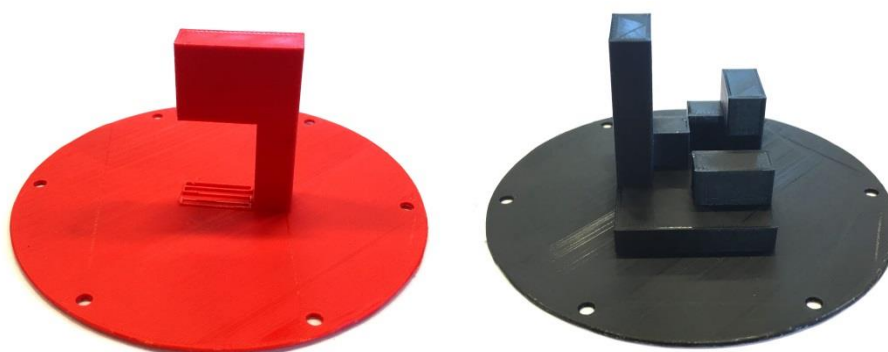


Figure 34 FDM print the cubical inserts (V.2.4)

Fourth, it seemed easier to merge the two surface plates in one unique surface. By doing so the thickness of the insert would be reduced as only one adjoining wall is needed between two cubes of different concentration instead of the two cube walls. A version (V.3) therefore focussed on designing a unique separating surface that is shaped to separate all the cubes from different concentration with only one wall (cf. Figure 35, left). This version does not contain any insert plate and is designed to be glued to the imaging segments. Because the interface between the imaging segment and the inserts is glued, less gaskets are needed which gives more space for the imaging chambers. (up to 47mm high). Different updates of this cubical insert version (V.3.1, V.3.2, V.3.3, and V.3.4) slightly changed the top and bottom bases sizes to better incorporate and glue the insert to the imaging segment (for example (V.3.4) in Figure 35 (right) , bases are thicker on the extremities and bottom base has a smaller diameter than the top base). At the end (V.3.4) was SLA printed with very few support (as shown in Figure 36). The SLA print was done at the EWI workshop using the EnvisionTEC Perfactory® P4 Mini printer with R5 a liquid photopolymer from EnvisionTec®. Due to the small dimension of the printer, the insert needed to be rotated with a 30° angle to fit in the printer, thus additional support needed to be added to the pillars and bases in order to hold them and print them properly.

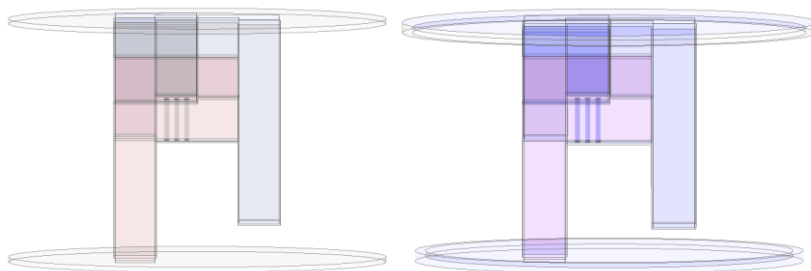


Figure 35 Phantom cubical inserts (V.3.1) (left) and (V.3.4) (right)



Figure 36 SLA print of the phantom cubical insert (V.3.4)

Global side view of the print, where the supports are visible as indicated by the black arrow on the left. Due to a lack of support, the bottom base of the print is not parallel to its top base (left). Zoom on the inside pillar of the insert (right). The pillars were supposed to be contained in the yellow cube drawn on the right; however, the support needed for their print spread on the neighbouring cubes.

Once printed, we realized that the chosen amount of support was too low for this print. This lack of support created weak bases that were not printed as flat as designed; thus more support needs to be added to the next print. However, we also realized that the inside pillars' supports already spread too much within the inside of the structure so we could not add more support there. A compromise needed to be made between: more supports for a better global base shape and less support for a less spread small inner pillars. At the end, a version (V.3.5), as shown in (Figure 37), was thus created to reinforce the base plate with more support as well as creating diagonal pillars that are already oriented in the 30° direction of the print. By doing so, the printer should not add extra support inside the insert and would only add support on the outside. This is not limiting as the extra supports on the outside of the insert can be easily cut off.

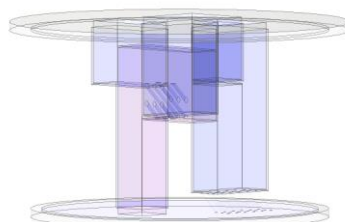


Figure 37 Phantom cubical insert design (V.3.5) with diagonal pillars and extra external support

Because the cubical phantom inserts of version (V.3.1 and above) were designed to be glued inside the phantom box imaging segment, less sealing gaskets were needed at the junction between the insert and the segment. Thus, all the previous cubical inserts version (V.3.1 and above) have been designed to fit in a bigger imaging segment of 45 to 47 mm height. As bigger imaging chamber permit to acquire bigger images and therefore extract more information this aspect was considered as a advantage of the cubical inset. However, all of those big inserts were not fitting in the phantom box designs (V.1.2) to (V.5).

At that point of the study, a final version of the phantom box (V.6.1) was set. And a cubical insert version (V.3.6) was designed to fit inside. This version, shorter than all the previous cubical inserts, is adapted to fit in an imaging segment of only 42mm height as designed in the box version (V.6.1). By doing so, standardized imaging segment of the same dimension (42 mm height) were created to host both kind of inserts (spherical (Figure 38) (left) or cubical (Figure 38) (right)). Having the same imaging segment size for all inserts allow the phantom user to really build a modular PET phantom by indifferently piling imaging segments containing different insert kind and image them altogether in one acquisition time

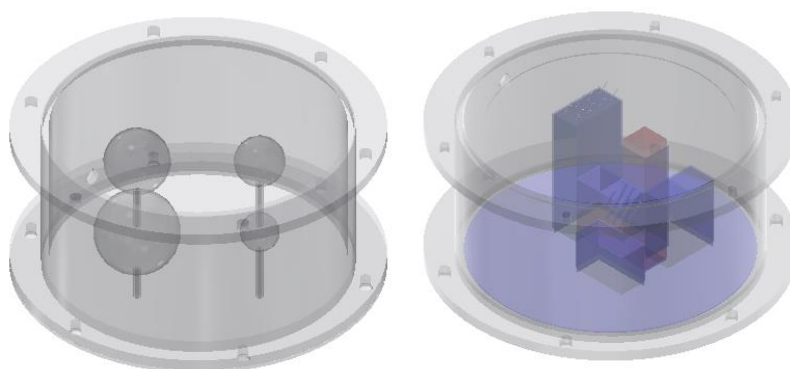


Figure 38 Imaging segment of 42mm containing: spherical insert (left) and cubical insert (right)

Finally, this cubical insert version (V.3.7) was SLA printed with more supports than previous printed version (V.3.4).As shown in (Figure 39) the printed result looked very promising with strong parallel bases and no extra support inside the insert.

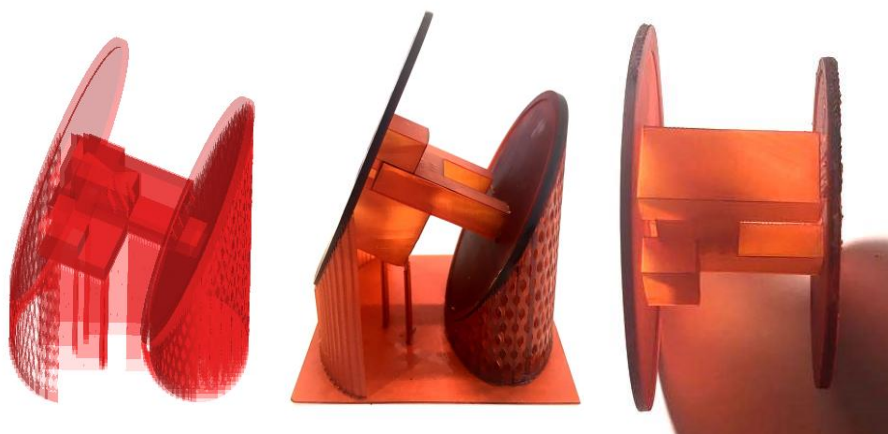


Figure 39 Additional external support added to design (3.6) by the SLA printed software: 3D design view (left), actual printed insert with supports (middle) and without (right)

A last design (V.3.7) was created to better adapt the inserts base diameter to the imaging segment tube dimensions. But, unfortunately this version could not have been printed as the EnvisionTEC Perfactory® P4 Mini printer was on maintenance for the last three months of the Master project. At the end, due to the limited allocated time of the Master thesis and this unlucky even, the production of cubical insert stopped there with a last design (V.3.7) still waiting to be printed.

4.4 DESIGN AND DEVELOPMENT CHAPTER SUMMARY

At the end three main directions have been followed during the design and development phase:

- the design of a PET phantom box
- the design of spherical inserts
- the design of cubical inserts

Each direction produced respectively 9, 7 and 3 main design versions. And totally 18, 10 and 15 sub-designs versions.

Out of all of these designs several parts have been manufactured and produced, yet not all of them were working:

- 1 phantom V.0 have been SLA printed
- 1 phantom box have been created from PMMA tube (V.7)
- 1 test segment have been created from PMMA tube (V.9)
- 8 spheres have been SLA printed
- 5 spheres plates have been FDM printed
- 1 cubical insert have been FDM printed
- 3 cubical insert have been SLA printed
- a sealed spherical insert box was made out of it

Indeed, among all of the produced objects, only three prototypes are actually usable:

- an entire phantom box have been created
- a sealed spherical insert box
- a cubical insert print

This is explained by the several issues faced and trade-offs made during the design and development phase (cf. Table 14)

Table 14 Phantom design trade-offs summary

Trade-off s	Description
Filling process	From no holes in the imaging chamber to holes there
Manufacturing process	From SLA semi-opac 3D printing to PMMA tubes
Tube size	From 1mm thick to 2mm thick
Imaging chamber height	From 44, to 45, to 48 to 42 mm height
Cubes height	From 7mm cubes to 8mm
Plate height	From 0.5mm to 1mm
Screws size	From M3 to M4
Erosion of the tube	Due to the M4 head screws diameters
Gluing process	From fine-looking transparent glue to yellowish epoxy glue
Leakages	From a modular design to a fixed chamber
SLA printer maintenance	From printable design to no manufacturing at all

5

CHAPTER 5: TEST AND VALIDATION RESULTS

In this fifth chapter, results of all the tests performed during the research study are introduced. First, pre-manufacturing tests done during the design and development phase regarding material selection (such as glue selection test) are detailed. Second, post manufacturing validation tests regarding the produced phantom compared to its primary requirements are described. These tests check whether the developed phantom meets its requirements. Material density of the developed PET phantom, water absorption of its wall, circularity of its printed inserts spheres and influence its semi porous cubical insert are assessed. Third, once each phantom part is validated and meets its requirement, the PET phantom is assembled and a post-assembly leak test is performed. Fifth, the phantom assembly and validated closing processes are evaluated and the relative irradiation dose receives while manipulating the phantom is calculated. Finally, the chapter end with a proof of concept test in the form of a FDG PET/CT scan of the designed and developed phantom is performed and concludes on the feasibility and efficacy of the designed research solution. From this chapter 5 and considering the unresolved trade-off of previous chapter 4, few conclusions and recommendations start to emerge and will be developed in next chapter 6.

5.1.1 PRE-MANUFACTURING GLUE SELECTION TEST

Once phantom box (V.6.2) design was fixed and set in production, the manufacturing of its components started. As designed by the Authors, the assembly of the different PMMA phantom walls pieces together necessitates the use of glue. Different glues can be used to assemble the PET phantom parts in an aesthetic and effective way. However the visual aspect of some glue, especially yellowish epoxy glues, usually counteracts with their relative fixative power. A trade-off between the relative strength of a glue compared to its visual aspect needed to be settled; therefore a glue selection test was performed during the study to compare two available glues: Araldite® 2022-1 and Araldite® 2020.

Araldite 2020 is a water like, liquid, transparent, epoxy glue with a short curing time. It is mainly used for glass gluing; (Figure 40) and (Table 15) present its main properties.



Figure 40 Araldite 2020 (retrieved from Araldite website)

Table 15 General properties of Araldite® 2020 (Huntsman 2020a, 2020b)

Name	Araldite® 2020
Sector of use	Assembly
Supplier	Araldite® by Huntsman Corporation
Physical state	Liquid
Colour	Transparent, water white
Odour	?
Flash point	>120°C
Density	1.11 g/cm ³ (at 20°C)

On the other hand, Araldite 2022-1, is a gap filling, non-liquid, yellowish methacrylate glue with a short curing time. Mainly used for various materials such as metal and plastics; this glue also have a large range of incompatible materials. (Figure 41) and (Table 16) present its main properties.

Table 16 General properties of Araldite® 2022-1 (Huntsman 2022b, 2022a)



Figure 41 Araldite 2022-1 (retrieved from Araldite website)

Name	Araldite® 2022-1
Sector of use	Assembly
Supplier	Araldite® by Huntsman Corporation
Physical state	Liquid, appearance of paste
Colour	Pale yellow
Odour	Acrylic like
Flash point	10°C
Density	A: 1.01-1.02 g/cm ³ (at 23°C) B: 0.94-0.95 g/cm ³ (at 23°C)

As presented in (Figure 42) two PMMA samples, one disk and one ring, have been glued together with both Araldite 2020 (left) and Araldite 2022-1 glues (right). The Araldite 2020 glue was applied in between the entire two surfaces where its water like texture completely faded in a see through interface which was almost not visible with naked eyes. On the contrary, the Araldite 2022-1 glue, which is supposed to be more adhesive, was applied only on the edges of the two samples and its superfluous quantity was removed with a spatula even though some yellowish remains are still visible (cf. the white arrow on Figure 42).

After a curing time of 24h, a tensile force was applied to separate the two and two pieces. Araldite 2020 glue did not performed as well as the Araldite 2022-1 glue. The two disks were easily separated, which suggests a relative weakness of the Araldite 2020 glue regarding its adhesive power to PMMA materials. On the contrary, Araldite 2022-1 glue performed well as the PMMA disk broke before the glue did.

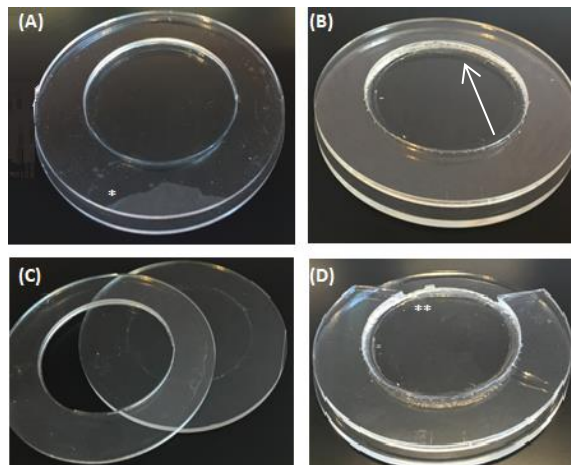


Figure 42 Gluing strength comparison between Araldite 2020 (A)(C) and 2022-1 (B)(D)

(A) Test sample where both entire surfaced were glued together with Araldite 2020 as extremely liquid glue. Only one spot is not glue (marked by an asterisk on the picture). (B) Test sample glued only on the edges with Araldite 2022-1. (C) shows the relative lower strength of Araldite 2020 compared to (D) 2022-1 when applying a steering force on the samples. In (D) the PMMA sample broke before the glue. The glue being still intact on the sample (market in D by two asterisks)

Test conclusion:

At the end, considering the fact that our PET phantom better needs to be resistant than aesthetic the Araldite 2022-1 glue was selected for its strength and resistance compared to the Araldite 2020. And a PET phantom prototype was built.

Once the PET phantom manufactured, validation tests are performed to evaluate if the prototype succeed or fail to meet the global PET phantom requirements. According to the PET phantom basic requirements previously listed in (Table 3 Ideal PET phantoms requirements) PET phantom pieces used in the phantom should be as much tissue equivalent as possible. This means, that:

- Manufacturing technique of the phantom inserts should be accurate enough and produce inserts shape as expected (Realistic insert shape design requirement)
- PET phantom parts should have a density in the range of human tissue density (Realistic insert shape design requirement)
- PET phantom walls should not absorb radioactive water and not appear as 'hot walls' in PET images (Wall-less insert design requirement)

Several post-manufacturing tests were therefore performed to check whether these requirements have been met (§5.1.2 Post-manufacturing spherical inserts circularity test, §5.1.3 Post-manufacturing phantom water absorption test, §5.1.4 Post-manufacturing **PHANTOM CT DENSITY TEST** and §5.1.5 Post-manufacturing cubical insert pillars influence).

5.1.2 POST-MANUFACTURING SPHERICAL INSERTS CIRCULARITY TEST

First an insert shape test was done to check how spherical the 3D printed spherical inserts were manufactured compared to their design. Spherical inserts of 0.3 and 0.4 mm thickness (V.3.2 and V.4) which have been 3D printed with the photopolymer R05 using SLA additive manufacturing were imaged in the LUMC using a Biograph™ mCT PET/CT scanner (Siemens Medical Solutions) in water and in air (cf. Figure 43). An image treatment protocol was especially developed to evaluate the sphericity of these printed shapes and can be found in (Appendix 7.3: Sphere shape analysis).



Figure 43 Transversal CT image view of the spherical V.3 inserts in air
 Transversal view of the sphere of 17mm inside diameter (left), blurry top view of the 22mm diameter sphere (middle), side view of the smallest sphere (10mm diameter).

The sphere shapes were compared to an ellipse and the ratio between the major and minor axis length was calculated. It was assumed that the closer to the value 1 this ratio is, the more spherical these shapes are. As presented in (Figure 44), the printed inserts have all a ratio close to 1, and therefore can be considered as "spherical".

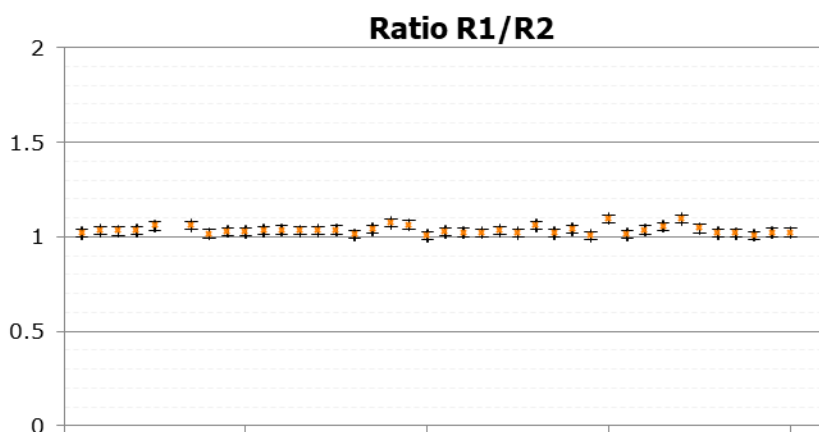


Figure 44 Ratio of the retrieved major & minor axis of the 3D printed spheres
 All spheres have a ratio around 1 (+/-0.2STD), which confirms the relative sphericity of the SLA printed spheres.

Test conclusion

SLA additive manufacturing technique seems to be a precise manufacturing modality which produces circular and accurate inserts.

5.1.3 POST-MANUFACTURING PHANTOM WATER ABSORPTION TEST

Second, the water absorption of the phantom was assessed. Several water absorption values of the different material composing the phantom have been found in the literature (cf. Table 17). The phantom box is made of PMMA tube and rings, sealed with rubber gaskets and held together using Araldite 2022-1 epoxy glue and nylon screws. Given the region of interest of the images extracted from the phantom box, the following approximation was made: “*the only material’s water absorption values that matter are the one from the material included in the view of view of the PET images extracted*” i.e. the PMMA tubes and the phantom inserts contained inside the phantom imaging segments.

PMMA material being widely used as part of other market PET phantoms and not being transformed in any kind while manufacturing the phantom box, a second approximation was made: “*the absorbance of PMMA tube forming the PET phantom box walls is considered as negligible*” and therefore was not furtherly analysed.

Table 17 Water absorption literature values found for the different materials used in the phantom

Material name	Test method	Water Absorption (%)
Photopolymer R05	ASTM D570-98	0.78 (EnvisionTEC 2017)
PMMA	ASTM D570-98	0.3-0.4 (Ide-mat 2003)
Nylon 6.6	ISO 62*	0.60-1.13 (Plasticshop 2011)

*ASTM D570-98 standard is equivalent to ISO 62 (ASTM international 2010).

At the end then, only the phantom SLA 3D printed inserts made of the photopolymer R05 needs to be tested for their water absorption. As found in the literature, R50 material has a low water absorption value ($\sim 0.78\%$ of its weight) (cf. Table 17) which can be considered as negligible. However, contrary to the PMMA tube, the additive manufacturing process used to produce the phantom inserts might have change the material absorbance properties. Indeed SLA printing is based on the polymerisation of R05 layer by layer. This superposition of layers in the inserts walls can make the wall less resistant, more porous and more absorbent than usual wall made of the plain same material. The relative thin printed walls (0.3mm to 1mm thick) could also lead to micro holes in the produced material which might lead to liquid absorbance. Hence, a test was conducted to check the relative absorbance of the printed photopolymer R05 used to manufacture the phantom inserts.

To this end, two pieces of SLA 3D printed R05 plastic *-sample-* were put in contact with a watery radioactive solution (Tc^{99m}) for 1h30. This duration is chosen similar to usual acquisition times planned to be used for the phantom image acquisition. The tested R05 pieces sample were approximately 10x20x0.3mm and 10x20x1mm. Tc^{99m} gamma emitter radionuclide was used instead of ^{18}F -FDG because of cheaper price and smaller available quantity

After this time, plastics is rinsed and remaining activity is acquired and compared with background values, to verify if R05 material absorbed radioactive water or not (the more detailed specific protocol can be found in (Appendix 7: Protocols)).

$$\lambda = \frac{\ln(2)}{T_{1/2}} \quad (1)$$

$$A(t) = A(0) \times e^{-\lambda t} \quad (2)$$

$$A(t) = A(0) \times \left(\frac{1}{2}\right)^{\frac{t}{T_{1/2}}} \quad (3)$$

$A(t)$: activity at time t

$A(0)$: initial activity at time zero

λ : radioactive decay constant

$T_{1/2}$: Radioactive half-life $T_{1/2}(Tc^{99m}) = 6.0067$ h

Radioactivity test results

Precise radioactivity values before and after rinsing are detailed in (Table 18). These values suggest that there is no real difference in radioactivity absorption from the thickness of the 3D printed R05 material. This implies that the thickness produced by SLA additive manufacturing technique does not influence the porosity of a material at that range (0.3 to 1mm).

Moreover, the remaining activity on R05 samples after rinse is in the order of magnitude of the background activity ($A_{Bg}+0.02\text{MBq}$). This suggests that R05 SLA printed materials of 0.3mm or 1mm thick have negligible radioactive solution absorption.

Table 18 Results of the radioactivity absorbance test

	Date	Time	Gross Radioactivity (MBq)	Net Radioactivity (MBq)	Calculated radioactivity at 08:37 (MBq)
Tc ^{99m} source calibration	10/08/2017	08:37	16.24	16.16	X
Background	10/08/2017	13:35	0.083	0	X
Tc ^{99m} source	10/08/2017	13:38	8.98	8.90	16.03
Tc ^{99m} + 0.86 mL water	10/08/2017	13:47	8.84	8.76	16.02
Remaining in the syringe	10/08/2017	13:47	1.14	1.06	2.07
R05 1mm not rinsed	10/08/2017	15:11	0.161	0.08	0.34
R05 0.3 mm not rinsed	10/08/2017	15:12	0.231	0.15	0.49
R05 1mm rinsed	10/08/2017	15:14	0.0986	0.02	0.21
R05 0.3 mm rinsed	10/08/2017	15:16	0.092	0.01	0.20

Test conclusion:

The PET phantom walls meets its requirement and does not absorb radioactive water and should appear as 'hot walls' in PET images

5.1.4 POST-MANUFACTURING PHANTOM CT DENSITY TEST

In order to check whether the produced phantom meets its design requirements a second test has been performed to evaluate the CT density (HU) of all the material constituting the PET phantom prototype. Hounsfield unit (HU) scale is defined as:

$$HU = 1000 \times \frac{\mu_{material} - \mu_{water}}{\mu_{water} - \mu_{air}} \quad (4)$$

(here μ_{water} and μ_{air} are respectively the linear attenuation coefficients of water and air measured in cm^{-1})

The Hounsfield units of water and air are fixed by definition: $HU_{water} = 0$ and $HU_{air} = -1000$ at standard temperature and pressure (STP). From a quick literature review, soft tissues HU are estimated to range between $[+20; +100]$ (cf. Table 19), thus the material density of the phantom inserts should ideally be included in this range in order to mimic as much as possible tumour properties.

Table 19 Literature HU values for typical human tissues types

Material	Hounsfield Unit	Range
Cortical bone	1000+	
Diverse bone	+400 to +1000	(Das 2014), (Rao, Srirangam, and Preminger 2006)
Diverse Calcification	>+150	(Rao, Srirangam, and Preminger 2006)
- Renal tract calculus containing calcium and oxalate	+400 to +1200	(Rao, Srirangam, and Preminger 2006)
- Stones containing cysteine and uric acid	+100 to +200	(Rao, Srirangam, and Preminger 2006)
Acute haemorrhage	+50 to 90	(Rao, Srirangam, and Preminger 2006)
Clotted blood	+70	(Rao, Srirangam, and Preminger 2006)
Muscle	+50	(Das 2014), (Rao, Srirangam, and Preminger 2006)
Soft tissue	+40 to +80	(Das 2014), (Rao, Srirangam, and Preminger 2006)
- Oesophageal tumours	+35 to +70	(Kim et al. 2012)
- Right lobe liver	+50	(Lamba et al. 2014)
- Spleen	+35 to +45	(Lamba et al. 2014)
- Renal cortex	+25 to +30	(Lamba et al. 2014)
- Grey matter	+40	(Walter Huda 2010)
- White matter	+30	(Walter Huda 2010)
Water	0	(Das 2014), (Rao, Srirangam, and Preminger 2006)
Fat	-50 to -120	(Das 2014), (Rao, Srirangam, and Preminger 2006)
- Midline anterior subcutaneous fat	-100 to -115	(Lamba et al. 2014)
- Posterolateral flank subcutaneous fat	-110 to -115	(Lamba et al. 2014)
Lung	-400 to -600	(Das 2014), (Rao, Srirangam, and Preminger 2006)
Air	-1000	(Das 2014), (Rao, Srirangam, and Preminger 2006)

In order to assess the phantom materials' density, preliminary CT scans have been conducted during the manufacturing of the phantom. Those scans were acquired in the LUMC using a Biograph™ mCT PET/CT scanner (Siemens Medical Solutions) in an abdominal setting in air and water. Hounsfield units (HU) of the different phantom materials were extracted from the acquired image sequences and compared to available literature values.

The following phantom parts have been imaged:

- R05 Box and insert (V.0)
- R05 spherical inserts (V.3.2 and V.4)
- PLA cubical inserts (V.2.4)
- R05 cubical inserts (V.3.4 and V.3.6)
- PMMA phantom box (V.7)

All are presented in (Figure 45) and CT density values (HU) of the material composing them were extracted from them, namely the density of: PMMA, NBR, R05, and PLA material.

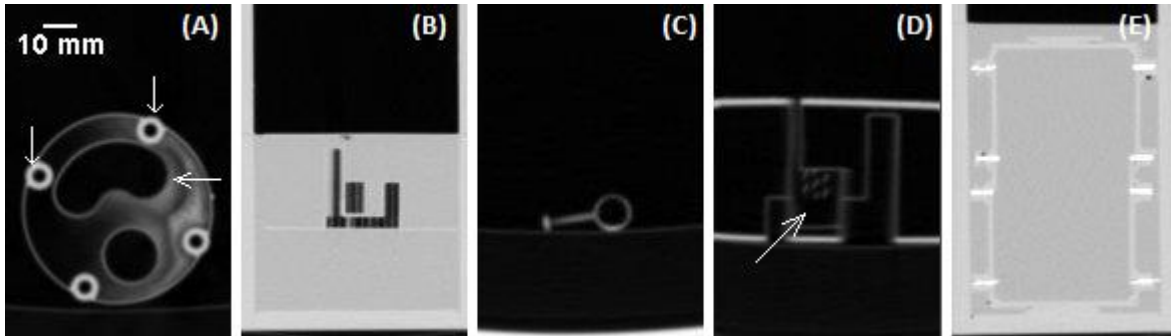


Figure 45 CT images extracted from the different parts of the phantom

Images were acquired using the Biograph™ mCT PET/CT scanner (Siemens Medical Solutions) in two different configurations (in air and in water). Only one of the two set up is presented here depending on the best contrast visualisation of the parts of interest. (A) Top view of the first SLA print of the phantom box and insert (V.0) in air, the filling corridors (vertical arrows) create non-ideal high density rings right next to the inserts shapes (horizontal arrow). (B) Transversal view of cubical insert (V.2.4) FDM printed of sin water. Trapped air (in black in the picture) is clearly visible inside the insert. (C) Transversal view of spherical insert (V.4) SLA printed of 10 mm ID in air. (D) Transversal view of cubical insert (V.3.6) SLA printed in air with clearly visible inside pillars. (E) Transversal views of phantom box (V.7) in water. Density difference between the PMMA and the rubber rings is visible.

Test results

First, known values like HU values of water and of air have been extracted from the acquired images using our protocol and compared to their known values, which are by definition respectively 0 and -1000. (Figure 46) and (Figure 47) present extracted CT density values of water and air from each images and both conclude that the extracted values of water and air using our protocol correspond to their characteristic values.

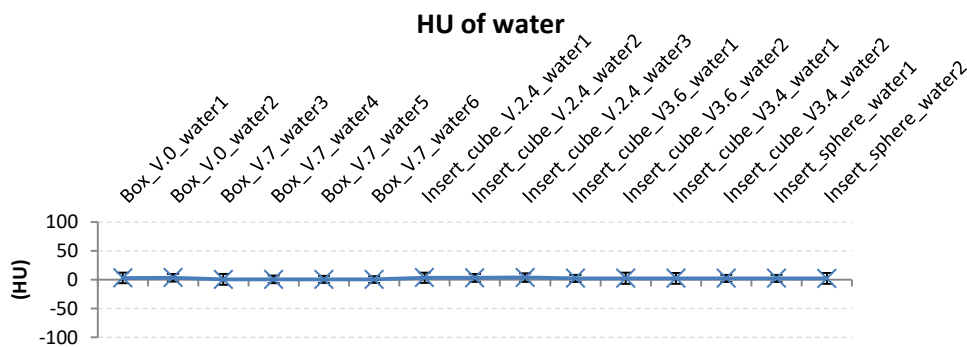


Figure 46 Retrieved CT density (HU) values of water from different imaging conditions

$HU_{WATER} = 2_{(+/-)}$ averaged value over 15 different image acquisitions and is similar to the calculated value of $HU_{AIR} = 0$. The 15 imaging conditions are named according to the code: "namepart_version_milieu" the final name number refers to the image acquisition number (first, second or third acquisition) which only differ on the slice thickness chosen (2mm, 4mm, or 5 mm). As no real differences in HU values have been noticed between each acquisition thickness the thickness is not detailed here and acquisition are only numbered.

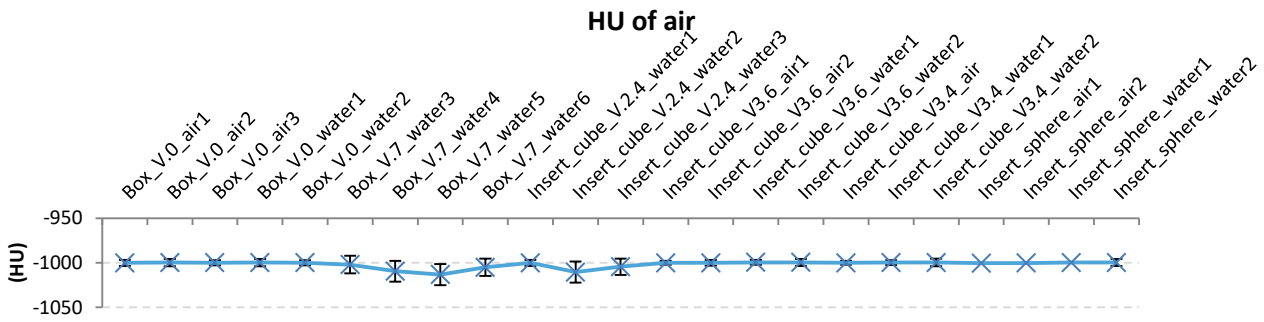


Figure 47 Retrieved CT density (HU) values of air from different imaging conditions

$HU_{AIR} = -1002_{(+/-4)}$ averaged value over 23 different image acquisitions and is similar to the calculated value of $HU_{AIR} = -1000$.

Second, unknown values like the HU values of material composing the phantom box (i.e. NBR, PMMA) and material composing the phantom inserts (i.e. R05 or PLA) have been extracted from the acquired images following the sae protocol. These values are presented in (Figure 49), (Figure 50), (Figure 51) and (Figure 52) and summarized in a density scale presented in (Figure 53).

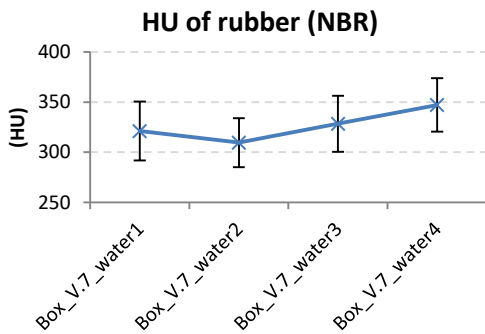


Figure 49 Retrieved CT density (HU) values of NBR $HU_{NBR} = 325_{(+/-15)}$ averaged value over four different image acquisitions

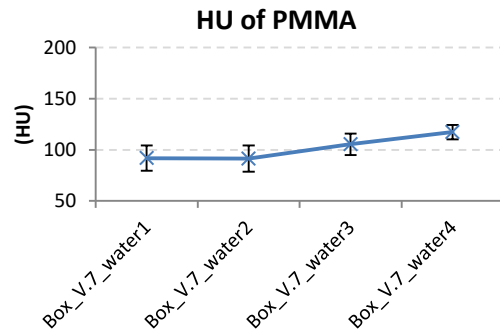


Figure 48 Retrieved CT density (HU) values of PMMA $HU_{PMMA} = 100_{(+/-15)}$ averaged value over four different acquisitions

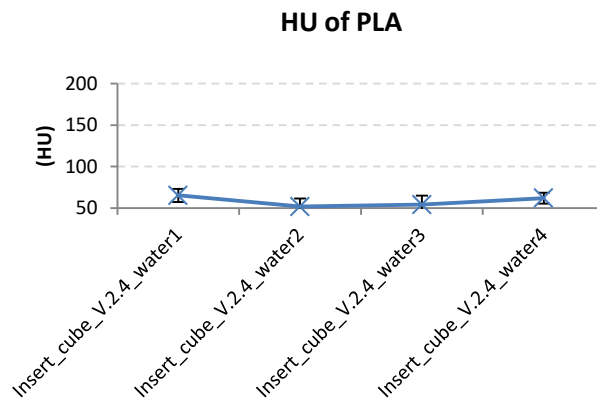


Figure 50 Retrieved CT density (HU) values of PLA $HU_{PLA} = 60_{(+/-6)}$ averaged value over four different image acquisitions

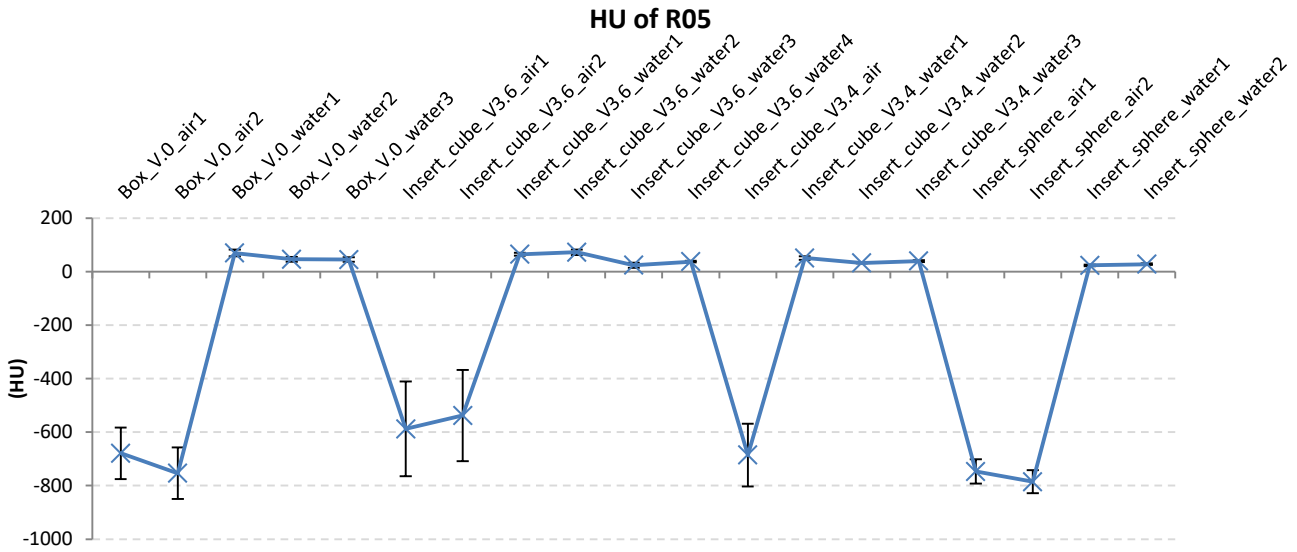


Figure 51 Retrieved CT density (HU) values of the photopolymer R05 in air and water. Two distinct values seem to appear according to the image acquisition settings (in water or in air) leading to two different values (approximately around -700 and around 50). This is due to the partial volume effect of the thin R05 walls pixel whose averaged values are lowered in due to the extremely low value of air (-1000) partially composing them. R05 density value is therefore retrieved from water (which has a less extreme value and therefore a minor effect).

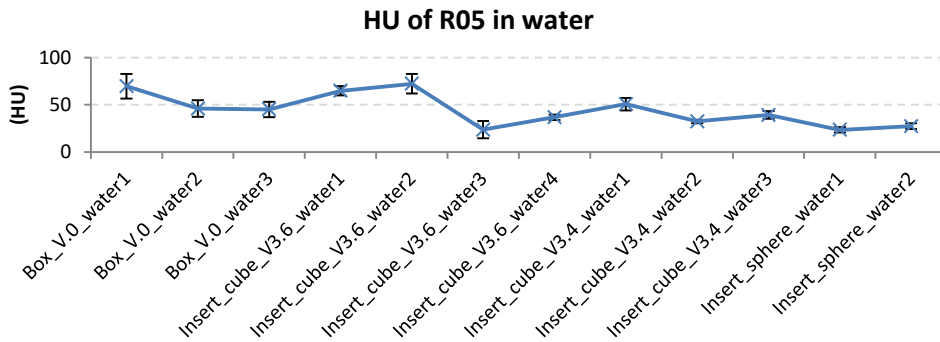


Figure 52 Retrieved CT density (HU) values of the photopolymer R05 in water only. $HU_{R05} = 45(+/ -15)$ in water averaged value over twelve different image acquisitions.

Test conclusion

From the density scale (Figure 53), selected materials (NBR, PMMA, PLA and R05) had their density compared to the expressed ideal density values required to properly mimic usual human tumour density (ranging from +20 to +100). This comparison led to the conclusion that PMMA, PLA and R05 are included in the range of proper density. However, NBR has a higher density than needed; therefore a modification of the rubber ring material should be considered in the next iteration of this project.

Remark:

PMMA has a density value is at the edge of what has been considered as ideal densities: 100 HU within an ideal range of [+20; +100]. However no modifications are implied here as PMMA is one of the most used materials in PET phantom market and no main issues have been raised from its use so far.

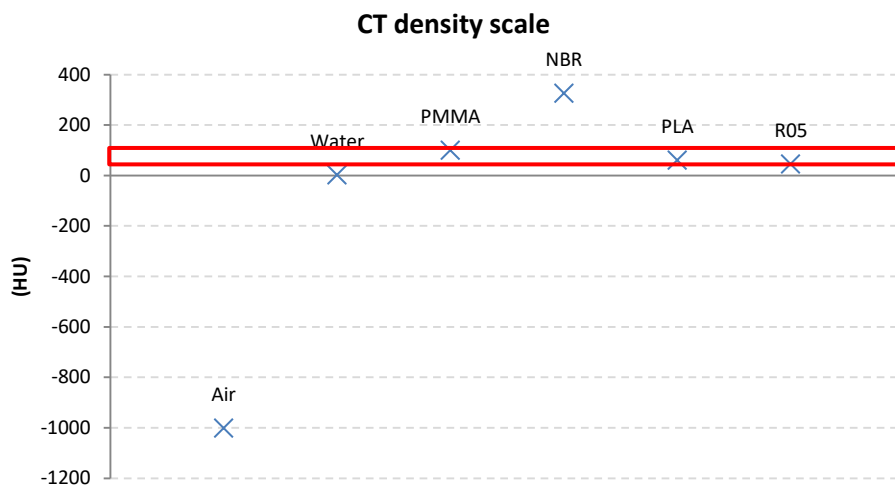


Figure 53 CT density scale (HU) from extracted values of air, water, PMMA, NBR, PLA and R05

As explained at the beginning of this section, this test has been run to check whether the material used for the phantom had a density that matches the usual tumour density [+20; +100]. All the extracted values $HU_{PMMA}=100_{(+/-15)}$, $HU_{PLA}=60_{(+/-6)}$, $HU_{R05}=45_{(+/-15)}$ apart from $HU_{NBR}=325_{(+/-15)}$ are included in this range. A modification of the rubber sealing material is therefore suggested as a recommendation for the continuation of the project.

5.1.5 POST-MANUFACTURING CUBICAL INSERT PILLARS INFLUENCE TEST

Third, once produced, the cubical inserts inner pillar needed to be imaged to analyse their influence on CT density and radioactivity concentration. These pillars have been added inside of the cubical inserts in order to slightly influence the global concentration of radioactivity contained in the insert at that position. By adding an extra material the global radioactivity concentration contained in a specific volume should be lowered as there is less space for the radioactive solution in that cube. However, the design and development of non-leaking cubical inserts not being complete yet, the influence of such pillars on radioactivity concentration has not been tested yet. However, a CT density analysis regarding these pillars influence on CT images has been conducted. It was done to verify that the pillars circumference is small enough to not be seen on PET or CT images.



Figure 54 CT acquisition of semi filled cubical insert

CT images of 0.58x0.58x2mm (left) and 0.58x0.58x5mm (right) extracted using the Biograph™ mCT PET/CT scanner (Siemens Medical Solutions). The ROIs in yellow on the images are 8.20 by 8.20 mm squares and represent a cube size as designed by the author. Usually

To this end, CT images were acquired of a SLA printed version of cubical insert V.3.6 (cf. Figure 45). From these images, ROIs of 8.20x8.20mm were selected centred on the pillars localisation and their mean value measured. These ROIs have a mean grey value of approximately – 870 HU, which is slightly different than the rest of the cubical insert inside grey value which is around – 990 HU. This proves that the addition of small pillars within a volume influences a little the CT values of this volume. By averaging the surrounding volume environment CT density (HU_{BG}) with the CT density of the plastic composing the pillars (HU_P), the global volume CT density value (HU_V) differs from both environment and plastic values. Here, for example, the pillars higher the CT density of the volume as the pillars has a higher density ($HU_P = HU_{R05} = 45$) than the surrounding milieu: air ($HU_{AIR} = -1000$) leading to a global HU of the volume around $HU_V = -870$.

Test conclusion

Therefore the use of pillars seems influence a little the CT density of one of our phantom's cube. Which is an undesired effect as those CT values are used to correct PET images during reconstruction. Ideally the pillars should be thin and small enough to not be seen on PET nor CT images, should not influence much the CT density of the volume while still impacting the PET radioactive concentration values in the volume

As PET images have a transverse resolution around 5mm (Saha 2010) the size of the tested pillars (1mm diameter) would be averaged in a non-visible entity within PET images. However they are still slightly visible and slightly influencing CT images but we will consider here that the pillars effect on CT images stays minimal.

One should not forget that another image acquisition using radioactivity still needs to be performed to fully evaluate the influence of a porous material (i.e. the addition of small pillars within a volume) on a radiotracer activity concentration in PET/CT images.

At the end, all of these post-manufacturing validation tests (§5.1.2 Post-manufacturing spherical inserts circularity test, §5.1.3 Post-manufacturing phantom water absorption test, §5.1.4 Post manufacturing phantom CT density test and §5.1.5 Post-manufacturing cubical insert pillars influence) validate the produced PET phantom parts separately. All these parts can now be assembled and tested as a whole.

5.1.6 POST-ASSEMBLY LEAKAGES TESTS

While assembling the different phantom parts of the validated PET phantom, leaks appeared at the junction of several interfaces (Figure 55) (Figure 56). Different closing and sealing techniques were therefore tested for both spherical inserts closing (Table 20) and segment assembling (Table 21).



Figure 55 Assembly of the spherical inserts with their holding plate, leaks appear at the bottom of the plat where each sphere is closed by a M3 screw

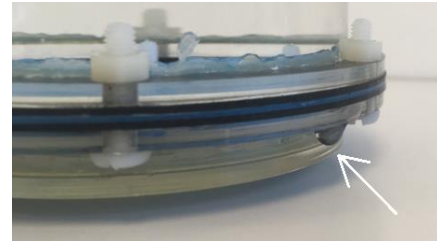


Figure 56 Assembly of imaging segment (top) with an insert plate (blue), and a bottom segment held by M4 screws and bolt with a leak (arrow).

First sealing processes of the spherical inserts were developed and tested as presented in (Table 20). From these tests, the assembly M3 screws + large rubber O-ring + plastic ring was selected as a sealing process for the spherical insert closing.








Tested closing process		Results
	M3 screws alone	✗
	M3 screws + large rubber Oring	✗
	M3 screws + thin rubber Oring	✗
	M3 screws + large rubber Oring + fiber ring	✓
	M3 screws + thin rubber Oring + fiber ring	✗
	M3 screws + large rubber Oring + plastic ring	✓
	M3 screws + thin rubber Oring + plastic ring	✓ but screw deformation

Table 20 Tested configuration overview for spherical insert closing leak tests

Second, sealing process of the segment junction was developed and tested as presented in (Table 21). First, different screws types have been tested: screws alone, screws and bolts, hexagonal screws, flat head screws. But the results of changing screws were non-conclusive. Second, plate shapes have been tested: blue plate V.6.1 having extrusion with an angle of 90 degrees versus white plate V.6.2 with a small slope extrusion of 45 degrees). But the influence of plate shape was not conclusive. Third, flanges with 12 screws have been tested (from phantom box V.9 design). The addition of screws in flanges was planned to reduce the strength applied to each of the screws and to homogeneously compress the rubber gasket all around the flange using more pressure points. The first test with this 12 screws flange was not conclusive. However the second test was. This second test used an insert plate which had been smoothed with thin sand paper. This drastically reduced the irregularity at the plate surface which was manufactured via FDM 3D printing. This sec-

and conclusive test led to the deduction that neither the screws type, size nor the plate shape influence a junction seal; but it is the smoothness of each interface surface that really matters. Fourth, to confirm this conclusion, extra tests were realized using smaller and smaller rubber rings. And all of them were conclusive when using smooth surfaces and confirmed that the sealing only holds when using a smoother flat surface.




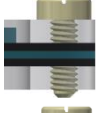


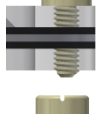


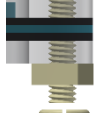


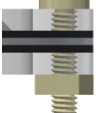


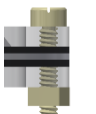


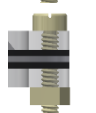





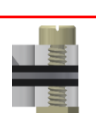
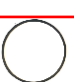

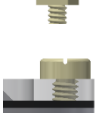


	Tested closing process	Gasket shape	Results
	6x hexagonal M4 screws + 6 holes gasket + blue plate (V.6.1)		
	6x Flat M4 screws + 6 holes gasket + blue plate (V.6.1)		
	6x Flat M4 screws + 6 holes gasket + flatter white plate (V.6.2)		
	6x Flat M4 screws + bolt + 6 holes gasket + blue plate (V.6.1)		
	6x Flat M4 screws + bolt + 6 holes gasket + flatter white plate (V.6.2)		
	12x Flat M3 screws + bolt + 12 holes gasket + flatter white plate (V.7)		
	12x Flat M3 screws + bolt + 12 holes gasket + smoother & flatter white plate (V.7)		
	12x Flat M3 screws + bolt + 12 holes thinner gasket + smoother & flatter white plate (V.7)		
	12x Flat M3 screws + bolt + thin rubber o-ring + smoother & flatter white plate (V.7)		
	6x Flat M4 screws + bolt + thin rubber o-ring + smoother & flatter white plate (V.6.2)		

Table 21 Tested configurations overview for assembly leak tests

Test conclusion:

These tests give a better understanding of sealing processes in general and conclude that the width of a rubber does not especially matter, the pressure applied on it and the smoothness of the surface it seals do. From all of these tests on segment junction, the assembly of twelve M3 screws or six M4 screws + thin rubber O-ring + smoother and flatter plate were selected as a sealing process for the phantom box closing. This is ideal as the NBR rubber gasket CT density is quite high (~300HU), recuing the material width to a minimum is therefore always good.

Remark:



M3 and M4 screws tested here are made of nylon 6.6. This material is relatively deformable; therefore elongation and changes in the threading of the screws appeared when applying a lot of strength while screwing (cf. Figure 57). This can be overcome when increasing the number of screws leading to a spreading of the strength on more screws and thus less individual stress for each screw

Figure 57 Picture of a M3 screw elongation of 1.27 mm (left) compared to a normal M3 screw with a global height of 12.5 mm (right)

5.1.7 POST-ASSEMBLY ESTIMATED IRRADIATION TIME

As the design evolved from 6 assembling screws per flanges (design box V.7) to 12 screws per flanges (design box V.9) during the Master thesis, a quick evaluation of the additional needed time to completely assemble the prototype was conducted. From this additional time the additional irradiation received by the user of the phantom has been evaluated in order to check the relative hazard caused by the designed phantom.

First, setting up the V.7 phantom and fastening all of its 36 screws takes approximately 30 minutes. The additional time needed to fasten 36 additional screws is therefore estimated to 30 more minutes. Leading to a set up time of at least 1 hour for phantom (V.9).

We consider now using spherical inserts in the phantom and calculate the relative absorbed dose it implies to the user. NEMA guidelines give a good estimation of radioactivity concentration used during phantom measurement with spherical inserts. Usually the NEMA phantom background activity concentration is set to 5.3 kBq/cc and its hot spheres are filled with N time the background concentration (N=4 or 8) (NEMA 2001a). Here, each phantom segment is a cylinder of r=4cm by h=4.2 containing five spheres (2 of 0.5cm, 2 of 0.85cm and 1 of 1.1cm inside radius). Two spheres (0.5cm and 0.85cm) are filled 8 times the background concentration and three (0.5cm, 0.85cm and 1.1 cm) are filled with four time the background concentration. As the phantom is composed of three of three segments, the total phantom activity is three time the activity contained in one these segments.

Activity of the phantom in a three spherical inserts configuration

$$A_{TOT} = 3 \times (A_{SEGMENT})$$

$$A_{TOT} = 3 \times (A_{BG} + A_{SPHERES})$$

$$A_{TOT} = 3 \times ((AC_{BG} \times V_{BG}) + (AC_{SPHERES} \times V_{SPHERES}))$$

$$A_{TOT} = 3 \times \left[\begin{aligned} &5.3 \frac{kBq}{cc} \times (4.2 \times 2\pi \times 4^2) cc \\ &+ 8 \times 5.3 \frac{kBq}{cc} \times \left(\frac{4}{3}\pi \times 0.5^3 + \frac{4}{3}\pi \times .85^3 \right) cc \\ &+ 4 \times 5.3 \frac{kBq}{cc} \times \left(\frac{4}{3}\pi \times 0.5^3 + \frac{4}{3}\pi \times .85^3 + \frac{4}{3}\pi \times 1.1^3 \right) cc \end{aligned} \right]$$

$$A_{TOT} = 3 \times (2236kBq + 131kBq + 183kBq)$$

$$A_{TOT} = 3 \times 2550 kBq$$

$$A_{TOT} = 7.5 MBq$$

Absorbed radiation dose rate $D_{T\ rate}$ for annihilation photons

Its estimation of radiation dose is difficult, it depends on the geometry of the source and whether shielding is used. Although the calculations itself may be correct it is difficult to calculate accurately the dose to the operator. However a global estimation is given as following:

$$D_{T\ rate} = 0.2 (\mu Gy/s)$$

from rule of thumb at 30cm away from a gamma point source of 511keV

Absorbed radiation dose D for a manipulation time of 1h

$$D_T = D_{T\ rate} \times Time = 0.2\mu Gy \times 60s$$

$$D_T = 11 (\mu Gy)$$

Equivalent dose H_T using radiation weighting factor W_R

$$H_T = \sum_R D_{T,R} \cdot W_R \text{ (Sv)}$$

Effective dose E , with all part of the body uniformly irradiated using

- radiation weighting factor of $W_R=1$ for photon and electrons
- tissue weighting factor of $W_T=1$ for the whole body

$$E = \sum_T H_T \cdot W_T = \sum_T \sum_R D_{T,R} \cdot W_R \cdot W_T = \sum_T \sum_R D_{T,R} \times 1 \times 1 = D_{T,R}$$

$$E = 11 \text{ (}\mu\text{Sv)}$$

The estimated effective dose received while screwing the 12 screws flanges is grossly around 11 μSv , which is way lower than the population limit of 50mSv/year. However this dose relates to β^+ irradiation which is mainly shielded by the PMMA plastic composing the phantom wall. Therefore a 12 screws design is still considered possible although not ideal regarding the potential hazard it generates.

More over the manipulation time here is set to 1h; which is quite long for assembling the phantom. This estimation does not take into account the learning curve or the user filling and while handling the phantom, 1h was the set-up time needed for the first test done with this phantom. It is probable that next set-up times will be faster.

5.1.8 FDG PET/CT IMAGING TEST AND PROOF OF CONCEPT

Finally a FDG PET/CT test acquisition is performed as a proof of concept of the study solution. This acquisition aims at verifying if the designed PET phantom properly functions. The tested phantom was assembled with five spherical inserts (10, 10, 17, 17 and 22 ID mm as positioned in Figure 58) and locked within the NEMA body PET phantom as shown in (Figure 59).

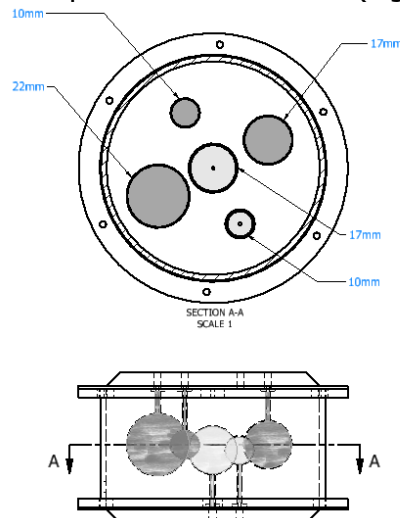


Figure 58 Transversal section view (top) and side view (bottom) of the tested PET phantom segment which contains spherical inserts

Two spheres of 17mm ID and 10mm ID are filled with a high radioactivity concentration (C1) in light grey in (Figure 59). Three other spheres (22mm, 17mm and 10mm ID) are filled with a lower radioactivity concentration (C2) in darker grey in (Figure 59). The segment itself is filled with a third lower concentration (C3) and placed inside the NEMA box phantom filled with the fourth lower concentration (C4) (cf. Figure 59).



Figure 59 PET phantom assembly of all the segments including the one containing the spherical inserts before filling (center).

According to (NEMA 2001b) the usual radioactivity concentrations needed in spherical PET phantom should be 5.3 kBq/mL (0.14 mCi/mL) within +/- 5% for the concentration of the background activity and a concentration of N times (N=4 or 8) that of the background for hot lesions (i.e. for spheres). Therefore, four different radioactivity concentrations should be used for the experiment:

- C4=1xbackground (5.3 kBq/mL)
- C3=2xbackground (10.6 kBq/mL)
- C2=4xbackground (21.2 kBq/mL)
- C1=8xbackground (42.4 kBq/mL)

In reality the concentrations injected during the test were approximately

- C4=1xbackground (3.4 kBq/mL @17:05)
- C3=2.5xbackground (8.5 kBq/mL @17:05)
- C2=3.5xbackground (12 kBq/mL @17:05)
- C1=6.7xbackground (23 kBq/mL @17:05)

Once the phantom filled, PET/CT images like (Figure 60) of this assembly were acquired using the Biograph™ mCT PET/CT scanner (Siemens Medical Solutions) with two bed positions and 15min per bed position. Six reconstructions were extracted from it as detailed in (Table 22). From these reconstructions and from the best image reconstruction (#6: TrueX + TOF + 900s + 512px + FWHM 5) a grey value analysis of the spheres was performed.

Reconstruction #	Reconstruction method	Time (s)	Image size	FWHM
1	TrueX + TOF	900	180	5
2	Iterative + TOF	900	180	5
3	TrueX + TOF	900	360	3
4	TrueX + TOF	600	360	3
5	TrueX + TOF	300	360	3
6	TrueX + TOF	900	512	3

Table 22 Chosen reconstruction parameters for the PET/CT image acquisition validation test

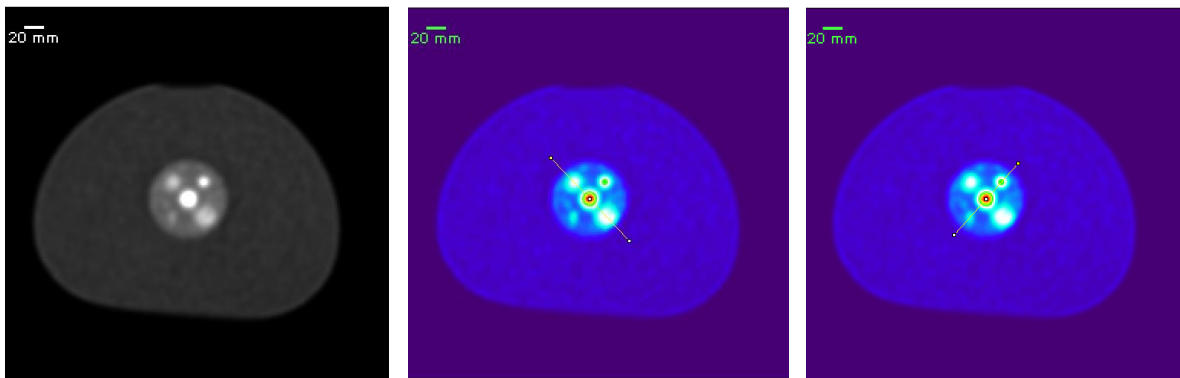


Figure 60 Transversal view of the PET image reconstructed with set up #6, grey colour scale (left); thermal colour scale (centre) and (right)

As presented in (Figure 61 and Figure 62) spheres intensity is a bit lower than the true intensity contained inside them in particular for small spheres with a low radioactivity concentration (such as the small sphere of 10mm ID filled with 12 kBq/mL) . This can be explained by the PV effect inherent of PET scanners, the image reconstruction effects or by the large amount of unknown variables for calculating the true activity concentrations.

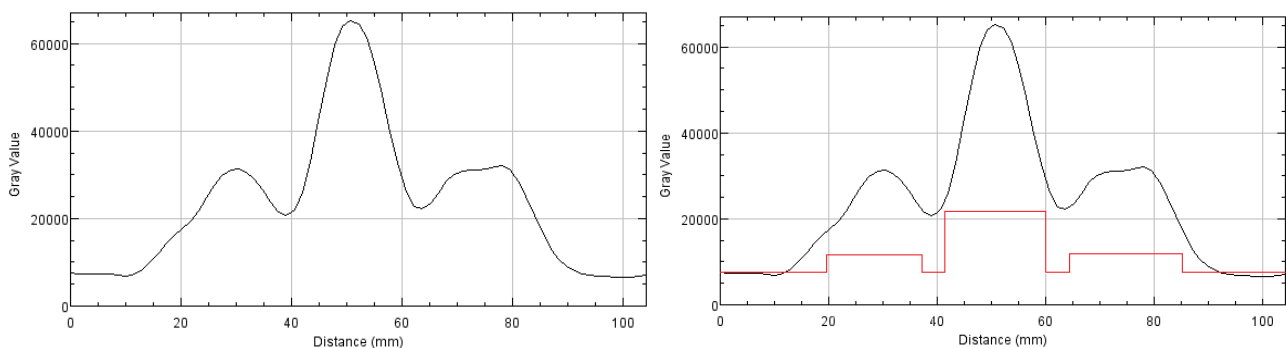


Figure 61 Plot line of grey values from (Figure 60) containing spheres of 17mm, 17mm, and 22mm ID (left). Each spheres true concentration and background are added in red (left).

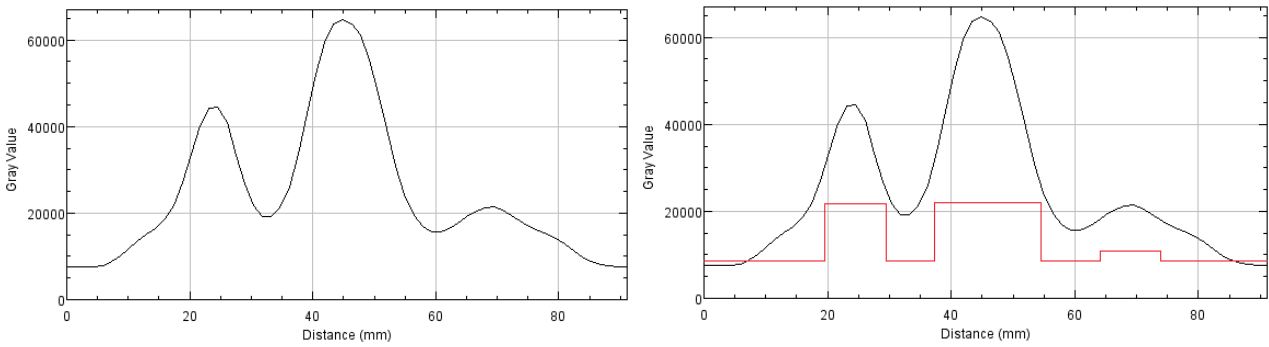


Figure 62 Plot line of grey values from (Figure 60) containing spheres of 10mm, 22mm and 10mm ID. Each spheres true concentration and background are added in red (left)

However if the plot lines are compared to the concentration ratio (1, 2.5, 3.5, or 6.7 time the background where the background is extracted from the images around 10 000 grey level) (in green in Figure 63) instead of compared to the grey value they were supposed to have (in red in Figures 60 and 61). Then the plot lines are closer to the sphere concentration ratio than to their actual radioactivity concentration. This suggests that probably the estimation of the radioactivity concentration is unprecise however the ratios match.

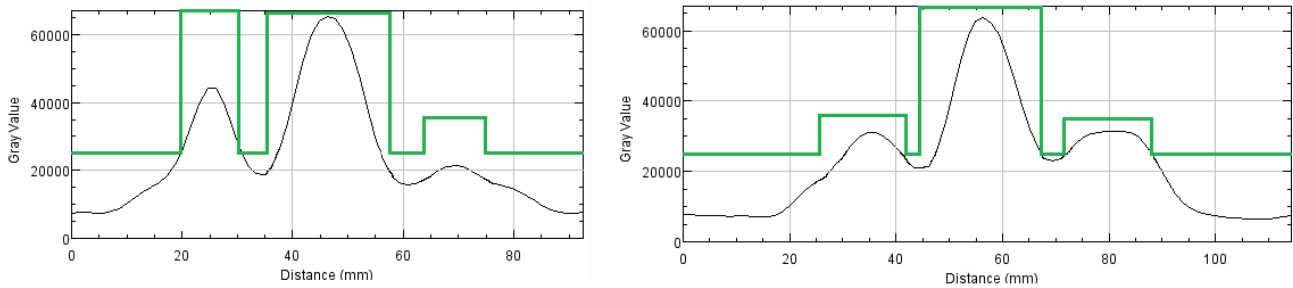


Figure 63 Plot line of grey values from (Figure 60) containing (left spheres of 10mm, 22mm and 10mm ID and 17mm, 22mm, 17mm ID (right)) Green line represents the ratio (1, 2.5, 3.5 or 6.7 time the background) of each spheres

At the end, this validation test proves the concept of the designed and developed spherical inserts. Further analysis of the data is still possible but will not be described in this report.

6

CHAPTER 6: RECOMMENDATIONS

At the end, all the limitations faced during the Master thesis and the validation tests results led to the creation of a list of recommendations that is introduced here in this sixth chapter.

This list of requirement is separated in four big categories: (1) insert development, (2) box development, (3) background improvement and (4) image acquisition.

Inserts design could be improved by

- Finishing to develop and print the cubical inserts
- PET image acquisition using radioactivity to analyse the influence of adding small pillars within a volume on the volume's radioactivity concentration.
- Improving the design of the cubical insert by closing the cubical inserts
- SLA printing of other geometric and easy shapes (donnuts, gaussians, etc) (cf. Figure 64)
- Literature review using PET/CT data base of tumour images to define the most usual tumour shapes and adapt these shape in a complex asymmetric and random insert design
- Exploiting the porousness of pillars within a small volume



Figure 64 Geometric shapes that can be developed later on

Box design could be improved by:

- Finishing the construction of a proper sealed prototype (V.8 and/or V.9)
- Improving the filling and closing time of the box by a new design
- Developing inserts with heterogeneous density (4D phantom)

Background representation in the PET phantom could be defined and improved by

- developing realistic shapes within the background of the PET phantom box
- developing heterogeneous density within the background of the PET phantom box

Lastly, image acquisition of the developed PET phantom could be further analysed by

- Using the new PET/CT scanner from Philip recently installed in the LUMC

This page is intentionally left blank

7

CHAPTER 7: CONCLUSION

This report summarizes the Master thesis research study completed in partial fulfilment of the Biomedical Engineering Master of Science specialized in Medical Physics. In this study, a new heterogeneous PET phantom allowing an extensive understanding of the key concept of heterogeneity quantification in PET images is designed, developed, tested and partially validated.

First, a preliminary phase of the Master study was conducted. This phase aimed at collecting, analysis and processing theoretical knowledges contextualising the research project. From this literature study and the highlighted gaps found in it, a precise research solution was proposed namely, the "Design and fabrication of a new heterogeneous PET phantom to improve heterogeneity quantification". To ensure the novelty of such a solution, its relevance has been checked. After this analysing phase, all the key elements needed to design and develop a new research solution are known, which introduced the second phase of the study: the definition of a design method and its processes.

Second, a definition of the design method and process was done directly following the literature review. This phase permitted to define the design approach that will be followed during the entire research study: from the preliminary design of the solution to its final prototype. Among all the different available design methods, we chose here to separate the Master thesis in four main phases: (1) already done analysis phase, currently done methodology phase (2), followed by upcoming design and development phase (3) and finishing with a last test, analysis and validation phase (4). The planned methodology was quick and straightforward. However, in reality, a lot of limitations and unforeseen events forced the design process to become more complex in an unpredicted way leading to the creation of several parallel design branches and various feedback loops and interaction between the phase (3) and (4).

Third, the study focussed on its "Design and Development" phase. In this phase, the design of the phantom has rapidly been split in two parallel designs: the design of the phantom box was separated from the design of its inserts parts. Moreover, the inserts design quickly evolved into the design of two different types of inserts: spherical inserts (inserts A) and cubic inserts (Inserts B). These three parallel designs were especially convenient during unforeseen events like material delivery delays, machine maintenance, or staff holiday, permitting to switch from one bottlenecked design to another one. Ultimately this permitted to be way more time efficient. However, iterations and updates of the designs were arising from almost all the different. Each separate pieces specifications like their size, shape, material... influenced the design other pieces. At the end, unforeseen events, impossible trade-offs and the interconnection of each design created a quite complex environment which was limiting the global speed of the project. Due to the limited allocated time, short cuts were made during the design and development phase of the Master thesis to only develop working pieces of the PET phantom instead of a global non-working entity.

Fourth, to this and a test and validation phase was conducted in parallel of the design and development phase. This step checked whether the produced pieces of the phantom fulfil their requirement and can be incorporated in our global PET phantom solution. In this phase pre manufacturing glue selection test, post manufacturing sphere circularity test, insert water absorption test, material density validation test, and cubical inset pillars influence test. This phase served also as a proof of concept of the semi-finalised research solution where a FDG PET/CT test was performed.

Globally, the practical contribution of the Master study can be separated in four main contributions. First, an extensive analysis of the literature performed to understand the issue regarding PET heterogeneity quantification and the current gaps in the literature that were needed to be filled. Due to the total novelty of this project, this analysis phase was considered as a key step of the project and a lot of efforts were put in this contribution to properly define the set-ups and direction of the project.

Second, once the project direction was defined, a clear description of a research solution was completed which constitutes the second main contribution of the study. Precise requirements of the solutions were listed according to current the state of the art of PET phantom limitations and regarding the global aim of the study. From the detailed solution specifications, a design could be developed.

Third, then, the design and development of a partial solution proceeded and constitute the third main contribution of the study. This contribution is the central point of the study as it aims at specifically answering the project problem. The solution development yields to several sub-contributions: an entire phantom box which unfortunately leaks, a working sealed spherical insert box, and a final cubical insert design that need to be printed. Besides these developed objects other contribution arise from the Master thesis, all in the form of: design process definition and workflow, design files and engineering drawings, manufacturing techniques and knowledges regarding PET phantom creation, limitations solution and usual trade-off faced while designing an object. At the end, of these sub-contributions expend the research solution development contribution with gained knowledges and additional produced information.

Last, the fourth contribution of the study stems from the limitation and un-resolved issues faced while developing the study solution. This last contribution is the creation of recommendations and suggestion of new directions for further work regarding this project.

In the end, the prior design and development phase of the research happened to be more difficult and time consuming than expected, which limited the number of validation tests conducted on the developed solution. But the Master thesis still reached its goal of designing and developing a brand new kind of PET phantom that now can be easily upgraded with complex heterogeneous inserts of mixed shapes and density. This research solution is fully functional and can also be used in numerous applications. This, however, should not prevent further updates of the PET phantom design to have something enhanced that is more practical and easily fillable for the user for example. As the project is very new, there is still room for a lot of improvement and applications.

REFERENCES

- Aerts, Hugo J W L, Emmanuel Rios Velazquez, Ralph T H Leijenaar, Chintan Parmar, Patrick Grossmann, Sara Cavalho, Johan Bussink, et al. 2014. "Decoding Tumour Phenotype by Noninvasive Imaging Using a Quantitative Radiomics Approach." *Nature Communications* 5 (June). Nature Publishing Group: 4006. doi:10.1038/ncomms5006.
- ASTM international. 2010. "D570-98 (2010): Standard Test Method for Water Absorption of Plastics." *ASTM Standards* 98: 25–28. doi:10.1520/D0570-98R10E01.2.
- Bazañez-Borgert, Marisa, Ralph A. Bundschuh, Michael Herz, Maria Jose Martínez, Markus Schwaiger, and Sibylle I. Ziegler. 2008. "Radioactive Spheres without Inactive Wall for Lesion Simulation in PET." *Zeitschrift Fur Medizinische Physik* 18 (1): 37–42. doi:10.1016/j.zemedi.2007.06.001.
- Berthon, B., C. Marshall, A. Edwards, M. Evans, and E. Spezi. 2013. "Influence of Cold Walls on PET Image Quantification and Volume Segmentation: A Phantom Study." *Medical Physics* 40 (8). American Association of Physicists in Medicine: 82505. doi:10.1118/1.4813302.
- Berthon, B, C Marshall, R Holmes, and E Spezi. 2015. "A Novel Phantom Technique for Evaluating the Performance of PET Auto-Segmentation Methods in Delineating Heterogeneous and Irregular Lesions." *EJNMMI Physics* 2 (1): 13. doi:10.1186/s40658-015-0116-1.
- Boellaard, Ronald, Nanda C Krak, Otto S Hoekstra, and Adriaan A Lammertsma. 2004. "Effects of Noise, Image Resolution, and ROI Definition on the Accuracy of Standard Uptake Values: A Simulation Study." *Journal of Nuclear Medicine* 45 (9): 1519–27. <http://jnm.snmjournals.org/content/45/9/1519.full.pdf>.
- Boellaard, Ronald, Wim J. G. Oyen, Corneline J. Hoekstra, Otto S. Hoekstra, Eric P. Visser, Antoon T. Willemsen, Bertjan Arends, et al. 2008. "The Netherlands Protocol for Standardisation and Quantification of FDG Whole Body PET Studies in Multi-Centre Trials." *European Journal of Nuclear Medicine and Molecular Imaging* 35 (12). Springer-Verlag: 2320–33. doi:10.1007/s00259-008-0874-2.
- Brook, Frank J., and Perry W Grigsby. 2015. "Low-Order Non-Spatial Effects Dominate Second-Order Spatial Effects in the Texture Quantifier Analysis of 18F-FDG-PET Images." *PLoS ONE* 10 (2). doi:10.1371/journal.pone.0116574.
- Brooks, Frank J. 2013. "On Some Misconceptions about Tumor Heterogeneity Quantification." *European Journal of Nuclear Medicine and Molecular Imaging*. doi:10.1007/s00259-013-2430-y.
- Brooks, Frank J, and Perry W Grigsby. 2013. "FDG Uptake Heterogeneity in FIGO IIB Cervical Carcinoma Does Not Predict Pelvic Lymph Node Involvement." *Radiation Oncology* 8 (1): 294. doi:10.1186/1748-717X-8-294.
- . 2014. "The Effect of Small Tumor Volumes on Studies of Intratumoral Heterogeneity of Tracer Uptake." *Journal of Nuclear Medicine* 55 (1): 37–42. doi:10.2967/jnumed.112.116715.
- Carles, M, I Torres-Espallardo, A Alberich-Bayarri, C Olivas, P Bello, U Nestle, and L Martí-Bonmatí. 2017. "Evaluation of PET Texture Features with Heterogeneous Phantoms: Complementarity and Effect of Motion and Segmentation Method." *Physics in Medicine and Biology* 62 (2). IOP Publishing: 652–68. doi:10.1088/1361-6560/62/2/652.
- Chalkidou, Anastasia, Michael J. O'Doherty, and Paul K. Marsden. 2015. "False Discovery Rates in PET and CT Studies with Texture Features: A Systematic Review." *PLoS ONE* 10 (5): 1–18. doi:10.1371/journal.pone.0124165.
- Cheng, Nai Ming, Yu Hua Dean Fang, Din Li Tsan, Ching Han Hsu, and Tzu Chen Yen. 2016. "Respiration-Averaged CT for Attenuation Correction of PET Images - Impact on PET Texture Features in Non-Small Cell Lung Cancer Patients." *PLoS ONE* 11 (3). doi:10.1371/journal.pone.0150509.
- Cheng, Nai Ming, Yu Hua Dean Fang, and Tzu Chen Yen. 2013. "The Promise and Limits of PET Texture Analysis." *Annals of Nuclear Medicine*. doi:10.1007/s12149-013-0759-8.
- Chu, A, C M Sehgal, and J F Greenleaf. 1990. "Use of Gray Value Distribution of Run Lengths for Texture Analysis." *Pattern Recognition Letters* 11 (6): 415–19. doi:10.1016/0167-8655(90)90112-F.
- Cook, Gary J R, Eva A Wegner, and Ignac Fogelman. 2004. "Pitfalls and Artifacts in 18FDG PET and PET/CT Oncologic Imaging." *Seminars in Nuclear Medicine*. doi:10.1053/j.semnuclmed.2003.12.003.
- Cortes-Rodicio, J., G. Sanchez-Merino, M.A. Garcia-Fidalgo, and I. Tobalina-Larrea. 2016. "Identification of Low Variability Textural Features for Heterogeneity Quantification of 18F-FDG PET/CT Imaging." *Revista Española de Medicina Nuclear E Imagen Molecular* 35 (xx): 2–7. doi:10.1016/j.remnm.2016.04.002.
- Das, B. K. 2014. *Positron Emission Tomography: A Guide for Clinicians*. doi:10.1007/978-81-322-2098-5.
- Dasarathy, Belur V, and Edwin B Holder. 1991. "Image Characterizations Based on Joint Gray Level-Run Length Distributions." *Pattern Recognition Letters* 12 (8): 497–502. doi:10.1016/0167-8655(91)80014-2.
- Desseroit, Marie-Charlotte, Florent Tixier, Wolfgang A. Weber, Barry A Siegel, Catherine Cheze Le Rest, Dimitris Visvikis, and Mathieu Hatt. 2017. "Reliability of PET/CT Shape and Heterogeneity Features in Functional and Morphologic Components of Non-Small Cell Lung Cancer Tumors: A Repeatability Analysis in a Prospective Multicenter Cohort." *Journal of Nuclear Medicine* 58 (3): 406–11. doi:10.2967/jnumed.116.180919.

- DiFilippo, Frank P., James P. Price, Daniel N. Kelsch, and Raymond F. Muzic. 2004. "Porous Phantoms for PET and SPECT Performance Evaluation and Quality Assurance." *Medical Physics* 31 (5). American Association of Physicists in Medicine: 1183–94. doi:10.1118/1.1711416.
- Doumou, Georgia, Musib Siddique, Charalampos Tsoumpas, Vicky Goh, and Gary J Cook. 2015. "The Precision of Textural Analysis in 18F-FDG-PET Scans of Oesophageal Cancer." *European Radiology* 25 (9): 2805–12. doi:10.1007/s00330-015-3681-8.
- Elmpt, Wouter van, Catharina M L Zegers, Bart Reymen, Aniek J G Even, Anne Marie C Dingemans, Michel Oellers, Joachim E. Wildberger, et al. 2016. "Multiparametric Imaging of Patient and Tumour Heterogeneity in Non-Small-Cell Lung Cancer: Quantification of Tumour Hypoxia, Metabolism and Perfusion." *European Journal of Nuclear Medicine and Molecular Imaging* 43 (2): 240–48. doi:10.1007/s00259-015-3169-4.
- EnvisionTEC. 2015. "Perfactory® Materials: Photopolymer R05: Safety Data Sheet according to Regulation (EC) No . 1907 / 2006 (REACH)." Vol. 2006.
- . 2017. "Perfactory® Materials: Photopolymer R05: Description Sheet."
- Fletcher, James W, Benjamin Djulbegovic, Heloisa P Soares, Barry A Siegel, Val J Lowe, Gary H Lyman, R Edward Coleman, et al. 2008. "Recommendations on the Use of 18F-FDG PET in Oncology." *Journal of Nuclear Medicine* 49 (3): 480–508. doi:10.2967/jnumed.107.047787.
- Forgacs, Attila, Hermann Pall Jonsson, Magnus Dahlbom, Freddie Daver, Matthew D. DiFranco, Gabor Opposits, Aron K. Krizsan, Ildiko Gara, and Johannes Czernin. 2016. "A Study on the Basic Criteria for Selecting HeterogeneityParameters of F18-FDG PET Images." *PLoS ONE* 11 (10). doi:10.1371/journal.
- Galavis, Paulina E, Christian Hollensen, Ngoneh Jallow, Bhudatt Paliwal, and Robert Jeraj. 2010. "Variability of Textural Features in FDG PET Images due to Different Acquisition Modes and Reconstruction Parameters." *Acta Oncologica* 49 (7): 1012–16. doi:10.3109/0284186X.2010.498437.
- Galloway, Mary M. 1975. "Texture Analysis Using Gray Level Run Lengths." *COMPUTER GRAPHICS AND IMAGE PROCESSING* 4: 172–79.
- Gerlinger, Marco, Andrew J Rowan, Stuart Horswell, James Larkin, David Endesfelder, Eva Gronroos, Pierre Martinez, et al. 2012. "Intratumor Heterogeneity and Branched Evolution Revealed by Multiregion Sequencing." *N Engl J Med* 36610366 (10): 883–92. doi:10.1056/NEJMoa1113205.
- Gerlinger, M, and C Swanton. 2010. "How Darwinian Models Inform Therapeutic Failure Initiated by Clonal Heterogeneity in Cancer Medicine." *British Journal of Cancer* 103: 1139–43. doi:10.1038/sj.bjc.6605912.
- Gillies, Robert J., Paul E. Kinahan, and Hedvig Hricak. 2016. "Radiomics: Images Are More than Pictures, They Are Data." *Radiology* 278 (2): 563–77. doi:10.1148/radiol.2015151169.
- Grootjans, Willem, Florent Tixier, Charlotte S van der Vos, Dennis Vriens, Catherine C Le Rest, Johan Bussink, Wim J G Oyen, L.-F. de Geus-Oei, Dimitris Visvikis, and Eric P Visser. 2016. "The Impact of Optimal Respiratory Gating and Image Noise on Evaluation of Intratumor Heterogeneity on 18F-FDG PET Imaging of Lung Cancer." *Journal of Nuclear Medicine* 57 (11). Society of Nuclear Medicine: 1692–98. doi:10.2967/jnumed.116.173112.
- Hamill, J.J., E Arnsdorff, M.E. Casey, Xinli Liu, and WJ Raulstron. 2005. "A Ge-68 PET Hot Sphere Phantom with No Cold Shells." *Nucl Sci Symp Conf Rec* 3. IEEE: 1606–10. doi:10.1109/NSSMIC.2005.1596626.
- Hanahan, Douglas, and Robert A Weinberg. 2000. "The Hallmarks of Cancer." *Cell* 100 (1): 57–70. doi:10.1007/s00262-010-0968-0.
- . 2011. "Hallmarks of Cancer: The Next Generation." *Cell* 144: 646–74. doi:10.1016/j.cell.2011.02.013.
- Haralick, Robert M., K. Shanmugam, and Its'Hak Dinstein. 1973. "Textural Features for Image Classification." *IEEE Transactions on Systems, Man, and Cybernetics* SMC-3 (6): 610–21. doi:10.1109/TSMC.1973.4309314.
- Hatt, Mathieu, Mohamed Majdoub, M. Vallieres, Florent Tixier, C. C. Le Rest, David Groheux, E. Hindie, et al. 2015. "18F-FDG PET Uptake Characterization Through Texture Analysis: Investigating the Complementary Nature of Heterogeneity and Functional Tumor Volume in a Multi-Cancer Site Patient Cohort." *Journal of Nuclear Medicine* 56 (1): 38–44. doi:10.2967/jnumed.114.144055.
- Hatt, Mathieu, Florent Tixier, Catherine Cheze Le Rest, Olivier Pradier, and Dimitris Visvikis. 2013. "Robustness of Intratumour 18F-FDG PET Uptake Heterogeneity Quantification for Therapy Response Prediction in Oesophageal Carcinoma." *European Journal of Nuclear Medicine and Molecular Imaging* 40 (11): 1662–71. doi:10.1007/s00259-013-2486-8.
- Hatt, Mathieu, Florent Tixier, Larry Pierce, Paul E. Kinahan, Catherine Cheze Le Rest, and Dimitris Visvikis. 2017. "Characterization of PET/CT Images Using Texture Analysis: The Past, the Present... Any Future?" *European Journal of Nuclear Medicine and Molecular Imaging*. Springer Berlin Heidelberg. doi:10.1007/s00259-016-3427-0.
- Hjelmgren, Ola, Lars Johansson, Ulrica Prahl, Caroline Schmidt, Johan Fred??n-Lindqvist, and G??ran M L Bergstr??m. 2014. "A Study of Plaque Vascularization and Inflammation Using Quantitative Contrast-Enhanced US and PET/CT." *European Journal of Radiology* 83 (7): 1184–89. doi:10.1016/j.ejrad.2014.03.021.
- Hoekstra, Corneline J, Otto S Hoekstra, Sigrid G Stroobants, Johan Vansteenkiste, Johan Nuyts, Egbert F Smit, Maarten Boers, Jos W R Twisk, and Adriaan A Lammertsma. 2002. "Methods to Monitor Response to Chemotherapy in Non-Small Cell Lung Cancer with 18F-FDG PET." *Journal of Nuclear Medicine: Official Publication, Society of Nuclear Medicine* 43 (10): 1304–9.

- <http://jnm.snmjournals.org/content/43/10/1304.full.pdf>.
- Holmes, Robin B., Sandra M.A. Hoffman, and Paul M. Kemp. 2013. "Generation of Realistic HMPAO SPECT Images Using a Subresolution Sandwich Phantom." *NeuroImage* 81: 8–14. doi:10.1016/j.neuroimage.2013.05.003.
- Hull, Charles W. 1986. "Apparatus for Production of Three-Dimensional Objects by Stereolithography." *US Patent 4,575,330*, 1–16. doi:10.1145/634067.634234.
- Hunt, Dylan Christopher, Harry Easton, and Curtis B. Caldwell. 2009. "Design and Construction of a Quality Control Phantom for SPECT and PET Imaging." *Medical Physics* 36 (12). American Association of Physicists in Medicine: 5404–11. doi:10.1118/1.3250855.
- Huntsman. 2020a. "Araldite® 2020: Description Sheet." https://samaro.fr/pdf/FT/Araldite_FT_2020_EN.pdf.
- . 2020b. "Araldite® 2020: Safety Data Sheet." <http://www.farnell.com/datasheets/1521397.pdf>.
- . 2022a. "Araldite® 2022-1: Description Sheet."
- . 2022b. "Araldite® 2022-1: Safety Data Sheet." Vol. 3.
- Ide-mat. 2003. "PMMA Properties from Ide-Mat, Retrieved from Retrieved from Matbase Website." <https://www.matbase.com/material-categories/natural-and-synthetic-polymers/thermoplastics/commodity-polymers/material-properties-of-polymethyl-methacrylate-extruded-acrylic-pmma.html#properties>.
- Jaskowiak, Chris J, Jesus A Bianco, Scott B Perlman, and Jason P Fine. 2005. "Influence of Reconstruction Iterations on 18 F-FDG PET/CT Standardized Uptake Values." *J Nucl Med* 46: 424–28. <http://jnm.snmjournals.org/content/46/3/424.full.pdf>.
- Juhász, Csaba, Shalini Dwivedi, David O Kamson, Sharon K Michelhaugh, and Sandeep Mittal. 2014. "Comparison of Amino Acid Positron Emission Tomographic Radiotracers for Molecular Imaging of Primary and Metastatic Brain Tumors." *Molecular Imaging* 13. <http://www.ncbi.nlm.nih.gov/pubmed/24825818>.
- Junttila, Melissa R., and Frederic J. de Sauvage. 2013. "Influence of Tumour Micro-Environment Heterogeneity on Therapeutic Response." *Nature* 501 (7467): 346–54. doi:10.1038/nature12626.
- Kim, S. H., Ki Nam Lee, E J Kang, D W Kim, and S H Hong. 2012. "Hounsfield Units upon PET/CT Are Useful in Evaluating Metastatic Regional Lymph Nodes in Patients with Oesophageal Squamous Cell Carcinoma." *British Journal of Radiology* 85 (1013): 606–12. doi:10.1259/bjr/73516936.
- Krak, Nanda C., R. Boellaard, Otto S. Hoekstra, J. W R Twisk, Corneline J. Hoekstra, and Adriaan A. Lammertsma. 2005. "Effects of ROI Definition and Reconstruction Method on Quantitative Outcome and Applicability in a Response Monitoring Trial." *European Journal of Nuclear Medicine and Molecular Imaging* 32 (3): 294–301. doi:10.1007/s00259-004-1566-1.
- Lamba, Ramit, John P. McGahan, Michael T Corwin, Chin Shang Li, Tien Tran, J Anthony Seibert, and John M Boone. 2014. "CT Hounsfield Numbers of Soft Tissues on Unenhanced Abdominal CT Scans: Variability between Two Different Manufacturers' MDCT Scanners." *American Journal of Roentgenology* 203 (5): 1013–20. doi:10.2214/AJR.12.10037.
- Lambin, Philippe, Emmanuel Rios-Velazquez, Ralph Leijenaar, Sara Carvalho, Ruud G P M Van Stiphout, Patrick Granton, Catharina M L Zegers, et al. 2012. "Radiomics: Extracting More Information from Medical Images Using Advanced Feature Analysis." *European Journal of Cancer* 48 (4): 441–46. doi:10.1016/j.ejca.2011.11.036.
- Lasnon, Charline, Mohamed Majdoub, Brice Lavigne, Pascal Do, Jeannick Madelaine, Dimitris Visvikis, Mathieu Hatt, and Nicolas Aide. 2016. "18F-FDG PET/CT Heterogeneity Quantification through Textural Features in the Era of Harmonisation Programs: A Focus on Lung Cancer." *European Journal of Nuclear Medicine and Molecular Imaging* 43 (13): 2324–35. doi:10.1007/s00259-016-3441-2.
- Leijenaar, Ralph T. H., Sara Carvalho, Emmanuel Rios Velazquez, Wouter J. C. van Elmpt, Chintan Parmar, Otto S. Hoekstra, Corneline J Hoekstra, et al. 2013. "Stability of FDG-PET Radiomics Features: An Integrated Analysis of Test-Retest and Inter-Observer Variability." *Acta Oncologica* 52 (7): 1391–97. doi:10.3109/0284186X.2013.812798.
- Leijenaar, Ralph T.H., Georgi Nalbantov, Sara Carvalho, Wouter J.C. van Elmpt, Esther G.C. Troost, Ronald Boellaard, Hugo J.W.L. Aerts, Robert J Gillies, and Philippe Lambin. 2015. "The Effect of SUV Discretization in Quantitative FDG-PET Radiomics: The Need for Standardized Methodology in Tumor Texture Analysis." *Scientific Reports* 5 (1): 11075. doi:10.1038/srep11075.
- Lu, Lijun, Wenbing Lv, Jun Jiang, Jianhua Ma, Qianjin Feng, Arman Rahmim, and Wufan Chen. 2016. "Robustness of Radiomic Features in [11C]Choline and [18F]FDG PET/CT Imaging of Nasopharyngeal Carcinoma: Impact of Segmentation and Discretization." *Molecular Imaging and Biology* 18 (6): 935–45. doi:10.1007/s11307-016-0973-6.
- Marie Sydoff Sören Mattsson, Sigrid Leide-Svegborn, Martin Andersson. 2014. "Use of Wall-Less 18F-Doped Gelatin Phantoms for Improved Volume Delineation and Quantification in PET/CT." *Phys Med Biol* 59 (5): 1097–1107. doi:10.1088/0031-9155/59/5/1097.
- Markiewicz, P J, G I Angelis, F Kotasidis, M Green, W R Lionheart, A J Reader, and Matthews JC. 2011. "A Custom-Built PET Phantom Design for Quantitative Imaging of Printed Distributions." *Phys. Med. Biol* 56. <http://iopscience.iop.org/0031-9155/56/21/N01>.
- Marusyk, Andriy, Vanessa Almendro, and Kornelia Polyak. 2012. "Intra-Tumour Heterogeneity: A Looking Glass for Cancer?" *Nature Publishing Group* 12. doi:10.1038/nrc3261.
- Miller, Michael. A., and Gary D. Hutchins. 2007. "Development of Anatomically Realistic PET and PET/CT

- Phantoms with Rapid Prototyping Technology." In *2007 IEEE Nuclear Science Symposium Conference Record*, 4252–57. IEEE. doi:10.1109/NSSMIC.2007.4437056.
- Minn, Heikki, Kenneth R Zasadny, Leslie E Quint, and Richard L Wahl. 1995. "Lung Cancer: Reproducibility of Quantitative Measurements for Evaluating 2-[F-18]-Fluoro-2-Deoxy-D-Glucose Uptake at PET." *Radiology* 196 (1): 167–73. doi:10.1148/radiology.196.1.7784562.
- Nahmias, Claude, and Lindi M Wahl. 2008. "Reproducibility of Standardized Uptake Value Measurements Determined by 18F-FDG PET in Malignant Tumors." *Journal of Nuclear Medicine* 49 (11): 1804–8. doi:10.2967/jnumed.108.054239.
- Naqa, I El, P. W. Grigsby, A Apte, E Kidd, E Donnelly, D Khullar, S Chaudhari, et al. 2009. "Exploring Feature-Based Approaches in PET Images for Predicting Cancer Treatment Outcomes." *Pattern Recognition* 42 (6). NIH Public Access: 1162–71. doi:10.1016/j.patcog.2008.08.011.
- NEMA. 2001a. "National Electrical Manufacturers Association (NEMA) NU 2-2001: Performance Measurements of Positron Emission Tomographs." *NEMA Standards Publication NU 2-2001*. <http://dea.unsj.edu.ar/mednuclear/PET-NEMA-NU2-2001.pdf>.
- . 2001b. "NEMA IEC Body Phantom Set™," 61675.
- Nyflot, Matthew J, Fei Yang, Darrin Byrd, Stephen R Bowen, George A Sandison, and Paul E Kinahan. 2015. "Quantitative Radiomics: Impact of Stochastic Effects on Textural Feature Analysis Implies the Need for Standards." *Journal of Medical Imaging* 2 (4): 41002. doi:10.1117/1.JMI.2.4.041002.
- O'Connor, James P B, Chris J. Rose, John C. Waterton, Richard A D Carano, Geoff J M Parker, and Alan Jackson. 2015. "Imaging Intratumor Heterogeneity: Role in Therapy Response, Resistance, and Clinical Outcome." *Clinical Cancer Research*. doi:10.1158/1078-0432.CCR-14-0990.
- Oliver, Jasmine A, Mikalai Budzevich, Geoffrey G Zhang, Thomas J Dilling, Kujtim Latifi, and Eduardo G Moros. 2015. "Variability of Image Features Computed from Conventional and Respiratory-Gated PET/CT Images of Lung Cancer." *Translational Oncology* 8 (6): 524–34. doi:10.1016/j.tranon.2015.11.013.
- Orlhac, Fanny, Christophe Nioche, Michaël Soussan, and Irène Buvat. 2017. "Understanding Changes in Tumor Texture Indices in PET: A Comparison Between Visual Assessment and Index Values in Simulated and Patient Data." *Journal of Nuclear Medicine* 58 (3): 387–92. doi:10.2967/jnumed.116.181859.
- Orlhac, Fanny, Michaël Soussan, Jacques-Antoine Maisonobe, Camilo A Garcia, Bruno Vanderlinden, and Irène Buvat. 2014. "Tumor Texture Analysis in 18F-FDG PET: Relationships Between Texture Parameters, Histogram Indices, Standardized Uptake Values, Metabolic Volumes, and Total Lesion Glycolysis." *Journal of Nuclear Medicine* 55 (3): 414–22. doi:10.2967/jnumed.113.129858.
- Orlhac, Fanny, B. Theze, Michaël Soussan, Raphaël Boisgard, and Irène Buvat. 2016. "Multiscale Texture Analysis: From 18F-FDG PET Images to Histologic Images." *Journal of Nuclear Medicine* 57 (11): 1823–28. doi:10.2967/jnumed.116.173708.
- Parmar, Chintan, Emmanuel Rios Velazquez, Ralph Leijenaar, Mohammed Jermoumi, Sara Carvalho, Raymond H Mak, Sushmita Mitra, et al. 2014. "Robust Radiomics Feature Quantification Using Semiautomatic Volumetric Segmentation." *PLoS ONE* 9 (7). doi:10.1371/journal.pone.0102107.
- Phelps, Michael E. 2004. *PET Molecular Imaging and Its Biological Applications*. Springer.
- Plasticshop. 2011. "Nylon 66 Technical Properties Data Sheet."
- Rajendran, Joseph G., and Kenneth A. Krohn. 2015. "F-18 Fluoromisonidazole for Imaging Tumor Hypoxia: Imaging the Microenvironment for Personalized Cancer Therapy." *Seminars in Nuclear Medicine* 45 (2): 151–62. doi:10.1053/j.semnuclmed.2014.10.006.
- Rao, Nagaraja P., Shalom J. Srirangam, and Glenn M. Preminger. 2006. *Urological Tests in Clinical Practice*. Springer.
- Reuzé, Sylvain, Fanny Orlhac, Cyrus Chargari, Christophe Nioche, Elaine Limkin, François Riet, Alexandre Escande, et al. 2017. "Prediction of Cervical Cancer Recurrence Using Textural Features Extracted from 18 F-FDG PET Images Acquired with Different Scanners." *Oncotarget* 8 (26). Impact Journals: 43169–79. doi:10.18632/oncotarget.17856.
- Saha, Gopal B. 2010. *Basics of PET Imaging*. doi:10.1007/978-1-4419-0805-6.
- Shiri, Isaac, Arman Rahmim, Pardis Ghaffarian, Parham Geramifar, Hamid Abdollahi, and Ahmad Bitarafan-Rajabi. 2017. "The Impact of Image Reconstruction Settings on 18F-FDG PET Radiomic Features: Multi-Scanner Phantom and Patient Studies." *European Radiology*. doi:10.1007/s00330-017-4859-z.
- Skretting, Arne, Jan F Evensen, Ayca M Løndalen, Trond V Bogsrud, Otto K Glomset, and Karsten Eilertsen. 2013. "A Gel Tumour Phantom for Assessment of the Accuracy of Manual and Automatic Delineation of Gross Tumour Volume from FDG-PET/CT." *Acta Oncologica (Stockholm, Sweden)* 52 (3): 636–44. doi:10.3109/0284186X.2012.718095.
- Soffientini, Chiara D., Elisabetta De Bernardi, Rosangela Casati, Giuseppe Baselli, and Felicia Zito. 2017. "Technical Note: A New Zeolite PET Phantom to Test Segmentation Algorithms on Heterogeneous Activity Distributions Featured with Ground-Truth Contours." *Medical Physics* 44 (1): 221–26. doi:10.1002/mp.12014.
- Sun, Chengjun, and William G. Wee. 1983. "Neighboring Gray Level Dependence Matrix for Texture Classification." *Computer Vision, Graphics and Image Processing* 23 (3): 341–52. doi:10.1016/0734-189X(83)90032-4.
- Thibault, Guillaume, Bernard Fertil, Claire Navarro, Sandrine Pereira, Pierre Cau, Nicolas Levy, Jean Sequeira, and Jean-Luc Mari. 2009. "Texture Indexes and Gray Level Size Zone Matrix Application to

- Cell Nuclei Classification." *Pattern Recognition and Information Processing*, 140–45. doi:Artn 1357002\|Doi 10.1142/S0218001413570024.
- Tixier, Florent, Ashley M Groves, Vicky Goh, Mathieu Hatt, Pierre Ingrand, Catherine Cheze Le Rest, and Dimitris Visvikis. 2014. "Correlation of Intra-tumor 18F-FDG Uptake Heterogeneity Indices with Perfusion CT Derived Parameters in Colorectal Cancer." *PLoS ONE* 9 (6). doi:10.1371/journal.pone.0099567.
- Tixier, Florent, Mathieu Hatt, C. C. Le Rest, Adrien Le Pogam, Laurent Corcos, and Dimitris Visvikis. 2012. "Reproducibility of Tumor Uptake Heterogeneity Characterization Through Textural Feature Analysis in 18F-FDG PET." *Journal of Nuclear Medicine* 53 (5): 693–700. doi:10.2967/jnumed.111.099127.
- Tixier, Florent, Mathieu Hatt, Clemence Valla, Vincent Fleury, Corinne Lamour, Safaa Ezzouhri, Pierre Ingrand, Remy Perdrisot, Dimitris Visvikis, and C. C. Le Rest. 2014. "Visual Versus Quantitative Assessment of Intratumor 18F-FDG PET Uptake Heterogeneity: Prognostic Value in Non-Small Cell Lung Cancer." *Journal of Nuclear Medicine* 55 (8): 1235–41. doi:10.2967/jnumed.113.133389.
- Tixier, Florent, Catherine Cheze Le Rest, Mathieu Hatt, Nidal Albarghach, Olivier Pradier, J.-P. Metges, Laurent Corcos, and Dimitris Visvikis. 2011. "Intratumor Heterogeneity Characterized by Textural Features on Baseline 18F-FDG PET Images Predicts Response to Concomitant Radiochemotherapy in Esophageal Cancer." *Journal of Nuclear Medicine* 52 (3). Society of Nuclear Medicine: 369–78. doi:10.2967/jnumed.110.082404.
- Tixier, Florent, Dennis Vriens, Catherine Cheze-Le Rest, Mathieu Hatt, Jonathan A Disselhorst, Wim Jg Oyen, Lioe-Fee de Geus-Oei, Eric P Visser, and Dimitris Visvikis. 2016. "Comparison of Tumor Uptake Heterogeneity Characterization between Static and Parametric 18F-FDG PET Images in Non-Small Cell Lung Cancer." *Journal of Nuclear Medicine: Official Publication, Society of Nuclear Medicine* 57 (7): 1033–39. doi:10.2967/jnumed.115.166918.
- Turkington, T.G., T.R. Degrad, and W.H. Sampson. 2002. "Small Spheres for Lesion Detection Phantoms." *2001 IEEE Nuclear Science Symposium Conference Record (Cat. No.01CH37310)* 4: 2234–37. doi:10.1109/NSSMIC.2001.1009268.
- Ultimaker. 2017. "Safety Data Sheet PLA." Accessed September 26. <https://ultimaker.com/download/67935/SDS PLA v3.004.pdf>.
- Vallières, M, C R Freeman, S R Skamene, and I El Naqa. 2015. "A Radiomics Model from Joint FDG-PET and MRI Texture Features for the Prediction of Lung Metastases in Soft-Tissue Sarcomas of the Extremities." *Physics in Medicine and Biology* 60 (14): 5471–96. doi:10.1088/0031-9155/60/14/5471.
- Velasquez, Linda M, Ronald Boellaard, Georgia Kollia, Wendy Hayes, Otto S Hoekstra, Adriaan A Lammertsma, and Susan M Galbraith. 2009. "Repeatability of 18F-FDG PET in a Multicenter Phase I Study of Patients with Advanced Gastrointestinal Malignancies." *Journal of Nuclear Medicine* 50 (10): 1646–54. doi:10.2967/jnumed.109.063347.
- Velden, Floris H P van, Gerbrand M. Kramer, Virginie Frings, Ida A. Nissen, Emma R. Mulder, Adrianus J. de Langen, Otto S. Hoekstra, Egbert F. Smit, and Ronald Boellaard. 2016. "Repeatability of Radiomic Features in Non-Small-Cell Lung Cancer [18F]FDG-PET/CT Studies: Impact of Reconstruction and Delineation." *Molecular Imaging and Biology* 18 (5): 788–95. doi:10.1007/s11307-016-0940-2.
- Velden, Floris H P van, Ida A Nissen, Femke Jongstra, Linda M Velasquez, Wendy Hayes, Adriaan A Lammertsma, Otto S Hoekstra, and Ronald Boellaard. 2014. "Test-Retest Variability of Various Quantitative Measures to Characterize Tracer Uptake And/or Tracer Uptake Heterogeneity in Metastasized Liver for Patients with Colorectal Carcinoma." *Molecular Imaging and Biology* 16 (1): 13–18. doi:10.1007/s11307-013-0660-9.
- Walter Huda. 2010. *Review of Radiologic Physics. Physics in Medicine and Biology*. Vol. 41. doi:10.1088/0031-9155/41/12/018.
- Weber, Wolfgang A, Sibylle I Ziegler, R Thödtmann, A R Hanauske, and Markus Schwaiger. 1999. "Reproducibility of Metabolic Measurements in Malignant Tumors Using FDG PET." *J Nucl Med* 40 (11): 1771–77. <http://jnm.snmjournals.org/content/40/11/1771.full.pdf>.
- Welch, Danny R. 2016. "Tumor Heterogeneity - A 'Contemporary Concept' Founded on Historical Insights and Predictions." *Cancer Research*. doi:10.1158/0008-5472.CAN-15-3024.
- Westerterp, Marinke, Jan Pruijm, Wim Oyen, Otto Hoekstra, Anne Paans, Eric Visser, Jan Van Lanschot, Gerrit Sloof, and Ronald Boellaard. 2007. "Quantification of FDG PET Studies Using Standardised Uptake Values in Multi-Centre Trials: Effects of Image Reconstruction, Resolution and ROI Definition Parameters." *European Journal of Nuclear Medicine and Molecular Imaging*. doi:10.1007/s00259-006-0224-1.
- Willaime, J M Y, F E Turkheimer, L M Kenny, and E O Aboagye. 2013. "Quantification of Intra-Tumour Cell Proliferation Heterogeneity Using Imaging Descriptors of 18F Fluorothymidine-Positron Emission Tomography." *Physics in Medicine and Biology* 58 (2). IOP Publishing: 187–203. doi:10.1088/0031-9155/58/2/187.
- Wollenweber, S. D. 2014. "A Multi-Contrast, Multi-Resolution Phantom for Radionuclide Imaging Using a Single Activity Concentration Fill." *IEEE Transactions on Nuclear Science* 61 (5): 2503–9. doi:10.1109/TNS.2014.2350917.
- Yan, Jianhua, Jason Lim Chu-Shern, Hoi Yin Loi, Lih Kin Khor, Arvind K Sinha, Swee Tian Quek, Ivan W K Tham, and David Townsend. 2015. "Impact of Image Reconstruction Settings on Texture Features in 18F-FDG PET." *Journal of Nuclear Medicine* 56 (11): 1667–73. doi:10.2967/jnumed.115.156927.

- Yip, Stephen, Keisha McCall, Michalis Aristophanous, Aileen B Chen, Hugo J W L Aerts, and Ross Berbeco. 2014. "Comparison of Texture Features Derived from Static and Respiratory-Gated PET Images in Non-Small Cell Lung Cancer." *PLoS ONE* 9 (12). doi:10.1371/journal.pone.0115510.
- Yip, Stephen S F, and Hugo J W L Aerts. 2016. "Applications and Limitations of Radiomics." *Physics in Medicine and Biology* 61 (13): R150–66. doi:10.1088/0031-9155/61/13/R150.
- Zito, Felicia, Elisabetta De Bernardi, Chiara Soffientini, Cristina Canzi, Rosangela Casati, Paolo Gerundini, and Giuseppe Baselli. 2012. "The Use of Zeolites to Generate PET Phantoms for the Validation of Quantification Strategies in Oncology." *Medical Physics* 39 (9): 5353–61. doi:10.1118/1.4736812.

APPENDICES

Appendices	i
Appendix 0: Literature research method	ii
Appendix 1: Parameters influencing PET uptake values as found in the literature	iv
Appendix 2: Parameters influencing PET texture features as found in the literature.....	vi
Appendix 3: NEMA Body Phantom specific dimensions and requirements.....	viii
Appendix 4: Box design versions details	ix
Appendix 5: Spherical inserts design versions details	xi
Appendix 6: Cubical inserts design versions details.....	xii
Appendix 7: Protocols	xiii
Appendix 7.1: Radioactivity absorbance test of the photopolymer R05 protocol	xiii
Appendix 7.2: CT image background values extraction protocol	xiv
Appendix 7.3: Sphere shape analysis protocol	xv
Appendix 8: Master Thesis Log journal	xvi

APPENDIX O: LITERATURE RESEARCH METHOD

The first literature review was conducted during the first months of this Master thesis. It aimed to define the background, the different aspects, limitations and parameters influencing heterogeneity quantification. It was conducted following the Preferred Reporting Items for Systematic Review and Meta-Analyses (PRISMA) guidelines (Moher et al. 2009) and was done on PubMed and Google scholar browser using the following key words: "positron emission tomography", "PET", "heterogeneity", "texture", "artefact", "limitation", "impact", "quantification" (cf. Table 19).

Table 23 Vocabulary used during first literature review

Source	Search	Results
PubMed	(((((PET OR positron emission tomograph*)) AND ((Heterogene* OR texture)))) AND (Artifact OR Limitation OR Impact OR quantification))	284 full text papers 174 in the last 5 years
Google scholar	allintitle: PET Heterogeneity Limitation OR Impact OR quantification	23 full text papers 18 in the last 5 years

Few old papers were read for a global understanding of the history of heterogeneity quantification, but globally the focus is set on latest as possible publications as better challenge the conclusions drawn by previous papers (filtering the publications between 2012-2017). During the screening phase, duplicated papers and those fulfilling the following exclusion criteria were removed:

- publication based on non-tumour images
- publication based on non-human patients
- publications not based on quantitative assessment of heterogeneity or texture in images

While reading, another extra set of papers were identified and added to support the literature review. These articles were not found using PubMed or Google scholar queries. (cf. "additional record" in (Figure 65)) but were extracted from the read papers' references.

During the first literature research (query in Table 23) a total of 212 papers were found. From those papers, 201 (without duplicates) were screened and classified as relevant or not. (cf. PRISMA chart on (Figure 65)). From the 98 remaining relevant papers, a selection of 67 papers have been read, and classified in two categories: (1) PET heterogeneity quantification applications & results; and (2) PET heterogeneity quantification limitation and variability. The overall methodology of this literature review is illustrated in (Figure 65).

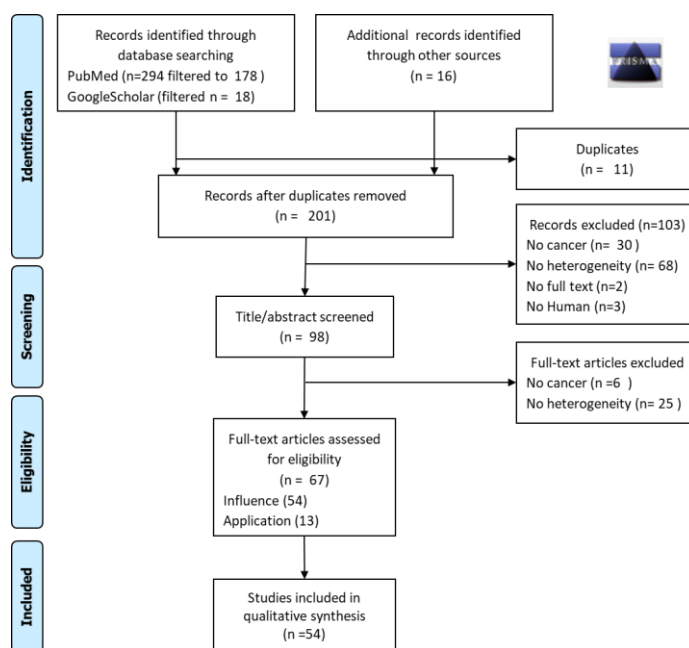


Figure 65 PRISMA flow chart of the literature study

Following the first systematic review, some extra research was conducted focusing on how PET heterogeneity quantification problems can be solved, and how current PET phantoms fail to solve them. This second literature review on the state of the art of heterogeneous phantom was also conducted during the first months on the Master thesis and was based on key words like "phantom", "PET" or "positron emission tomography", "heterogeneity" (Table 24).

Source	Search	Results
PubMed	((((PET OR positron emission tomograph*)) AND (Heterogene* OR texture)) AND Phantom	68 full text papers

Table 24 Vocabulary used during second literature review

During this second literature review, research has been conducted only on PubMed (query on (Table 24). A total of 68 papers (including later on added papers and without duplicates) were found on the topic of PET phantoms. From those papers, a selection of 19 papers regarding the state of the art of research PET phantoms and their limitation were presented in the literature review report.

APPENDIX 1: PARAMETERS INFLUENCING PET UPTAKE VALUES AS FOUND IN THE LITERATURE

Table 25 Biological or physiological parameters influencing PET uptake values

Parameters	Reference
Plasma glucose level	(Boellaard et al. 2008)
Insulin level	(Cook, Wegner, and Fogelman 2004)
FDG plasma clearance	(Boellaard et al. 2008)
Pre or postmenopausal subjects with hormone replacement therapy	(Cook, Wegner, and Fogelman 2004)
Menstruation	(Cook, Wegner, and Fogelman 2004)
Granulomatous processes	(Cook, Wegner, and Fogelman 2004)
Inflammatory processes	(Boellaard et al. 2008), (Cook, Wegner, and Fogelman 2004)
Infective processes or Helicobacter pylori infection	(Cook, Wegner, and Fogelman 2004)
Autoimmune thyroiditis, Graves' thyrotoxicosis, autoantibody positivity	(Cook, Wegner, and Fogelman 2004)
Breathing	(Boellaard et al. 2008)
Colonic /bowel activity	(Cook, Wegner, and Fogelman 2004)
Urinary activity	(Cook, Wegner, and Fogelman 2004)
Testicular activity	(Cook, Wegner, and Fogelman 2004)
Skeletal muscle activity	(Boellaard et al. 2008), (Cook, Wegner, and Fogelman 2004)
Brown fat metabolic activity	(Cook, Wegner, and Fogelman 2004)
Liquid drank before acquisition	(Cook, Wegner, and Fogelman 2004)
Time between FDG administration and acquisition	(Boellaard et al. 2008)
Radiotracer uptake period	(Boellaard et al. 2008)

Table 26 Pre-acquisition parameters influencing PET uptake values

Parameters	Reference
Scanner calibration	(Boellaard et al. 2008), (Westerterp et al. 2007)
Net dose given to the patient	(Boellaard et al. 2008)
Residual activity in the syringe after injection	(Boellaard et al. 2008)
Paravenous administration	(Boellaard et al. 2008)
Clocks synchronisation between PET system and dose calibrator used	(Boellaard et al. 2008)
Dose calibration time/dose injection time	(Boellaard et al. 2008)

Table 27 Acquisition parameters influencing PET uptake values

Parameters	Reference
Noise	(Boellaard et al. 2004)
Time per bed position	(Boellaard et al. 2008)
Amount of overlap between subsequent bed positions	(Boellaard et al. 2008)
Acquisition mode (2D or 3D)	(Boellaard et al. 2008)
Inter-institute variability	(Westerterp et al. 2007)
Intra-institute variability - Test and re-test variability	(Minn et al. 1995), (Weber et al. 1999), (Hoekstra et al. 2002), (Krak et al. 2005), (Nahmias and Wahl 2008), (Velasquez et al. 2009), (van Velden et al. 2014), (van Velden et al. 2016)

Table 28 Image reconstruction parameters influencing PET uptake values

Parameters	Reference
Image reconstruction methods and settings	(Boellaard et al. 2008), (Westerterp et al. 2007), (Krak et al. 2005), (Jaskowiak et al. 2005), (Boellaard et al. 2004)
Image matrix size	(Westerterp et al. 2007)
Attenuation corrections from CT data (mismatch due to respiration/contrast agent/ CT tube current)	(Boellaard et al. 2008), (Cook, Wegner, and Fogelman 2004)
Region of interest (ROI) variability (manual or semiautomatic procedures)	(Boellaard et al. 2008), (Westerterp et al. 2007), (Krak et al. 2005), (Boellaard et al. 2004)
Normalization	(Boellaard et al. 2008)

APPENDIX 2: PARAMETERS INFLUENCING PET TEXTURE FEATURES AS FOUND IN THE LITERATURE

Table 29 Biological and physiological parameters influencing PET texture features

Parameters	Reference
Patient size	(Nyflot et al. 2015), (Cortes-Rodicio et al. 2016)
Patient weight	(Cortes-Rodicio et al. 2016)
Patient BMI	(Cortes-Rodicio et al. 2016)
Patient glucose level	(Cortes-Rodicio et al. 2016)
Tumour volume	(Willaime et al. 2013), (Hatt et al. 2013), (Brooks and Grigsby 2013), (Brooks and Grigsby 2014), (Orlhac et al. 2014), (Brook and Grigsby 2015), (Hatt et al. 2015), (Nyflot et al. 2015), (Forgacs et al. 2016)
Tissue type	(Willaime et al. 2013)
Tumour rotation and deformation motion	(Oliver et al. 2015)
Respiratory motion	(S. Yip et al. 2014), (Oliver et al. 2015), (Cheng et al. 2016), (Grootjans et al. 2016), (Carles et al. 2017)
Biologic heterogeneity	(Orlhac et al. 2016) ³
Uptake heterogeneity (radiotracer distribution)	(Orlhac et al. 2016) ⁴ , (Orlhac et al. 2017)
Reproducibility (Physiologic variability in test-retest)	(Tixier et al. 2012), (Leijenaar et al. 2013), (Willaime et al. 2013), (van Velden et al. 2014), (van Velden et al. 2016), (Desseroit et al. 2017)
Reproducibility (Phantom variability in test-retest)	(Nyflot et al. 2015), (Forgacs et al. 2016)

Table 30 Acquisition parameters influencing PET TF

Parameters	Reference
Acquisition stochastic image noise	(Nyflot et al. 2015), (Grootjans et al. 2016)
Acquisition protocol : 2D vs 3D	(Galavis et al. 2010)
Acquisition protocol : 3D vs 4D (respiratory motion)	(S. Yip et al. 2014), (Oliver et al. 2015)
Acquisition protocol: static vs parametric	(Tixier et al. 2016)
Scanner type	(Desseroit et al. 2017), (Reuzé et al. 2017)
Time per bed position	(Shiri et al. 2017)

Table 31 Reconstruction and Post-processing Parameters influencing PET texture features

Parameters	Reference
Partial volume effect (PVE) correction (PVC)	(Hatt et al. 2013)
Reconstruction algorithms	
- OSEM vs Iterative-Vue Point algorithm	(Galavis et al. 2010)
- PSF reconstruction vs OSEM	(Lasnon et al. 2016)
- OSEM vs OSEM+PDF vs OSEM+TOF vs OSEM+PSF+TOF	(Yan et al. 2015), (Shiri et al. 2017)
- normal algorithm vs respiratory gated algorithm *	(Cheng et al. 2016), (Grootjans et al. 2016), (Carles et al. 2017)
- BLOB-OS+TOF vs 3D-RAMLA	(Cortes-Rodicio et al. 2016)
- Usual algorithm with or without TOF and/or TrueX	(Forgacs et al. 2016)
- BLOB-OS+TOF+Gaussian filter vs BLOB-OS+TOF+ maximum likelihood expectation maximization deconvolution	(van Velden et al. 2016)
Reconstruction iterations number	
- 2 vs 4 iterations	(Galavis et al. 2010)
- 1 vs 2 vs 3 iterations	(Yan et al. 2015)
- 2 vs 6 iterations (with change in FWHM: 5vs 8.6mm respectively)	(Nyflot et al. 2015)
Reconstruction sub-iteration (subset x iteration)	
- 2x16 vs 3x16 vs 4x16 vs 5x8 vs 2x21 vs 3x21 vs 4x21	(Shiri et al. 2017)
- 15 vs 18 vs 24 vs 27 vs 36 vs 40 vs 48 vs 54 vs 64 vs 72	
Reconstruction subset	
- 8 vs 16 vs 21 vs 24	(Shiri et al. 2017)
- 4 vs 6 vs 8 vs 9 vs 12 vs 16 vs 18 vs 24 vs 32	
Voxel size	
- 4 mm vs 2 mm	(Cortes-Rodicio et al. 2016), (Orlhac et al. 2017)
- Scale values of 1 vs 2 vs 3 vs 4 vs 5 mm and initial in-plane resolution	(Vallières et al. 2015)
- 4mm vs 3.13 mm	(Forgacs et al. 2016)
- 5.3x5.3x3.4 mm vs 2.7x2.7x3.4 mm vs 2x2x2 mm	(Reuzé et al. 2017)

³ ¹⁶ Has only been evaluated on clinical PET and mouse

Grid-size of the reconstruction algorithm	
- 128x128 vs 256x256	(Galavis et al. 2010), (Yan et al. 2015)
Post-reconstruction filter	
- Filter FWHM 3 vs 5 vs 6 mm	(Galavis et al. 2010)
- Filter FWHM 2 vs 2.5 vs 3 vs 3.5 vs 4.0 m vs full width	(Doumou et al. 2015)
- Filter FWHM 2.5 vs 3.5 vs 4.5 vs 5.5 mm	(Yan et al. 2015)
- Filter FWHM 4 vs 5 mm	(Forgacs et al. 2016)
- Filter FWHM 3 vs 4 vs 5 vs 6 vs 7 mm	(Shiri et al. 2017)
- Filter FWHM 0, 0.5, 1, 1.5, 2, 2.5, 3, 3.5, 4, 4.5, 5, 5.5, 6, 6.5, 7 mm	(Shiri et al. 2017)
- with or without filter	(Lasnon et al. 2016)

Table 32 Feature extraction parameters influencing PET texture features

Parameters	Reference
Segmentation/Delineation	
- Inter-observer variability in manual delineation	(Leijenaar et al. 2013)
- Fixed threshold ($VOI_{42\%}$) vs adaptive threshold (VOI_{COA}) vs fuzzy locally adaptive Bayesian (FLAB) algorithm	(Hatt et al. 2013)
- Fixed threshold ($VOI_{40\%}$) vs adaptive threshold (VOI_{COA})	(Orlhac et al. 2014)
- Fixed threshold ($VOI_{50\%}$) vs FLAB algorithm	(Lasnon et al. 2016)
- Manual delineation vs semi-automatic (GrowCut) algorithm	(Parmar et al. 2014)
- Manual delineation vs semi-automatic (isocontour at 50%)	(van Velden et al. 2016)
- Fixed thresholds ($VOI_{45\%}$, $VOI_{50\%}$, $VOI_{55\%}$, $VOI_{60\%}$)	(Doumou et al. 2015)
- Manually vs fixed threshold ($VOI_{41\%}$, $VOI_{50\%}$, $VOI_{70\%}$) vs adaptive threshold (Nestle) vs watershed gradient-based method vs region growing	(Lu et al. 2016)
- Inclusion of tumour edges or not	(Orlhac et al. 2017)
- Fixed threshold ($VOI_{40\%}$) vs adaptive threshold (VOI_{COA})	(Carles et al. 2017)
Number of voxel per VOI	
- 4 vs 5 vs 10 voxels radius	(Orlhac et al. 2017)
- Random voxel number were tested	(Brook and Grigsby 2015)
Discretization (i.e. resampling image intensity values)	(Brook and Grigsby 2015)
- No sampling vs with sampling	(Orlhac et al. 2014)
- 8 vs 64	(Orlhac et al. 2014)
- 16 vs 64	(Orlhac et al. 2014)
- 32 vs 64	(Orlhac et al. 2014)
- 128 vs 64	(Orlhac et al. 2014)
- 8 vs 16 vs 32 vs 64 grey levels	(Vallières et al. 2015)
- 8 vs 16 vs 32 vs 64 vs 128 grey levels	(Tixier et al. 2012), (Doumou et al. 2015), (Leijenaar et al. 2015), (Desseroit et al. 2017)
- 8 vs 16 vs 32 vs 64 vs 128 vs 256 grey levels	(Hatt et al. 2015)
- Equal-probability vs Lloyd-Max quantization algorithms	(Vallières et al. 2015)
- Bin size B of 0.05 vs 0.1 vs 0.2 vs 0.5 vs 1 of SUV	(Leijenaar et al. 2015), (Lu et al. 2016)
Texture matrices	
- Entropy/contrast extraction from different matrices	(Galavis et al. 2010)
- Average of 13 matrices in 13 directions vs 1 matrix with 13 direction	(Hatt et al. 2015)
- Matrix size	(Shiri et al. 2017)
Parameters correlations	
- Between texture features	(Orlhac et al. 2014), (Hatt et al. 2015)
- Between features and MATV, SUV, TLG	(Orlhac et al. 2014), (Hatt et al. 2015)
- Between features and MATV, SUV, SD-SUV	(Cortes-Rodicio et al. 2016)
- Between MATV and SUV_{MAX} and SUV_{MIN}	(Hatt et al. 2015)

APPENDIX 3: NEMA BODY PHANTOM SPECIFIC DIMENSIONS AND REQUIREMENTS

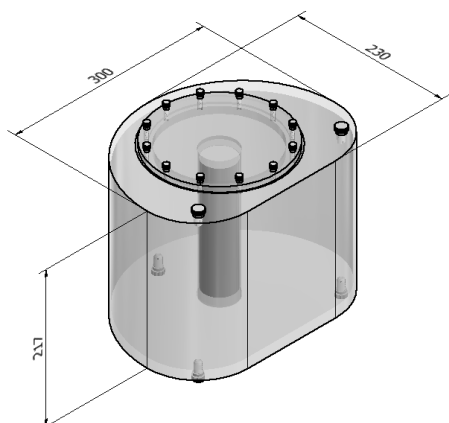


Figure 66 3D drawing of the NEMA Body PET Phantom

NEMA IEC Body Phantom Set™

Thorax like box, containing a cylindrical lung insert and six fillable spheres. The NEMA box can be opened by unscrewing 12 plastic screws holding a cap into place.

Specifications:

- Exterior length of phantom: 217x280x300 mm
- Interior length of phantom: 180 mm
- 6 fillable spheres with inner diameters of:
 - 10/13/17/22/28/37 mm.
- Distance from sphere plane to inside wall: 70 mm
- Volume of empty cylinder: 9.7 liters
- Cylindrical insert dimension:

- Outside diameter: 51 mm
- Length: 195 mm *(and not 180 as specified by the constructor)*

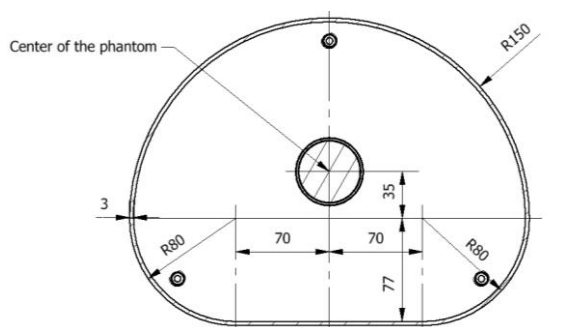


Figure 67 Transversal engineering drawing view of the NEMA Body PET phantom ⁵

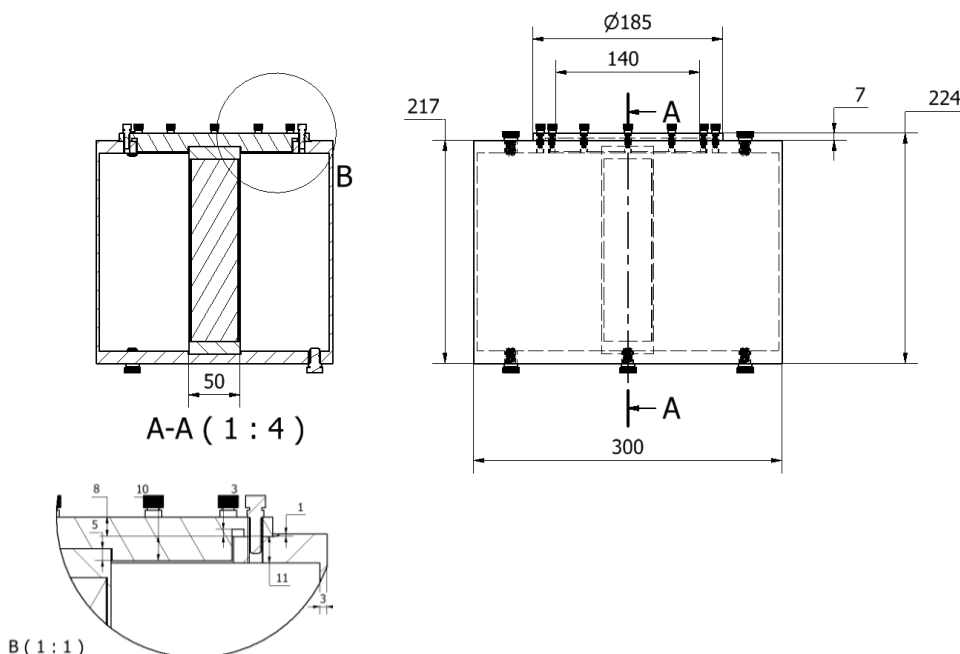


Figure 68 Frontal engineering drawing views of the NEMA Body PET phantom Normal frontal view of the NEMA box, cap and insert (right), sagittal section of the box and lung insert (left-up) (A-A), and detail view of the sagittal section of the bow and its closing cap and screws (left-down) (B).

⁵ (by L.M.H Ghesquiere-Dierickx using Inventor software)

APPENDIX 4: BOX DESIGN VERSIONS DETAILS

Table 33 Phantom Box design iterations details

Design Step	V#	Manufacturing process	Cylinder size (ID/OD)	Top/Bottom extrusion height	Imaging/Filling chambers height	Filling process	Assembling process	Creation Date	Extra Remarks	
Pre-Manufacturing	0	SLA printing	80/82mm 1mm	5&3mm	<i>undefined</i>	Only via filling chambers using capillaries	<i>undefined</i> Interference fit		Preliminary Design by (W.Grootjans)	
	First ideas on the filling and assembling design									
	1.1	SLA printing	78/80mm 1mm thick	5&3mm	<i>undefined</i>	Each chamber has a single 2mm hole No closing defined yet	80/100mm outside ring <i>No watertight defined yet</i> <i>No closing defined yet</i>	16/03/17	Filling and closing processes are in progress (luer lock or rubber cap or screws + gasket or ...)	
	1.2	SLA printing	78/80mm 1mm thick	5&3mm	45mm 10mm	2mm holes 6x6x5 cubes (x7) M2 screws (x7)	80/100mm ring 2mm holes M2 screws (x36) Gasket	23/03/17	Definition of the filling process. Definition of the water tight closing in the assembling process (2 gaskets of 1mm thick)	
	Change on the manufacturing process									
	2.1	PMMA tubes x2 Erode the inside	78/80mm 1mm thick	5&3mm	45mm 10mm	2mm holes +6x6x5 cubes (x7) + M2 screws (x7)	80/90mm ring 2mm holes M2 screws (x36)	05/04/17	Change in the manufacturing process	
	2.2	PMMA tubes x2	76/80mm 2mm thick	5&3mm	45mm 10mm	2mm holes +6x6x5 cubes (x7) + M2 screws (x7)	80/90 ring 2mm holes M2 screws (x36)	06/04/17	Trade-off in the wall thickness (from 1mm to 2mm)	
	2.3	PMMA tubes x2	76/80mm 2mm thick	5&3mm	45mm 10mm	2mm holes +6x6x5 cubes (x7) + M2 screws (x7)	80/90mm ring 2mm holes M2 screws (x36)	11/04/17	Exploded CAD view	
	2.4	PMMA tubes PMMA cut plate	76/80mm 2mm thick	5&3mm	45mm 10mm	2mm holes +6x6x5 cubes (x7) + M3 screws (x7)	80/96mm ring 3mm holes M3 screws (x36)	19/04/17	Locking rings cut out of a plate and not a tube M3 screws	
	Changes in size of the imaging chambers									
	3.1	PMMA tubes PMMA cut plate	76/80mm 2mm thick	5&3mm	48mm 7mm (too small to fill)	-	80/96mm ring 3mm holes M3.8 screws (x36)	21/04/17	Longer imaging chamber of 48 mm height	
	3.2	PMMA tubes PMMA cut plate	76/80mm 2mm thick	5&3mm	48mm 5mm or 8mm	3mm holes +8x8x3 cubes (x3) + M3 screws (x7)	80/96mm ring 3mm holes M3.20 screws (x24)	21/04/17	Merging of filling chambers, locking ring and filling cubes	
	Small changes in filling cubes or design									
	4.1	PMMA tubes PMMA cut plate	76/80mm 2mm thick	3&3mm	44mm 7,5mm or 13mm	3mm holes +7x7x3 cubes (x5) +7x7.5x3 cubes(x2) + M3 screws (x7)	80/96mm ring 3mm holes M3.8 screws (x36)	26/04/17	Back to M3.8 screws Precise screw holes dimension are still undefined	

4.2	PMMA tubes PMMA cut plate	76/80mm 2mm thick	3&3mm	44mm 7,5mm or 13mm	2.7&3.4mm holes + 7x7x~3 cubes(x5) +7x7.5x~3 cubes(x2) + M3 screws (x7)	80/96mm ring 2.7 &3.4mm holes M3.8 screws (x36)	09/05/17	Fileted filling cubes to fit a circular shape Adapted screws holes to thread or solely holes (3mm holes become either 2.7 or 3.4 mm dia)
4.3	PMMA tubes PMMA cut plate	76/80mm 2mm thick	3&3mm	44mm/ 7,5mm or 13mm	2.7&3.4mm holes + 7x7x~3 cubes(x5) +7x7.5x~3 cubes(x2) + M3 screws (x7)	80/96mm ring 2.7 &3.4mm holes M3.8 screws (x36)	16/05/17	Top & bottom closing cap glue on the top and not inside the top and bottom chambers
Plates of 1 mm (i.e. imaging chamber of 43mm)								
5	PMMA tubes PMMA cut plate	76/80mm 2mm thick	3&3mm	43mm/ 7,5mm or 13mm	2.7&3.4mm holes + 7x7x~3 cubes(x5) +7x7.5x~3 cubes(x2) + M3 screws (x7)	80/96mm ring 2.7 &3.4mm holes M3.8 screws (x36)	30/05/17	Adaptation for plate of 1mm instead of 0.5mm
Cubes of 8mm height (i.e. imaging chamber of 42mm)								
6.1	PMMA tubes PMMA cut plate	76/80mm 2mm thick	3&3mm	42mm/ 8mm or 14mm	2.7&3.4mm holes + 12x8x~3 cubes(x7) + M3 screws (x7)	80/96mm ring 2.7 &3.4mm holes M3.8 screws (x36)	16/06/17	Adaptation for cubes of 8mm
6.2	PMMA tubes PMMA cut plate	76/80mm 2mm thick	3&3mm	42mm/ 8mm or 14mm	2.7&3.4mm holes + 12x8x~3 cubes(x7) + M3 screws (x7)	79.3/96mm ring 2.7 &3.4mm holes M3.8 screws (x36)	19/07/17	Update of the flanges inside diameter
M4 screws								
7	PMMA tubes PMMA cut plate	76/80mm 2mm thick	3&3mm	42mm/ 8mm or 14mm	2.7&3.4mm holes + 12x8x~3 cubes(x7) + M3 screws (x7)	79.3/96mm ring 2.7 & 4mm holes M4 screws (x36)	02/08/17 24/08/17	Issue when ordering the flanges, the received screw holes were too big: M3 screws need to be M4 M4 head screws are bigger than M3 → Need to erode the tube glass
Back to M3 screws and adaptation to all kind of inserts								
8	PMMA tubes PMMA cut plate	76/80mm 2mm thick	3&3mm	40-42mm/ 8mm or 14mm	2.7&3.4mm holes + 12x8x~3 cubes(x7) + M3 screws (x7)	80/96mm ring 2.3 &3mm holes M3 screws (x36)	09/08/17	Correct M3 re-ordering of some part for another version of the phantom (where the cubic plates will be glued to the casing) Adaptation of imaging segment height to both kind of inserts
Locking rings of 12 holes								
9	PMMA tubes PMMA cut plate	76/80mm 2mm thick	3&3mm	40-42mm/ 8mm or 14mm	2.7&3.4mm holes + 12x8x~3 cubes(x7) + M3 screws (x7)	80/96mm ring 2.3 &3mm holes M3 screws (x72)	06/09/17	Increase of number of screws to lock the assembly of the phantom to prevent leakages at the junction of the segments and inserts.

APPENDIX 5: SPHERICAL INSERTS DESIGN VERSIONS DETAILS

Table 34 Spherical inserts design iterations

Design Step	V#	Manufacturing process	Plate thickness	Plate shape	Spheres Dimension (ID mm)	Spheres wall thickness	Creation Date	Extra Remarks
Pre-Manufacturing	1 sphere per plate							
	1	Sphere: SLA print Plate: undefined	0.3mm	Disk 80mm OD	10/13/17/22/28/37	1mm	26/05/17	1 sphere per plate
	4 spheres per plates							
	2.1	Sphere: SLA print Plate: undefined	0.3mm	Disk 80mm OD	10/13/17/22	1mm	29/05/17	4 plates per plate
	2.2	Sphere: SLA print Plate: undefined	0.3mm	Disk 80mm OD	10/13/17/22	0.3mm	06/06/17	Thinner spheres of 0.3mm instead of 1mm
	3.1	Sphere: SLA print Plate: undefined	1mm	Disk 80mm OD	10/13/17/22	0.3mm	07/06/17	Thicker plate of 1 mm
3.2	Sphere: SLA print Plate PMMA laser cut	1mm	Disk 80mm OD	10/13/17/22	0.3mm	23/06/17	Correction of the error between ID and OD of the spheres in (V.3.1) → SLA print of the 0.3mm version (26/06/2017)	
0.4 mm sphere thickness								
4	Sphere: SLA print Plate: PMMA laser cut	1mm	Disk 80mm OD	10/13/17/22	0.4mm	26/06/17	0.3mm thick inserts' prints has holes led to a 0.4mm thick spheres → SLA print of the 0.4mm version (27/06/2017)	
Back to 0.3 mm sphere thickness + closing process of each sphere								
Post-Manufacturing	5	Sphere: SLA print Plate: FDM print	1mm +4mm	Disk 80mm OD + 2nd disk 75mm OD	10/13/17/22	0.3mm	07/08/17	Update of the sphere plate: thicker plate on one side, closing of each sphere via M3 screws. Change in the manufacturing: from PMMA laser cut to FDM 3D printed. → Manufacturing of it (28/08/2017)
	6.1	Sphere: SLA print Plate: FDM print	1mm +6mm	Disk 80mm OD + 2nd disk 75mm OD +slope	10/13/17/22	0.3mm	05/09/17	Higher plate (6mm thick instead of 4mm) and slope added → Manufacturing of it (05/09/2017)
	6.2	Sphere: SLA print Plate: FDM print	1mm +6mm	Disk 80mm OD + 2nd disk 75mm OD +slope	10/13/17/22 + 10/17	0.3mm + 0.4 mm	11/09/17	Adaptation of the number of filling hole to the number of available spheres (4+2) → Manufacturing of it (11/09/2017)
	Plate with 12 holes for assembling process							
7	Sphere: SLA print Plate: FDM print	1mm +6mm	Disk 80mm OD + 2nd disk 75mm OD +slope	10/13/17/22 + 10/17	0.3mm + 0.4 mm	18/09/17	Adaptation to the box design (V.9) with 12 assembling holes → Manufacturing of it (18/09/2017) → Smothered on (19/09/2017)	

APPENDIX 6: CUBICAL INSERTS DESIGN VERSIONS DETAILS

Table 35 Cubical insert design iterations

Design Step	V#	Manufacturing process	Structure Height (inside+2xplates thickness)	Base Plate dimension	Base plate thickness	Pixels External/Internal dimension	Pixels wall thickness	Creation Date	Extra Remarks
	0	-	-	-	-	8x8x8	Plain design	18/05	Preliminary design from XXX publication
						First ideas on the pixels size			
	1.1	SLA printing	46mm+2x0.5 = 47mm	2x96mm dia + holes	0.5mm	E: 8x8x8 I: 7,7x7,7x7,7	0.3 or 0.6	15/06	Issue with the pixel inside volume (too small)
	1.2	SLA printing	46mm+2x0.5 = 47mm	2x96mm dia + holes	0.5mm	E: 8,6x8,6x8,6 I: 8x8x8	0.3 or 0.6	17/05	
						Adaptive size of the pixels			
Pre-Manufacturing	2.1	SLA printing	46mm+2x0.5 = 47mm	2x96mm dia + holes	0.5mm	Adaptive size (8x8x8 or .6x8.6x8)	0.3 or 0.6	23/05	Outside column for the concentration change in the L shape
	2.2	SLA printing	46mm+2x0.5 = 47mm	2x96mm dia + holes	0.5mm	Adaptive size (8x8x8 or .6x8.6x8)	0.3 or 0.6	24/05	Inside column for the concentration change in the L shape
	2.3	SLA printing	45mm+2x1 = 47mm	2x96mm dia + holes	1mm	Adaptive size (8x8x8 or .6x8.6x8)	0.3 or 0.6	30/05	Thicker base of 1mm instead of 0.3mm
	2.4	SLA printing	45mm+2x1 = 47mm	2x96mm dia + holes	1mm	Adaptive size (8x8x8 or .6x8.6x8)	0.3 or 0.6	12/06	Same as 2.3 but not hollow → FDM printing of it
	2.5	SLA printing	45mm+2x1 = 47mm	2x96mm dia + holes	1mm	Adaptive size (8x8x8 or .6x8.6x8)	0.3 or 0.6	14/06	The number of pixel contained in the base (row0) of the M shape is reduced to match the row1.
							Merged plates in 1 structure		
Post-Manufacturing	3.1	SLA printing	47mm	2x 76mm dia: fitting all inside the imaging tube	1mm	Adaptive size (8x8x8 or 8.6x8.6x8)	0.3	31/05	Merged M and L shapes in 1 plate + Base dimension changes as the merged insert will be glued inside the phantom
	3.2	SLA printing	47mm	80mm dia (on top) 76mm dia (inside)	1mm 2mm on edges	Adaptive size (8x8x8 or 8.6x8.6x8)	0.3	02/06	Extra thickness on the plates edges for a better fitting and gluing with the box
	3.3	SLA printing	47mm	80mm dia (on top) 76mm dia (inside)	1mm 2mm on edges	Adaptive size (8x8x8 or 8.6x8.6x8)	0.3	08/06	Resizing of few pixels, to correct inside size as 8x8x8mm
	3.4	SLA printing	46mm	80mm dia (on top) 76mm dia (inside)	1mm 2mm on edges	Adaptive size (8x8x8 or 8.6x8.6x8)	0.3	15/06	Adapting for cubes of 8mm instead of 7.5/7 mm → SLA printing of version 3.4 with almost no support
	3.5	SLA printing	46mm	80/70mm (on top) 70/65mm dia (inside)	1.5mm 2mm on edges	Adaptive size (8x8x8 or 8.6x8.6x8)	0.3	19/06	Diagonal pillars inside the L shape and on top of the M shape
	3.6	SLA printing	42mm	80/70mm (on top) 70/65mm dia (inside)	1.9 mm 2.4 mm on edges	Adaptive size (8x8x8 or 8.6x8.6x8)	0.3	21/06	Size adaptation so the imaging windows are the same for the spherical and cubical shaped inserts. Thickening of the plates base → (28/06/2017) SLA print of it → 02-03/07/2017 SLA print with more support
	3.7	SLA printing	42mm	80/70mm (on top) 75.7/65mm dia (inside)	1.9 mm 2.4 mm on edges	Adaptive size (8x8x8 or 8.6x8.6x8)	0.3	22/06	Resizing of the top and bottom plates diameters so they are closer to the box dimensions (76/80mm)

APPENDIX 7: PROTOCOLS

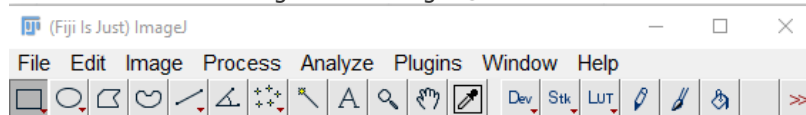
APPENDIX 7.1: RADIOACTIVITY ABSORBANCE TEST OF THE PHOTOPOLYMER R05 PROTOCOL

- 1) Acquire background and source syringe's activities using **XXX**
- 2) A solution of water mixed with Tc^{99m} is poured on the plastic pieces in a surface of 1x2mm
- 3) Wet plastic pieces are stored in normal conditions
- 4) After 1h30 water is removed from the plastic pieces by gently tilting them
- 5) Remaining radioactivity on plastic pieces is acquired
- 6) Plastic pieces are rinsed during 1 min with clear water to try to remove the maximum of remaining radioactivity
- 7) Remaining radioactivity on plastic pieces is acquired

APPENDIX 7.2: CT IMAGE BACKGROUND VALUES EXTRACTION PROTOCOL

1) Open ImageJ® software

Figure 69: ImageJ® toolbar



2) File> Import > Image Sequence and select one of the .tif or .IAM files you want to import

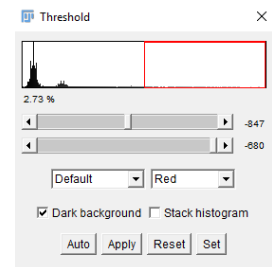
3) Verify pixels size and voxel depth (CTRL+MAJ+P) of the imported image sequence.

4) Verify intensity range (CTRL+H) of the sequence, to check if any resampling has been done on the images pixel intensity. Grey values should roughly be between -1000 to 800.

5) If necessary, you can crop the image sequence (Image>Crop or CTRL+MAJ+X) and save it (File>Save as>Image sequence...) in a new dedicated file.

6) SELECT a ROI grey value threshold by using

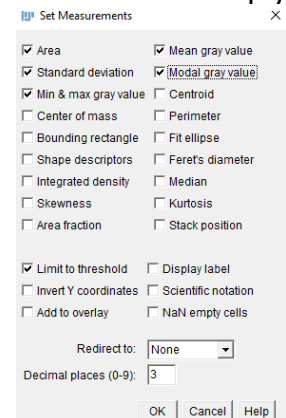
- Image>Adjust>Threshold or CTRL+MAJ+T
- Select the correct pixel grey value range that only include the objects of interest (here the phantom inserts parts included between -844 and -440)
- The threshold method should be set on "Default" and "Red"
- Dark background and stack histogram should be selected
- Do NOT press on "Apply"



7) Open the ROI Manager Process>Tools>ROI Manager and check that the ROI list is empty. If not press the Delete bottom of the ROI Manager.

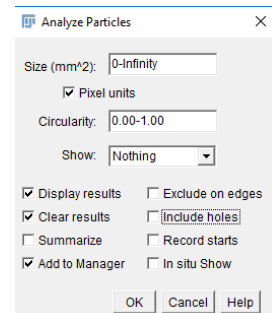
8) Set the measurements you want to apply on your images by going in Analyse>Set Measurements and selecting the one of interest. Please ensure that the following boxes are crossed:

- "Area"
- "Mean grey value"
- "Standard deviation"
- "Modal grey value"
- "Min & max grey value"
- "Limit to threshold"



9) Define ROIs and analyse them using Analyse>Analyse Particle

- Size :0-Infinity (but 0 can be set to a higher value to only select big ROIs)
- Pixel unit box unchecked
- Circularity : 0.00-1.00
- Show : Nothing
- Display results, clear results, add to manager boxes should be checked
- Press OK



10) Verify that the found ROIs are relevant by going through the ROI manager and selecting each ROI at a time and visualising it in the image sequence

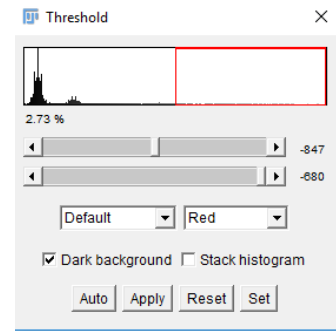
11) ROIs can be save by pressing the "More>>" and Save in the ROI manager window.

12) Results can be save using File>Save As.

APPENDIX 7.3: SPHERE SHAPE ANALYSIS PROTOCOL

1) Import image in ImageJ following steps 1 to 5 from previous protocol (Appendix 3.2).

- 2) SELECT a ROI grey value threshold by using
 - a. Image>Adjust>Threshold or CTRL+MAJ+T
 - b. Select the correct pixel grey value range that only include the objects of interest (values range that will permit to only select the insert shape $\sim[-840;-400]$ for spheres in air)
 - c. The threshold method should be set on "Default" and "Red"
 - d. Dark background and stack histogram should be selected
 - e. Do NOT press on "Apply"

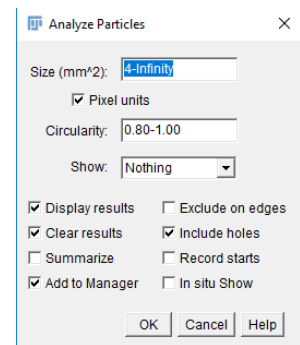


3) Open the ROI Manager Process>Tools>ROI Manager and check that the ROI list is empty. If not press the Delete bottom of the ROI Manager.

4) Set the measurements you want to apply on your images by going in Analyse>Set Measurements and selecting "Fit Ellipse" and "Limit to threshold"

5) Define ROIs and analyse them using Analyse>Analyse Particle as follow:

- a. Size :4-Infinity
- b. Pixel unit box checked
- c. Circularity : 0.80-1.00
- d. Show : Nothing
- e. "Display results", "Clear results", "Add to manager" and "Include holes" boxes should be checked
- f. Press OK



6) Verify that the found ROIs are relevant by going through the ROI manager and selecting each ROI at a time and visualising it in the image sequence

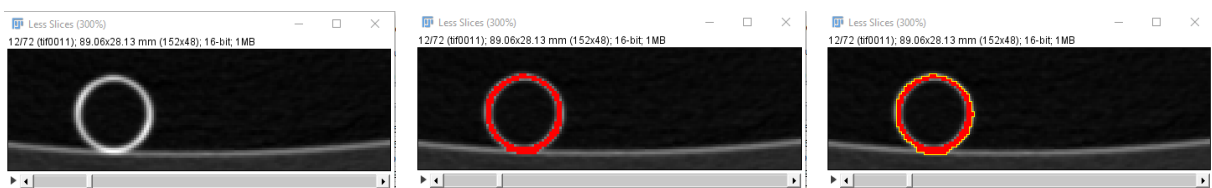


Figure 70 Shape selection in CT images using ImageJ
Image without any selection (left), threshold visualisation on the image (centre) and respective selected ROI overlapped with original image (right).

7) ROIs can be save by pressing the "More>>" and Save in the ROI manager window.

8) Results can be save using File>Save As

	Major	Minor	Angle
1	5.427	3.222	84.701
2	7.898	5.978	157.487
3	15.081	14.029	162.933
4	15.075	14.643	123.739
5	5.542	3.392	73.748

Figure 71: Results retrieved from shape extraction protocol

APPENDIX 8: MASTER THESIS LOG JOURNAL

<p>10/05/2017 (LUMC) Preparation colloquium 11/05/2017 Colloquium: Presentation and Feedbacks 12/05/2017 Literature review report update + RHP level 3 lecture --/--/---- 15/05/2017 Design: Cubical inserts (V.1.1) 16/05/2017 Design: Box (V.4.3) 17/05/2017 Design: Cubical inserts (V.1.2) (.../...) 18/05/2017 Design: Cubical inserts (V.1.2) (.../...) 19/05/2017 <i>Holidays</i> --/--/---- 22/05/2017 <i>Holidays</i> 23/05/2017 Design: Cubical inserts (V.2.1) 24/05/2017 Design: Cubical inserts (V.2.2) (LUMC) 25/05/2017 <i>Hemelvaartsdag</i> 26/05/2017 Design: Spherical inserts (V.1) --/--/---- 29/05/2017 Design: Spherical inserts (V.2.1) 30/05/2017 Design: Cubical inserts (V.2.3) Design: Box (V.5) 31/05/2017 Design: Cubical inserts (V.3.1) 01/0/2017 Report: Versioning of all the box and inserts designs 02/06/2017 Design: Cubical inserts (V.3.2) (LUMC) --/--/---- 05/06/2017 <i>Tweede Pinksterdag</i> 06/06/2017 Design: Spherical inserts (V.2.2) 07/06/2017 Design: Spherical inserts (V.3.1) 08/06/2017 Design: Cubical inserts (V.3.3) (.../...) 09/06/2017 Design: Cubical inserts (V.3.3) (.../...) (LUMC) --/--/---- 12/06/2017 <i>Graduation defence of Pablo M.</i> Design: Cubical inserts (V.2.4) Manufacturing: FDM print of it 13/06/2017 Manufacturing: Second FDM print of it 14/06/2017 Design: Cubical inserts (V.2.5) 15/06/2017 Design: Cubical inserts (V.3.4) 16/06/2017 Design: Box (V.6.1) (LUMC) --/--/---- 19/06/2017 Design: Cubical inserts (V.3.5) (.../...) 20/06/2017 Design: Cubical inserts (V.3.5) (.../...) 21/06/2017 Design: Cubical inserts (V.3.6) 22/06/2017 Design: Cubical inserts (V.3.7) 23/06/2017 Design: Spherical inserts (V.3.2) (LUMC) --/--/---- 26/06/2017 Manufacturing: Print of the 0.3mm spherical inserts Design: Spherical inserts (V.4) 27/06/2017 Manufacturing: Print of the spherical inserts (V.4) 27/06/2017 Manufacturing: Tube ordering: 4 weeks delivery time 28/06/2017 Manufacturing: SLA first print of the cubical inserts 29/06/2017 Design: update of the SLA printing file Manufacturing: Ordering of the tube 30/06/2017 Manufacturing: SLA prints of the cubes (V.3.7) (LUMC) --/--/---- 03/07/2017 Manufacturing: SLA prints of the cubes (V.3.7)(success) 04/07/2017 <i>Holidays</i> 05/07/2017 <i>Holidays</i> 06/07/2017 <i>Holidays</i> 07/07/2017 <i>Holidays</i> --/--/---- 10/07/2017 Manufacturing: cut off the SLA print support parts 11/07/2017 Report: Writing of the literature review (LUMC) 12/07/2017 Report: Writing of the literature review 13/07/2017 Report: Writing of the literature review 14/07/2017 <i>Holidays</i></p>	<p>17/07/2017 Report: Writing of the literature review 18/07/2017 Report: Writing of the literature review 19/07/2017 Design: Box and flanges update (V.6.2) 20/07/2017 SLA printer is away on the 24/07/2017 21/07/2017 Test: CT imaging of the SLA cube (V.0) (LUMC) --/--/---- 24/07/2017 Test: Analysis of the CT images 25/07/2017 Manufacturing: Ordering flanges acrylic parts 26/07/2017 Report: Draft of the literature report (LUMC) 27/07/2017 Test: (LUMC) waiting for PET/CT availability 28/07/2017 Test: (LUMC) CT imaging of FDM cubes (V.2.4), SLA cubes (V3.4, V3.7) & SLA spheres (V3.2 & V.4) --/--/---- 31/07/2017 Test: Analysis of the CT images 01/08/2017 Test: Analysis of the CT images 02/08/2017 Manufacturing: Tubes& flanges reception (LUMC) Design: Box (V.7.1) 03/08/2017 Manufacturing: Cutting and threading of the tube 04/08/2017 Manufacturing: Gluing of the tube in the box --/--/---- 07/08/2017 Design: Spherical inserts plate (V.5) (.../...) 08/08/2017 Design: Spherical inserts plate (V.5) 09/08/2017 Design: Box (V.8) Manufacturing: Re-ordering of flanges 10/08/2017 Test: Radioactivity absorbance test (LUMC) 11/08/2017 Test: Radioactivity remaining calculation analysis --/--/---- 14/08/2017 Manufacturing: Reception of the rubber ring 15/08/2017 Report: CT density and absorbance properties 16/08/2017 <i>Graduation defence of Praneeta R.</i> 17/08/2017 Manufacturing: Ordering of the screws M3 ad M4 Test: CT images of the phantom's parts (LUMC) 18/08/2017 Report: Final version of the literature review --/--/---- 21/08/2017 Manufacturing: Reception of the flanges' box (V.8) 22/08/2017 Test: Analysis of the CT images 23/08/2017 <i>Graduation defence of Timon B.</i> 24/08/2017 <i>Graduation ceremony of Timon B.</i> 25/08/2017 Manufacturing: Reception of the screws Design: Box (V.7.2) Manufacturing: remove glue Manufacturing: adapt flanges to screws head --/--/---- 28/08/2017 Report: update versioning and SLA print check Manufacturing: print of the spheres' plate (V.5) 29/08/2017 Manufacturing: remove glue and Manufacturing: adapt flanges to screws head 30/08/2017 Test: Gluing tests Manufacturing: Threads in flanges 31/08/2017 (LUMC) 01/09/2017 Report: Master thesis report --/--/--- 04/09/2017 Report: Master thesis report 05/09/2017 Test: Watertight test Design: spheres' plate (V.6.1) design and print 06/09/2017 Test: leakage tests Design: phantom box (V.8) with 12 holes 07/09/2017 Meeting Willem for Green Light meeting (LUMC) 08/09/2017 Test: leakage tests Green light Meeting --/--/---- 11/09/2017 Design: Design of spherical insert plate (V.6.2) Manufacturing: FDM 3D print of the plate (V.6.2) 12/09/2017 Manufacturing: re-print of the FDM 3D plate (V.6.2) 13/09/2017 Manufacturing: spheres glued on the plates</p>
-----------------------------------------------------------------------------------------------------------------------------------------------------------------------------------------------------------------------------------------------------------------------------------------------------------------------------------------------------------------------------------------------------------------------------------------------------------------------------------------------------------------------------------------------------------------------------------------------------------------------------------------------------------------------------------------------------------------------------------------------------------------------------------------------------------------------------------------------------------------------------------------------------------------------------------------------------------------------------------------------------------------------------------------------------------------------------------------------------------------------------------------------------------------------------------------------------------------------------------------------------------------------------------------------------------------------------------------------------------------------------------------------------------------------------------------------------------------------------------------------------------------------------------------------------------------------------------------------------------------------------------------------------------------------------------------------------------------------------------------------------------------------------------------------------------------------------------------------------------------------------------------------------------------------------------------------------------------------------------------------------------------------------------------------------------------------------------------------------------------------------------------------------------------------------------------------------------------------------------------------------------------------------------------------------------------------------------------------------------------------------------------------------------------------------------------------------------------------------------------------------------------------------------------------------------------------------------------------------------------------------------------------------------------------------------------------------------------------------------------------------------------------------------------------------------------------------------------------------------------------------------------------------------------------------------------------------------------------------------------------------------------------------------------------------------------------------------------------------------------------------------------------------------------------------------------------------------------------------------------------------------------------------------------------------------------------------------------------------------------------------------------------------------------------------------------------------------------------------------------------------------------------------------------------------------------------------------------------------------------------------	------------------------------------------------------------------------------------------------------------------------------------------------------------------------------------------------------------------------------------------------------------------------------------------------------------------------------------------------------------------------------------------------------------------------------------------------------------------------------------------------------------------------------------------------------------------------------------------------------------------------------------------------------------------------------------------------------------------------------------------------------------------------------------------------------------------------------------------------------------------------------------------------------------------------------------------------------------------------------------------------------------------------------------------------------------------------------------------------------------------------------------------------------------------------------------------------------------------------------------------------------------------------------------------------------------------------------------------------------------------------------------------------------------------------------------------------------------------------------------------------------------------------------------------------------------------------------------------------------------------------------------------------------------------------------------------------------------------------------------------------------------------------------------------------------------------------------------------------------------------------------------------------------------------------------------------------------------------------------------------------------------------------------------------------------------------------------------------------------------------------------------------------------------------------------------------------------------------------------------------------------------------------------------------------------------------------------------------------------------------------------------------------------------------------------------------------------------------------------------------------------------------------------------------------------------------------------------------------------------------------------------------------------------------------------------------------------------------------------------------------------------------------------------------------------------------------------------------------------------------------------------------------------------------------------------------------------------------------------------------------------------------------------------------------------------------------------------------------------------------------------------------------------------------------------------------------------------------------------------------------------------------------------------------------------------------------------------------------------------------------------------------------------------------------------------------------------------------------------------------------------------------------------------------------------------------------------------------------------------------------------------------------------------------------------------------------------------------------------------------------------------------------------------------------------------------------------------------------------------------------------------------------------------------------------------------------------------------------------------------------------------

12/09/2017 Manufacturing: re-print of it Manufacturing: Threading and gluing of the spheres	14/09/2017 Manufacturing: box (V.9) parts cut Manufacturing: gluing of the phantom parts
13/09/2017 Graduation Defence of R. Van Ossanen Manufacturing: Gluing of the spheres (.../...) Manufacturing Cut of the M3 screws	Manufacturing: creation of a sphere insert box
14/09/2017 Manufacturing: Gluing to the tube	15/09/2017 Test: leakage test of the sphere insert box + Meeting in the (LUMC) to prepare FDG tests
15/09/2017 Meeting Willem (LUMC)	--/--/----
--/--/----	18/09/2017 Design: spheres' plates (V.7) Manufacturing: Print of the 12 holes plate
18/09/2017 Leakages tests	Test: leak test of box (V.8) + spheres' plate (V.7)
	19/09/2017 Manufacturing of new gasket (box V.9.1 and 9.2) Manufacturing: Smoother spheres' plate (V.7) Test: leakage test of box (V.8) and plate (V.7)
	20/09/2017 Test: leakages test of phantom (V.7)
	21/09/2017 Test: FDG test with glued spherical phantom